Xiumian Hu *Editor*

Field Trip Guidebook on Chinese Sedimentary Geology

Science Press
Beijing

Springer

Field Trip Guidebook on Chinese Sedimentary Geology

Xiumian Hu
Editor

Field Trip Guidebook on Chinese Sedimentary Geology

Science Press
Beijing

Springer

Editor
Xiumian Hu
Nanjing University
Nanjing, China

ISBN 978-981-99-6935-7 ISBN 978-981-99-6936-4 (eBook)
https://doi.org/10.1007/978-981-99-6936-4

Jointly published with Science Press
The print edition is not for sale in China (Mainland). Customers from China (Mainland) please order the print book from: Science Press.

This Springer imprint is published by the registered company Springer Nature Singapore Pte Ltd.
The registered company address is: 152 Beach Road, #21-01/04 Gateway East, Singapore 189721, Singapore

Paper in this product is recyclable.

Mesozoic-Cenozoic Sedimentary Geology in the Tibetan Himalaya: Continental Collision, Palaeoceanography and Hyperthermal Events

Xiumian Hu, Xi Chen, Wei An, Jiangang Wang, Jingen Dai, Juan Li, Qun Liu, and Zhong Han

1 Geological Introduction

The Himalayan–Tibetan orogen is the youngest and most spectacular of all the continent–continent collisional belts on Earth, which occupies high-altitude Himalaya and Karakorum ranges in the south and the Tibetan plateau to the north (Yin and Harrison 2000). This orogenic system was largely created by the Indo-Asian collision over the past ~60 Ma (Hu et al. 2016; An et al. 2021). In the southern Tibet of

X. Hu (✉)
Nanjing University, Nanjing, China
e-mail: bobliu@pku.edu.cn

X. Chen · J. Dai
China University of Geosciences, Beijing, China
e-mail: xichen@cugb.edu.cn

J. Dai
e-mail: daijingen@cugb.edu.cn

W. An
Hefei University of Technology, Hefei, China
e-mail: anwei@hfut.edu.cn

J. Wang
Institute of Geology and Geophysics, CAS, Beijing, China
e-mail: wangjiangang@mail.iggcas.ac.cn

J. Li
Nanjing Institute of Geology and Paleontology, Nanjing, China

Q. Liu
Nanjing Xiaozhuang University, Nanjing, China

Z. Han
Chengdu University of Technology, Chengdu, China

X. Hu (ed.), *Field Trip Guidebook on Chinese Sedimentary Geology*,
https://doi.org/10.1007/978-981-99-6936-4_12

China, this orogen belt is east–west trending and extends more than 1000 km. From north to south, it can be divided into 5 tectonic units including the Gangdese Arc, Xigaze Forearc Basin, Yarlung Zangbo Suture Zone and Tethys Himalayas (Tibetan Himalayas). In this field trip, the geological characteristics of typical outcrops of different units will be investigated. Each of the unit experienced complicated history of evolution related to the subduction and closure of Neo-Tethys Ocean. Additionally, the paleoceanographic conditions of eastern Tethys Ocean are archived in the marine sedimentary successions and will be investigated including several hyperthermal events.

1.1 Gangdese Arc

The Gangdese magmatic arc refers to the Mesozoic–Palaeogene igneous rocks developed along the southern margin of the Lhasa block that were formed as a result of northward subduction of the Neo-Tethyan oceanic lithosphere. It is the middle part of the ~ 6,000-km-long Neo-Tethyan arc belt that extends from Kohistan-Ladakh, through southern Tibet and western Burma, to Sumatra in southeastern Asia (Figs. 1 and 2) (Zhang et al. 2019a, b).

Intrusive rocks of the Gangdese arc (Gangdese batholith) are mainly granodiorite and monzogranite, with subordinate gabbro, gabbro-diorite, diorite, tonalite and granite. Volcanic rocks spread across the Gangdese arc also show a wide range of composition, including basalt, andesite, dacites and rhyolite (e.g., Zhu et al. 2008; Kang et al. 2014). Pre-Cenozoic volcanic rocks had experienced green-schist facies metamorphism, and were intruded by later granitoids. Cenozoic volcanic rocks represented by the Linzizong volcanic successions are unmetamorphosed, only mildly

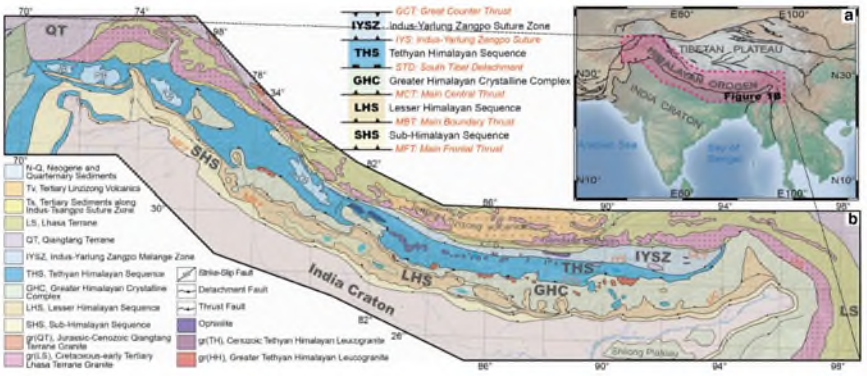

Fig. 1 **a** Tectonic and topographic map of the Tibetan Plateau, adapted from (Tapponnier et al. 2001) and (Yin 2006). The pink box indicates the simplified regional geologic map of the Himalayan Orogen (**b**), modified from Yin and Harrison (2000), Yin (2006), and Sciunnach and Garzanti (2012)

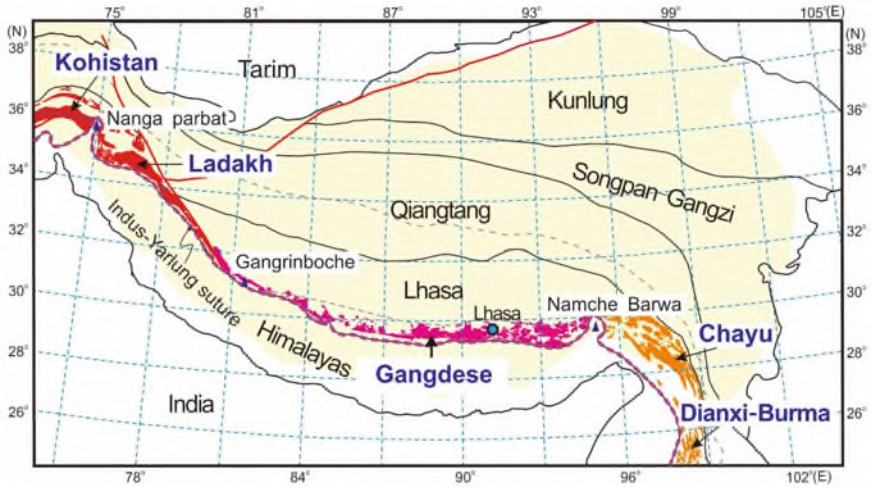

Fig. 2 Location and distribution of the Gangdese arc (Modified after Ji et al. 2009)

deformed, and overlain older rocks above a regional unconformity (Mo et al. 2008; Lee et al. 2009; Zhu et al. 2015). Sedimentary covers of the Gangdese arc are only patchily preserved, including Upper Jurassic–Lower Cretaceous carbonates and shallow-marine to nonmarine clastic rocks (Leier et al. 2007a, b; Wang et al. 2020).

Geochronological study indicated the Gangdese arc had a long-lived magmatic history from Early Mesozoic to Neogene (Fig. 3) (Ji et al. 2009; Hou et al. 2015). Magmatic activity in the Gangdese arc was started as early as Middle Triassic (~237 Ma, Wang et al. 2016a, b), although the Neo-Tethyan subduction zone was fully developed only since Early Cretaceous as indicated by tectonic and sedimentary evidences. Tectonic setting and petrogenesis of the pre-Cretaceous igneous rocks are still puzzled and controversial. Arc magmatism was mainly active during Cretaceous to Palaeogene, and shows two magmatic peaks at ~90 Ma and ~51 Ma, respectively (Ji et al. 2009). Postcollisional magmatic activity were represented by the Miocene potassic and ultrapotassic rocks, which commonly occur as isolated complexes and intruded into the Gangdese batholiths and volcano-sedimentary covers (Chung et al. 2003; Hou et al. 2004; Zhao et al. 2009).

Igneous rocks of the Gangdese arc are characterized by extremely depleted isotopic features, indicating magmatic derivation from a juvenile source (Ji et al. 2009; Zhu et al. 2011). Zircon crystals from these rocks are thereby characterized by very positive $\varepsilon_{Hf}(t)$ values (Ji et al. 2009; Hou et al. 2015), which make them highly recognizable during provenance study. Gangdese zircons have been widely used as sedimentary fingerprint to trace Asian active margin sediments in the foreland basin, remnant oceanic basin as well as synorogenic conglomerate, to constraint the timing of Indian-Asian continental collision, uplift and erosion of Gangdese-Himalayan orogenic belt and evolution of major drainages originated from the Tibetan plateau (e.g., Hu et al. 2015; Najman et al. 2017; Colleps et al. 2020).

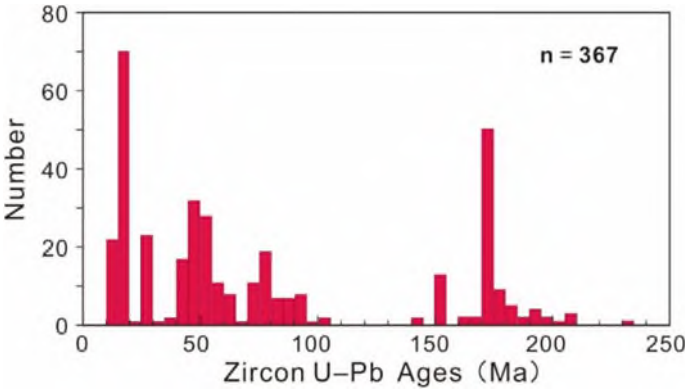

Fig. 3 A summary of published zircon U–Pb ages from the Gangdese arc

Structural analyses have shown that notable (~60%) crustal shortening had taken place on the Lhasa block during the Late Cretaceous (e.g., Murphy et al. 1997; Volkmer et al. 2007). As a result, the Gangdese belt might have reached elevations of up to 4 km in the Early Paleogene (Kapp et al. 2007), i.e., an Andean-type mountain has already been established stretching the Gangdese arc well before the India–Asian collision in Early Cenozoic (Ding et al. 2014). By contrast, crustal shortening of southern Asian margin after the India–Asian collision is limited. Recent rapid exhumation occurred in the Miocene, which might have related to the delamination of the subducting Indian slab or incise of the Yarlung-Zangbo (e.g., Harrison et al. 1992; Carrapa et al. 2014).

1.2 Xigaze Forearc Basin

The Xigaze forearc basin (XFB) is located to the south of the Gangdese arc in an east–west oriented belt extending over 500 km along the Yarlung Zangbo suture zone. With a width ranging from 50 to 22 km (Wang et al. 2012), the forearc basin is composed of flysch-dominated Xigaze Group and shallow marine succession including the Padana and Qubeiya formations and the overlying Palaeogene Cuojiangding Group (Fig. 4) (Liu et al. 1988; Wan et al. 2001).

The Xigaze Group is composed of the Chongdoi, Sangzugang and Ngamring Formations. The Chongdoi Formation comprises two members, the lower member of purplish-red radiolarian chert, siliceous mudstone interbedded with ophiolitic breccia and the upper of volcaniclastic turbidites, with numerous tuff layers throughout both members. The lower member is deposited directly upon the pillow basalts of the Xigaze ophiolite and its upper contact is conformable with the overlying Ngamring Formation (Girardeau et al. 1984; An et al. 2014; Wang et al. 2017a, b). The lower member contains a late Barremian–late Aptian radiolarian association (Ziabrev et al.

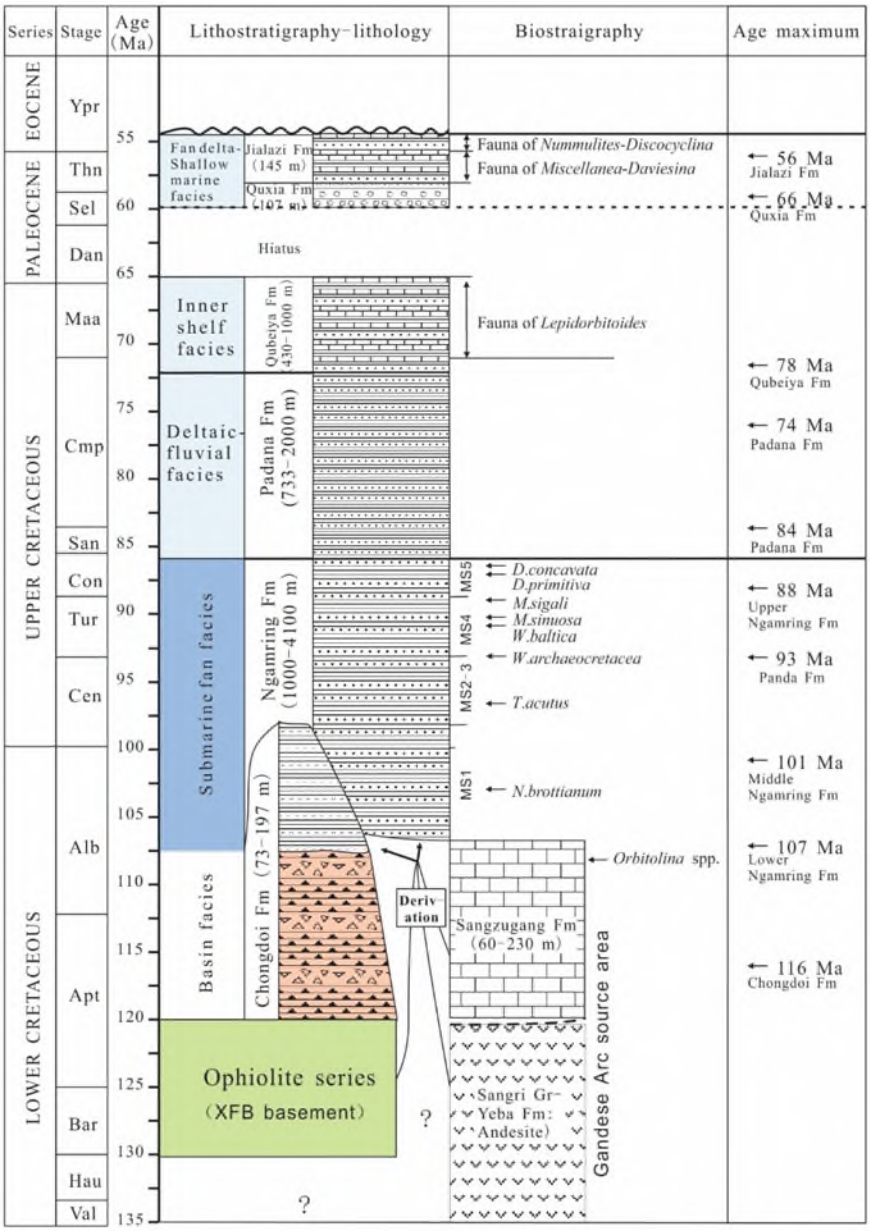

Fig. 4 Diagram showing the stratigraphic framework of the XFB with data of biostratigraphy, maximum age of detrital zircon U–Pb isotopes, and lithofacies (modified after Wang et al. 2012). In the column of the biostratigraphy, the fauna of the Qubeiya and Jialazi formations are from Wan et al. (2001), and the biozones of the Ngamring Formation are cited from Wan et al. (1998). The column of the age maximum is from Wu et al. (2010) and Hu et al. (2016)

2003) and tuffaceous zircon ages from ~119 to 113 Ma (Wang et al. 2017a, b), whereas the upper member contains detrital zircons with the youngest peak age of 116 Ma and tuffaceous zircon ages from ~113 to 110 Ma (late Aptian; Wu et al. 2010; Wang et al. 2017a, b).

The Sangzugang Formation consists of thick-bedded or massive dark-gray bioclastic limestones with abundant benthic foraminifera, rudists, corals, and minor bivalves. This unit is in fault contact with either the Ngamring Formation or the latest Oligocene-Early Miocene Kailas Formation, and its original stratigraphic relationships are uncertain (Wang et al. 2012). The Sangzugang Formation was deposited in reefal environments along the northern part of the forearc basin during the late Aptian to early Albian (Liu et al. 1988; An et al. 2014). It can be considered an equivalent to the rudistid-bearing Khalsi Limestone of the Ladakh Himalaya, which is paraconformably overlain by volcaniclastic turbidites that contain ammonoids of the late Albian age at the base (Garzanti and Van Haver 1988).

The Ngamring Formation consists of sandstone and shale, and is characterized by a series of large channelized conglomerates in the lower part. It is conformable with both the underlying Chongdoi Formation and the overlying Padana Formation in the south, and locally in fault contac with the Xigaze Ophiolite in the south or the Kailas Formation in the north (Wang et al. 2012). The Ngamring Formation forms a synclinorium striking W-E in the Xigaze area (Wang et al. 2012), with Aptian–Albian and Cenomanian–Turonian ages for the oldest strata in the northern and southern flanks respectively, and late Coniacian for the youngest strata along the axis indicated by foraminiferal associations (Wan et al. 1998). The depositional age is also supported by the youngest detrital-zircon ages being between 84 and 107 Ma (Albian–Santonian; Wu et al. 2010; An et al. 2014; Orme et al. 2014, 2016).

The shallow-water parts of the XFB with a total thickness of 1472 m provides auxiliary information about forearc basin development and consists of the Padana, Qubeiya, Quxia, and the Gyalaze formations, which were cropped out to the west of Ngamring county. The Santonian-Campanian Padana Formation is composed of varicolored sandstone interbedded with shales, minor conglomerates and limestones. Best exposed in Sangsang, this unit conformably overlies the Ngamring Formation and is in fault contact with the Xigaze Ophiolite to the south. It was interpreted to be shelf-deltaic-fluvial deposition at the filling stage of the forearc basin, with a depositional age of Santonian-Campanian constrained by the youngest detrital zircon ages and some fossils (Wu et al. 2010; An et al. 2014).

The overlying Qubeiya Formation consists of fine-grained sandy wackestones intercalated with fine-grained sandstones deposited on the inner shelf (Liu et al. 1988; Wan et al. 2001). A deposition age of Maastrichtian is indicated by benthic foraminiferal assemblages (Liu et al. 1988; Hu et al. 2016). The Quxia Formation contains a lower part of shales with thick-bedded sandstones, and an upper part of conglomerates, sandstones and shales arranged in fining-upward cycles. This unit was deposited in a fluvial-fan delta environment at the early Paleocene (Hu et al. 2016). The Jialazi Formation mainly consists of sandy foraminiferal limestones and interbedded sandstones deposited in shallow-marine, distal fan-delta environments.

The depositional age is constrained as Paleocene to earliest Eocene by larger benthic foraminifera and tuffaceous zircon ages (Hu et al. 2016; Jiang et al. 2021).

Evolution of the Xigaze forearc includes an early underfilled stage represented by abyssal cherts and turbidites of the Chongdui and Ngamring Formations and an overlying filled stage represented by the Padana, Qubeiya, Quxia and Jialazi formations, which matches well with a typical upward-shoaling sequence from deep-water turbidites to slope, shelfal, and eventually deltaic or even fluvial deposits of forearc basin. Based on both sedimentological (Wang et al. 2012) and provenance analysis, five successive stages are identified in the evolution of the Xigaze forearc basin (Fig. 5). (1) Late Barremian–Aptian (127–117 Ma): The Chongdui Formation records abyssal siliceous sedimentation in the initial phases of Neo-tethyan subduction, when negligible sediment was produced because the nascent arc was still largely submerged. The upper Aptian to lower Albian Sangzugang Formation developed subsequently (117–110 Ma), on the shallow-marine northern edge of the Xigaze forearc basin. (2) Albian–early Cenomanian (104–99 Ma): The Chongdui turbidites and lower Ngamring turbidites were deposited in deep-sea fan environments. Detritus was largely supplied by Lower Cretaceous magmatic rocks of the Gangdese arc, with minor contributions from its basement (as documented by the subordinate population of pre-Mesozoic zircons) and from erosion of the Sangzugang Formation (Fig. 5a). (3) Cenomanian–early Coniacian (99–88 Ma): The middle Ngamring turbidites were derived from both Cretaceous (ca. 100 Ma) and Jurassic (ca. 157 Ma) magmatic rocks of the Gangdese arc, and subordinately from the Sangzugang Formation (Fig. 5b). (4) Coniacian–Santonian (88–83 Ma): The upper Ngamring turbidites were derived from both the Gangdese arc and the central Lhasa terrane (Fig. 5c). (5) Early Campanian (83–76 Ma): The Padana Formation records coastal to fluvio-deltaic sedimentation with a slight increase in quartz, possibly due in part to the recycling of older siliciclastic sediments (Fig. 5d).

1.3 Xiukang Complex and Trench Basin

The Xiukang Complex, currently 10–20 km-wide and in tectonic contacts with the Yarlung-Zangbo Ophiolite in the north and with Tethyan Himalayan strata in the south, has been considered to be products of the Neotethyan subduction and subsequent India-Asia collision (Tapponnier et al. 1981; Cai et al. 2012; An et al. 2017; Metcalf and Kapp 2019). The mélange, including exotic blocks of sandstone, limestone, chert and basalt with various sizes and ages, displays a typical block-in-matrix fabric. The generally deformed matrix is represented by upper Triassic–lower Aptian abyssal chert, siliceous mudstone and local turbidites showing N-S trending stretching lineation and top-to-south S-C fabrics (Cai et al. 2012). The occurrence of *Globotruncanas* within the limestone blocks suggested a post-Late Cretaceous age for the formation of the mélange (Tapponnier et al. 1981). Three groups of sandstone blocks with different provenance and depositional setting are distinguished by their petrographic, geochronological and isotopic fingerprints (An et al. 2017). Blocks of

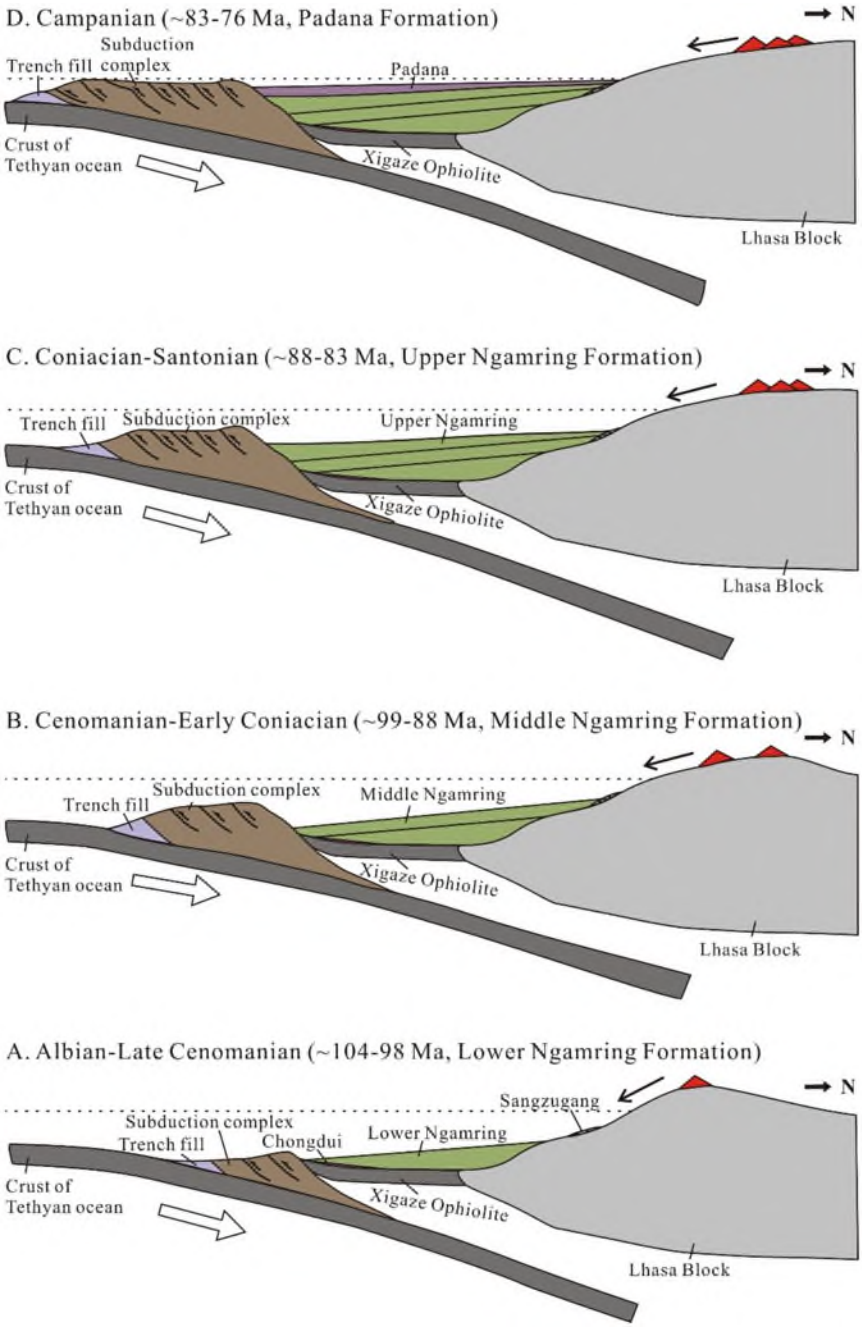

Fig. 5 Schematic sections illustrating the envisaged evolution of the Xigaze forearc basin from Albian to Campanian times (An et al. 2014)

turbiditic quartzarenite originally sourced from the Indian continent were deposited in pre-Cretaceous time on the northernmost edge of the Indian passive margin and eventually accreted at the early stage of the India–Asia collision. Two distinct groups of volcaniclastic-sandstone blocks were derived from the central Lhasa block and Gangdese magmatic arc. One group was deposited in the trench and/or on the trench slope of the Asian margin during the early Late Cretaceous (Cai et al. 2012; An et al. 2017), and the other group in a syn-collisional basin just after the onset of the India–Asia collision in the Early Eocene (An et al. 2017).

The abundant limestone blocks, varying in size from cm to km, are mostly bioclastic, with Middle–Late Permian crinoids and bryozoans, and Early Triassic, Early Jurassic and Late Cretaceous foraminifera (Tapponnier et al. 1981; Jin et al. 2015 and references therein). These exotic blocks have been variously interpreted to represent either remnants of seamounts within the Neotethys Ocean (Wang and Mu 1980), or of a carbonate platform situated on the northern fringe of Gondwana (Guo et al. 1991). Subsequent studies of the brachiopod fauna have documented transitional/mixed characters between Cathaysian and Gondwanan faunas, favoring deposition on the outer peri-Gondwanan shelf or on seamounts within Neotethys (Shen et al. 2003a, b). Blocks from seamounts within the Neotethys Ocean, as indicated by limestones and cherts directly deposited on OIB-type basalt, have been reported recently in Zhongba (Dai et al. 2012). Decimetric to metric basaltic blocks appear occasionally. They are mainly porphyritic and/or amygdaloidal, have experienced low-grade hydrothermal metamorphism, and display within-plate-basalt geochemical affinity, similar to Indian-Reunion "hotspot" lavas (Dupuis et al. 2005). Metric blocks of radiolarian chert have been identified as two groups, Middle–Upper Triassic ones with continental-margin affinity and Upper Jurassic–Lower Cretaceous ones with oceanic-basin affinity (Zhu et al. 2006).

Late Cretaceous and Paleocene trench basins have been recently reported along the central part of the Yarlung Zangbo suture zone, including the Jiachala Formation in Gyangze area (Fu et al. 2018), the Rongmawa Formation in the Dênggar area (Cai et al. 2012), and the Luogangcuo Formation and Sangdanlin-Zheya succession exposed in Saga area (An et al. 2018a, b; Hu et al. 2020). The Jiachala, Rongmawa, and Luogangcuo formations accumulated in Late Cretaceous during Neo-Tethyan ocean subduction whereas the Sangdanlin and Zheya formations accumulated in the middle Paleocene during the onset of the India-Asia collision, marking a transitional stage starting with pre-collisional sedimentation and ending with syn-collisional deformation.

The Jiachala Formation is composed of sandstone interbedded with shale deposited in a submarine-fan lobe environment (Fu et al. 2018). The Rongmawa Formation consists of lower and upper members with thin-bedded sandstone interlayered with siltstone, separated by a middle member of mud dominated interval interbedded with chert and sandstone. The Luogangcuo Formation is composed of conglomerate interlayered with sandstone and shale. Conglomerates was deposited by debris flows while sandstone by turbidity currents in a distal submarine fan (An et al. 2018a, b). Provenance analysis suggests that detritus of sandstones was derived

mainly from the Gangdese arc and central Lhasa terrane while the conglomerates were sourced from the Xiukang Complex.

In the Saga area, The Sangdanlin Formation is mainly composed of chert and siliceous shale with turbiditic sandstone beds increasing upwards. The Zheya Formation is composed of turbiditic sandstone intercalated with shale (Wang et al. 2011; DeCelles et al. 2014). The depositional age is precisely constrained by coccolith and radiolarian biostratigraphy coupled with zircon chronostratigraphy as middle Paleocene (59 ± 1 Ma; Hu et al. 2015). Turbiditic sandstones in the lower Sangdanlin Formation are either quartzose derived from India or feldspatholitho-quartzose volcaniclastic derived from the Gangdese arc and central Lhasa terrane (Wang et al. 2011; DeCelles et al. 2014). In the upper Sangdanlin and Zheya formations, instead, all turbidites are sourced transversally from the Gangdese arc and central Lhasa (Wang et al. 2011; DeCelles et al. 2014; Wu et al. 2014a, b; Hu et al. 2015, 2016; An et al. 2021).

1.4 Yarlung Zangbo Suture Zone

The Yarlung Zangbo Suture Zone (YZSZ) marks the southernmost and youngest suture in Tibetan Plateau (Yin and Harrison 2000; Fig. 6 inset). This suture includes remnants of the Neo–Tethyan oceanic lithosphere accreted to Eurasia (Allègre et al. 1984; Dai et al. 2011; Hébert et al. 2012). The Yarlung Zangbo ophiolite (YZO) comprises well preserved to dismembered ophiolitic massifs. Ophiolites are fragments of ancient oceanic lithosphere that are emplaced at convergent plate margins. Previous studies document that the YZO formed during 130–120 Ma (Dai et al. 2012, 2013, 2021; Li et al. 2009; Liu et al. 2016; Wang et al. 2006; Wu et al. 2014a, b; Zhang et al. 2016a, b; Zhang et al. 2016a, b; Fig. 6a, b). In the south, the YZO thrusts over a narrow belt of ophiolitic mélange which is composed of blocks of serpentinized peridotite, mafic rock, amphibolite, chert, limestone, and sandstone (Guilmette et al. 2009); while in the north, the YZO is overlain by flysch of the Xigaze Group (Dürr 1996; Wang et al. 2012). The nonconformable depositional contact between YZO lava and sediment of Chongdoi Formation defines the YZO as the base of the Xigaze forearc basin (An et al. 2014; Dai et al. 2015; Wang et al. 2017a, b).

1.4.1 Tectonic Settings of the Yarlung Zangbo Ophiolite (YZO)

Slow-Spreading Mid-Ocean-Ridge Model

Several tectonic models have been proposed for the YZO. In the early 1980s, detailed geological mapping was conducted in the Xigaze Ophiolite in the central YZO including the Dazhuqu to the Jiding massifs (Fig. 6b). These studies revealed that the YZO did not form at a magma-rich mid-oceanic spreading ridge because of the paucity of mafic rocks, but was generated at a slow-spreading ridge (Girardeau et al.

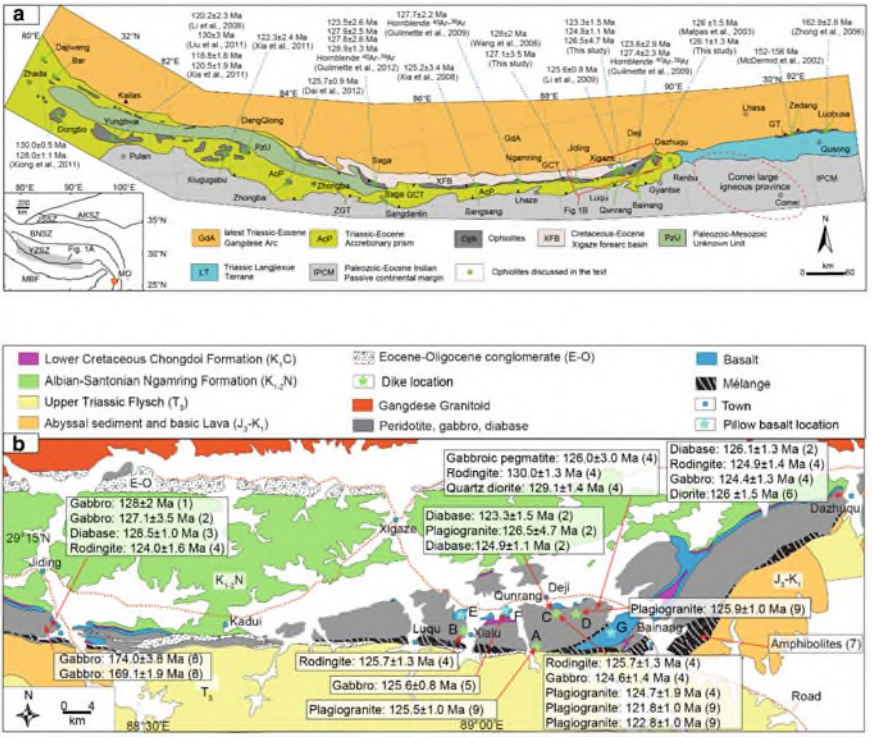

Fig. 6 **a** Schematic tectonic map of southern Tibet showing the ophiolitic massifs within the YZSZ (after Dai et al. 2013). Zircon U–Pb ages of the mafic rocks and hornblende $^{40}Ar/^{39}Ar$ ages of the amphibolites across the whole YZSZ are also presented. Major faults: GCT, Great Counter thrust; ZGT: Zhongba-Gyangze thrust; GT: Gangdese thrust. Inset is the simplified tectonic map of Tibetan Plateau showing major sutures. The major sutures are: AKSZ, A'nemaqin-Kunlun suture zone; JSSZ, Jinshajiang suture zone; BNSZ, Bangong-Nujiang suture zone; YZSZ, Yurlung Zangbo suture zone. MO, Myitkyina ophiolite, Myanmar. **b** Geological map of the Xigaze area (Wang et al. 1987) showing the locations of dated samples (after Dai et al. 2021). References: (1) Wang et al. (2006); (2) Dai et al. (2013); (3) Bao et al. (2013); (4) Zhang et al. (2016a, b); (5) Li et al. (2009); (6) Malpas et al. (2003); (7) Guilmette et al. (2009); (8) Wang et al. (2018); (9) Dai et al. (2021)

1985a; Nicolas et al. 1981). Limited thin crustal outcrops might be related to exhumation after ophiolite emplacement (Burg et al. 1987). This possibility was confirmed by thermochronological data from the Oligocene sediments within the YZSZ which reveal about 6 km (vertical) of rock removal (Carrapa et al. 2014).

The slow-spreading ridge tectonic model was developed by Wu et al. (2014a, b) and his group (Fig. 7a). Zhang et al. (2016a, b) argued that Xigaze Ophiolite basalts are typical N–MORBs without influence from subduction–related fluids. However, the following lines of evidence argues against this conclusion: (1) most mafic rocks show negative Nb anomalies and positive U and Pb anomalies, indicating that their source was affected by subduction–related fluids (Hébert et al. 2012); (2) although at least 85% of sedimentary Nd and Hf are recycled into the mantle, the Hf and

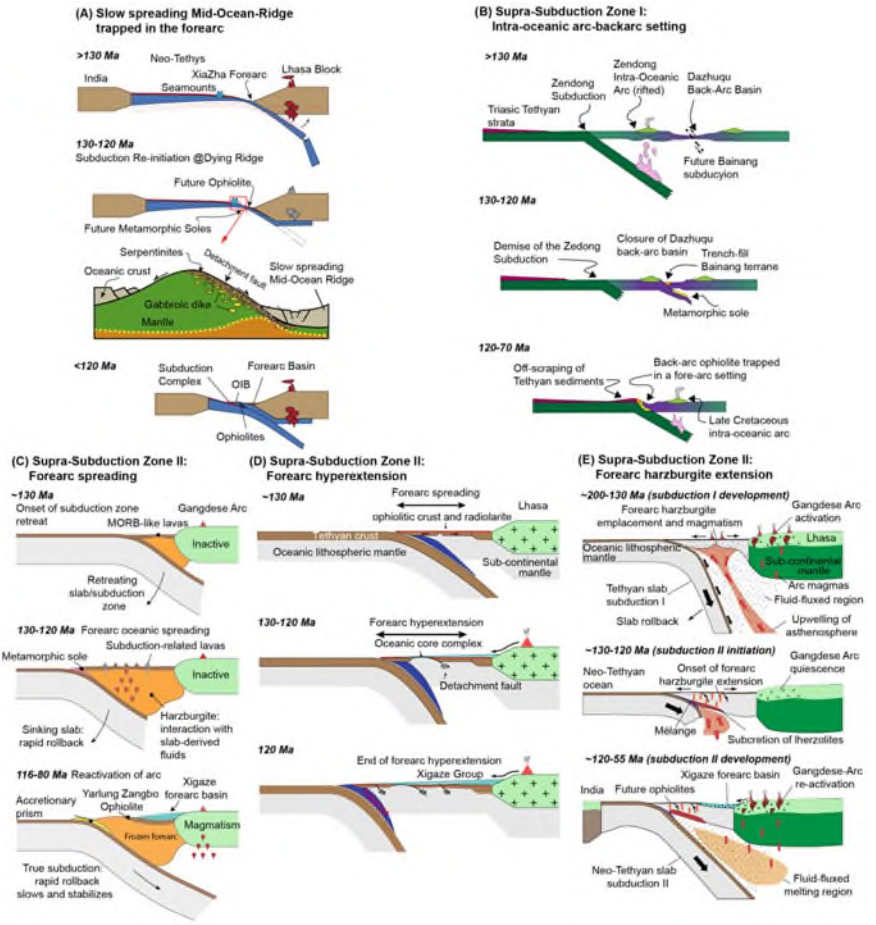

Fig. 7 Proposed tectonic models for the Yarlung Zangbo ophiolite (after Dai et al. 2021). **a** Slow spreading mid-ocean-ridge trapped in the forearc (Liu et al. 2014; Zhang et al. 2019a, b); **b** Supra–Subduction Zone I: complex intra–oceanic arc-backarc setting (Hébert et al. 2012; Guilmette et al. 2009); **c** Supra–Subduction Zone II: Forearc spreading (Dai et al. 2013, 2021); **d** Forearc hyperextension (Maffione et al. 2015); **e** Forearc harzburgite extension and lherzolite subcretion (Xiong et al. 2016)

Nd isotopic compositions of the Izu–Mariana arc lavas are not markedly different from those of MORBs (Chauvel et al. 2009). Therefore, the MORB–like Nd–Hf isotopic compositions do not rule out the possibility that mafic rocks witnessed subduction–related fluids.

Liu et al. (2016) proposed that Xigaze Ophiolite gabbroic rocks were generated beneath a fossil slow–spreading ridge because gabbro pods or dikes are associated with diabase dikes or sills, suggesting that the gabbros were exhumed when the diabases were generated. Rapid exhumation of mantle peridotites and gabbroic rocks

of the Xigaze Ophiolite may have allowed intrusion of the diabase dikes and sills. The above arguments do not constrain the tectonic setting of the Xigaze Ophiolite. If the Xigaze Ophiolite was formed in an SSZ environment, the mantle peridotites and gabbroic rocks could also be intruded by diabase dikes. In addition, Liu et al. (2018) observed that gabbroic intrusions in the Jiding sequence are more evolved than Dazhuqu and Bainang gabbroic rocks which are characterized by higher Cr_2O_3 but lower TiO_2 and REE contents in both clinopyroxene and bulk compositions. They proposed that the lower oceanic crust within the Xigaze Ophiolite is highly segmented and discontinuously distributed, similar to that exposed at modern slow– and ultra–slow–spreading ridges. Such variations may be related to both magma evolution and magma source, since they also proposed that melt–crystal reaction played a key role in magma generation. More recently, Liu et al. 2019 proposed that Dazhuqu mantle peridotites experienced 0–6% garnet–facies melting followed by 10–18% melting in the spinel stability field based on clinopyroxene trace element modeling. This is similar to the degree of garnet–facies melting inferred for many MOR peridotites rather than fore–arc peridotites. The occurrence of abyssal peridotite is not strong evidence that the Xigaze Ophiolite was generated in the slow–spreading MOR because a previous study revealed the occurrence of both fertile and depleted mantle in the Zedang area (Xiong et al. 2016). Specifically, previous studies revealed that more than half of the Luqu peridotites (Fig. 7b) have ultra–refractory compositions indicated by both whole rock and clinopyroxene compositions (Zhang et al. 2017).

The same group proposed a subduction re–initiation model at a dying mid–ocean–ridge (Zhang et al. 2019a, b; Fig. 7a) following previous studies of Guilmette et al. (2012). This interpretation was based on the high geothermal gradient recorded by the metamorphic sole in the Lhaze ophiolitic mélange which was also reported in other mélange massifs including Bainang, Buma and Saga (Guilmette et al. 2012). This model emphasized that the location of the subduction zone was close to the Eurasian continental margin (Zhang et al. 2019a, b), while previous models proposed that subduction was intra-oceanic (Guilmette et al. 2012). This model proposed (1) the entire YZO was a trapped remnant of MORB lithosphere that was generated in a slow–spreading MOR; and (2) the metamorphic sole originated from the MOR crust in the lower plate. However, the majority of MOR was generally subducted, not accreted, just as illustrated by the currently subducting Nazca Ridge beneath the northern South American margin (Hampel et al. 2004). All the above observations can be well explained in a subduction initiation model.

Supra-Subduction Zone Model

Most studies of mineral and whole–rock geochemical data from the YZO reveal a heterogeneous mantle that possesses refractory whole rock major element compositions and U–shape REE patterns (Dai et al. 2013; Zhang, et al. 2017; Xiong et al. 2017), as well as the high Cr# spinels for most YZO peridotites (Hébert et al. 2003; Zhang, et al. 2017; Xiong et al. 2017), indicating that they underwent hydrous melting. Mafic rocks show slight depletion in light REE, and have a small negative

Ta–Nb anomaly, suggesting the influence of a subduction component. The abundances of incompatible elements in the mafic rocks are similar to back–arc–basin basalts (BABB; Bédard et al. 2009; Hébert et al. 2012). Therefore, the YZO was proposed to belong to a complex intra-oceanic arc–back-arc setting, analogous to the Lau basin (Aitchison et al. 2000; Hébert et al. 2003; Guilmette et al. 2009; Fig. 7b). However, there is no evidence for a slightly older intra-oceanic arc along the YZSZ that a BAB could form behind (Wu et al. 2014b). Instead, the associated Gangdese magmatic arc lies to the north, separated from the ophiolites by the Xigaze forearc basin (Fig. 6b).

Based on geochemical similarities between basalts and late–stage mafic dikes in the YZO and forearc basalts and boninites in the IBM, Dai et al. (2013) was first to propose that the YZO formed in a forearc spreading setting (Fig. 7c). This forearc spreading model was further developed in the following two models: (1) Forearc hyperextension: paleomagnetic and field geological observations reveal the occurrence of extensional detachment faults in the YZO (Maffione et al. 2015). These exhumed mantle rocks and mélange on the seafloor and were subsequently covered by forearc basin strata (Fig. 7d). Forearc hyperextension might help explain dismemberment of the YZO. (2) Forearc harzburgite extension and lherzolite subcretion: both harzburgite and lherzolite outcrop in the Zedang Ophiolite of the eastern YZO (Xiong et al. 2016; Fig. 7e). The equilibration temperature of lherzolite is 250–150 °C higher than that of the harzburgite, suggesting that harzburgites formed earlier (possibly at 200–130 Ma during an earlier episode of subduction) and at shallower levels than lherzolite. The authors proposed that the subcretion of lherzolites, intrusion of dolerite dykes, and doming and extension of overlying harzburgitic lithosphere occurred coevally during 130–120 Ma of the second stage of subduction (Fig. 7e).

1.4.2 Geological Settings of the Xigaze Ophiolite (XO)

The Xigaze Ophiolite (XO), located in the central part of the Yarlung Zangbo suture zone (Dai et al. 2021), displays well preserved sections from mantle to crustal rocks, together with overlying sedimentary strata (Fig. 6b). Marine sedimentary rocks consist of mudstone, chert, felsic tuffs and fine–grained volcaniclastic deposits and are exposed along the northern margin of the XO, with Late Barremian to Late Aptian depositional ages (Ziabrev et al. 2003; Figs. 6b and 7b). The Xigaze Ophiolite mafic sequence is thin (approximately 2 km) (Girardeau et al. 1985b). A well–preserved sequence of pillowed lava occurs in several places such as Qunrang, Deji, and Luqu. Minor cumulate gabbro has only been reported at Dazhuqu, Bainang and Jiding massifs (Liu et al. 2018; Fig. 6b). Sheeted diabase is rarely observed except at Deji and Bainang massifs (Wang et al. 1987). The Xigaze Ophiolite is dominated by mantle peridotite (Figs. 6b and 7b). These are variably serpentinized (Hébert et al. 2003) and are intruded by various dikes, such as diabase, rodingite, plagiogranite, and gabbroic pegmatite (Fig. 8b).

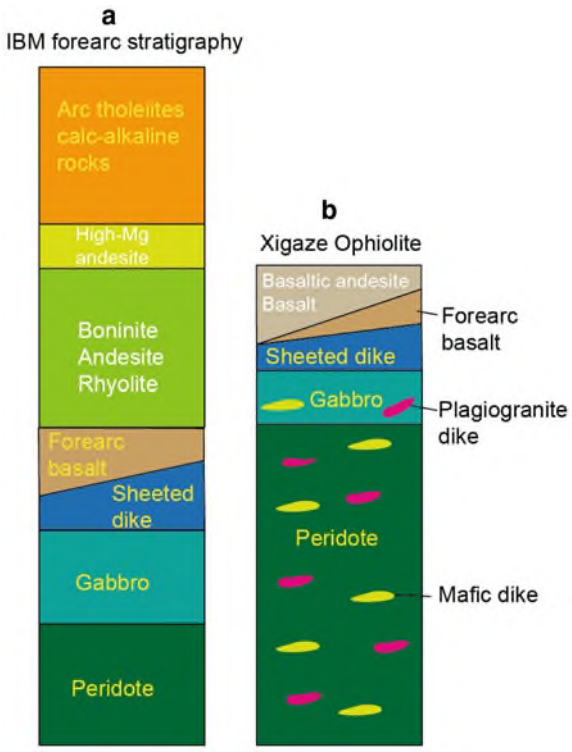

Fig. 8 Schematic columnar sections of Izu–Bonin–Mariana (IBM) forearc (**a**, modified from Ishizuka et al. 2011) and Xigaze Ophiolite (**b**, modified from Girardeau et al. 1985a)

In the XO, there are plenty of radiometric ages from mafic rocks including isotropic gabbro, diabase sill and various gabbroic/diabase dikes intruded into both the crustal and mantle section. These ages range from 124 ± 1.6 Ma to 130 ± 1.3 Ma (Fig. 7b; Bao et al. 2013; Dai et al. 2013, 2021; Liu et al. 2016; Zhang et al. 2016a, b), which are comparable to those of the plagiogranites (Four plagiogranite samples from three different locations of a, c, d in Fig. 6b yielded zircon U–Pb ages of 121.8 ± 1.0 Ma, 122.8 ± 1.0 Ma, 125.5 ± 1.0 Ma, 125.9 ± 1.0 Ma, respectively, Fig. 9a–d). These ages indicate that both mafic and felsic intrusive rocks in the Xigaze Ophiolite were generated in the Early Cretaceous, i.e., 121.8–130.0 Ma (Fig. 9e). However, Middle–Late Jurassic ages (174.0 ± 3.8 Ma and 169.1 ± 1.9 Ma) from two gabbro samples from the Dazhuqu and Jiding massifs have been reported recently in the Xigaze Ophiolite (Wang et al. 2018), products of an earlier stage of igneous activity in the Neo–Tethyan Ocean, unrelated to the Early Cretaceous magmatism. Most ages suggest that the duration of Xigaze Ophiolite magmatic activity during the Early Cretaceous stage was about 10 Ma, consistent with the conclusions of Hu and Stern (2020).

The main samples and field observations in this field guide book were focused around several massifs (a–d for gabbroic pegmatite, plagiogranite, diabase dike in the mantle and basaltic dike in the crust, e–g for pillow basalt; Fig. 6b).

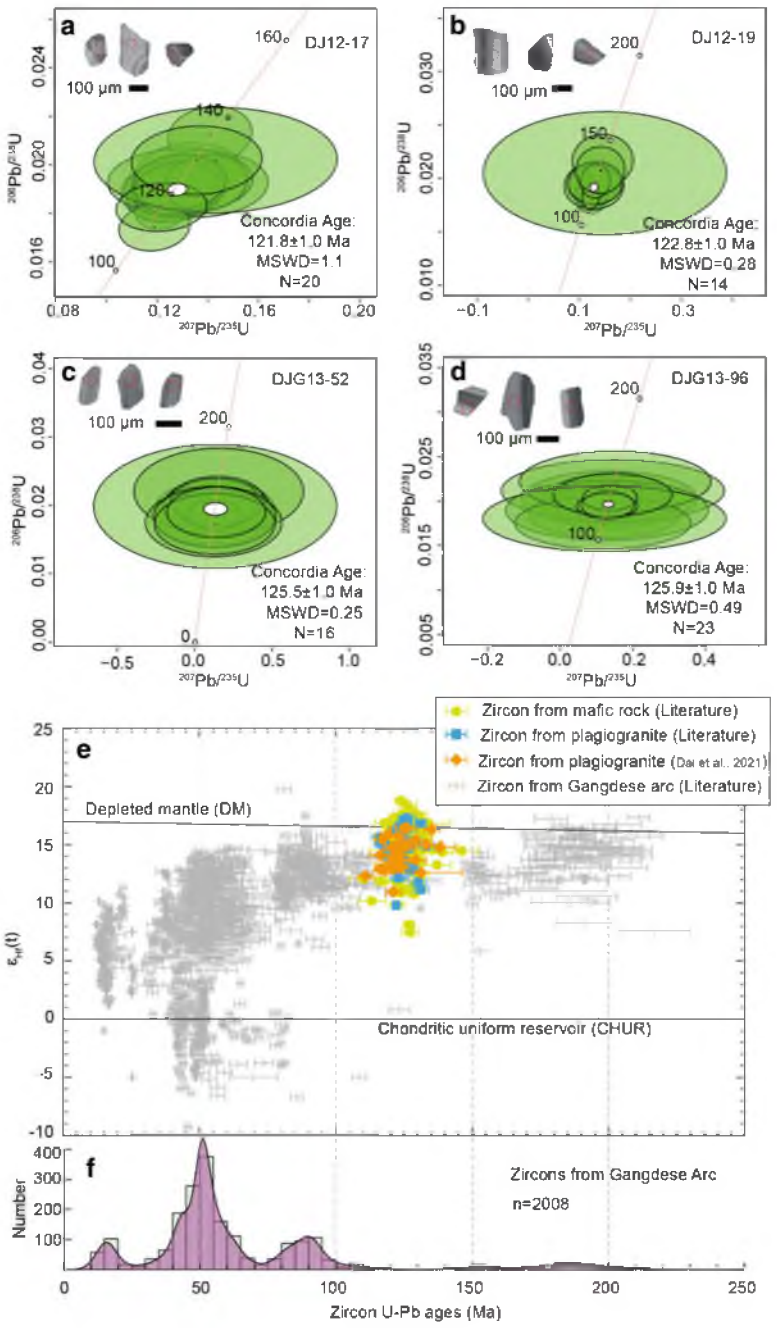
a
DJ12-17
100 μm
Concordia Age:
121.8±1.0 Ma
MSWD=1.1
N=20
b
DJ12-19
100 μm
Concordia Age:
122.8±1.0 Ma
MSWD=0.28
N=14
c
DJG13-52
100 μm
Concordia Age:
125.5±1.0 Ma
MSWD=0.25
N=16
d
DJG13-96
100 μm
Concordia Age:
125.9±1.0 Ma
MSWD=0.49
N=23
Zircon from mafic rock (Literature)
Zircon from plagiogranite (Literature)
Zircon from plagiogranite (Dai et al., 2021)
Zircon from Gangdese arc (Literature)
e
Depleted mantle (DM)
Chondritic uniform reservoir (CHUR)
f
Zircons from Gangdese Arc
n=2008
Number
Zircon U-Pb ages (Ma)

◀**Fig. 9** Zircon U–Pb concordia plots of four plagiogranite samples (**a**–**d**: DJ12–17, DJ12–19, DJG13–52, DJG13–96) and representative cathodoluminescence images of zircons. Plots of $\varepsilon_{Hf}(t)$ versus U–Pb ages of zircons from plagiogranite and mafic rock in the Xigaze Ophiolite (**e**) and zircon U–Pb ages of Gangdese Arc (**f**). Data source of mafic rock and plagiogranite from Dai et al. 2013; Liu et al. 2016; Zhang et al. 2016a, b; Please see Dai et al. (2021) for the detailed data source of the Gangdese arc

1.5 Syncollisional and Post-Collisional Basins

1.5.1 Syncollisional Basin

After initial continent–continent collision (i.e., the first contact of two continents after the end of an oceanic subduction), an underfilled seaway still exists between the two continents. The marine basin was inherited, and developed above former forearc and passive marginal basins. This syncollisional basin will be gradually filled until final retreat of seawater from the collision zone. Then, the landmasses were completely integrated and connected by fluvial systems (Hu et al. 2016b). In some literature, the syncollisional basin was called as an underfilled peripheral foreland basin (Sinclair 1997). A remarkable feature of syncollisional basin is that sediments from the active margin could be transported across the trench and deposited on the former passive margin.

In the Gangdese forearc, syncollisonal basin developed above the Xigaze forearc basin (Figs. 9 and 10). Syncollisional strata including the Quxia Formation and the Jialazi Formation were well preserved and exposed in the Cuojiangding area of Zhongba County (Fig. 10). The Quxia Formation is a suite of (~105-m-thick) coarse-grained clastic rocks, consists of conglomerates, sandstones and shales that were deposited in fluvial to fan-delta environments. The underlying latest Cretaceous sandy wackestones and fine-grained sandstones of the Qubeiya Fomration were deposited in deltaic to inner shelf environments, representing the final the final filling of the Xigaze forearc basin. The overlying Jialazi Formation was conformably contact with the Quxia Formation, and consists of ~240-m-thick sandy foraminiferal limestones and interbedded sandstones, deposition in shallow marine, distal fan-delta environments (Hu et al. 2016b). The Paleocene-Eocene Thermal Maximum (PETM) event was recognized in the Jialazi Fomration, as indicated by carbon-isotope excursion and facies change. It was accompanied by increasing siliciclastic supply, indicating enhanced hydrological circulation (Jiang et al. 2021).

Larger benthic foraminifera from the Qubeiya Formation indicates a late Maastrichtian depositional age, whereas those from the Jialazi Formation indicate late Paleocene-early Eocene age (SBZ3-SBZ5, ~58–54 Ma). Considering the limited thickness of the Quxia Formation and rapid depositional rate in the fan-delta environment, there should be a hiatus of ~7–8 Ma between the Qubeiya Formation and the Quxia Formation (Ding et al. 2005; Hu et al. 2016). Although this unconformity was not directly observed in the field because of poor outcrop conditions, abrupt facies change between the two formations support this speculation. Dramatic change

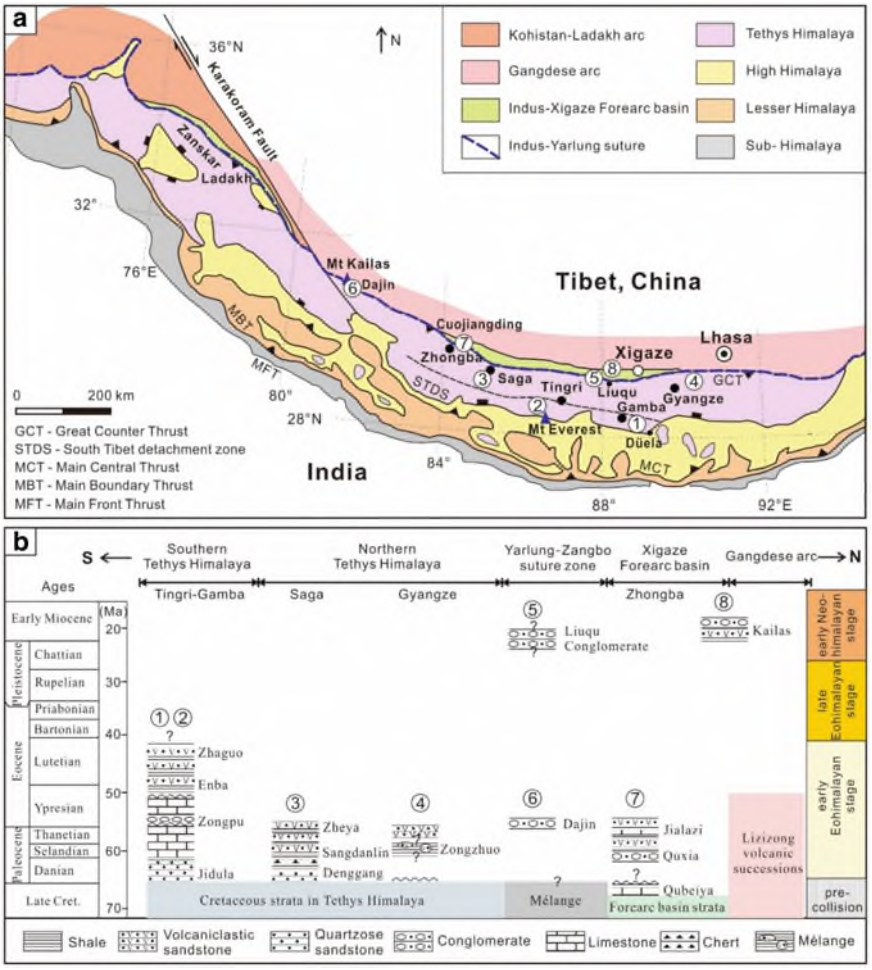

Fig. 10 **a** Simplified geological map shows location of major syncollisional and post-collisional sedimentary units along the Indian-Asian collision belt. **b** Stratigraphic correlation of syncollisional and post-collisional sedimentary records (Hu et al. 2017)

of depositional environments and the possible depositional hiatus were interpreted as a consequence of incipient collision between India and Asia. If this is the truth, sedimentary response to the collision onset would be constrained between 65 and ~58 Ma in the Gangdese forearc. Subsequently, the southern margin of Asia was uplifted and rapid exhumation ensued. Petrography pf sandstones changes from 'undissected arc' to 'dissected arc' through the stratigraphic sequence (Hu et al. 2016).

Further west in the Kailas region (Fig. 10), the earliest Eocene coarse-grained shallow-marine clastic rocks (Dajin Formation) contain large amounts of recycled sedimentary rock fragments. U–Pb age and Hf isotopic signatures of detrital zircons

indicate ultimate provenance of these rocks was the Gangdese arc. Sedimentary recycling of forearc-basin strata documented in the Dajin Formation may be also a consequence to the India-Asia collision (Wang et al. 2015).

South of the Yarlung suture in the Tethyan Himalaya, syncollisional basin could be divided into two belts, analogous to the Indian passive margin strata. The northern zone consists of deep-marine turbidites, chert and olistostromes, while the southern zone was filled shallow marine carbonates, and shelf to fluvial clastic rocks.

Syncolisional strata of the northern zone were well documented in the Saga area (Figs. 9 and 10). The Sangdanlin Formation and the conformably overlying Zheya Formation consist of hundreds-m-thick interbedded volcaniclastic sandstones, black mudstones, purple-reddish chert and siliceous shales. The appearance of chert and siliceous shale, and lack of carbonate sediments indicate a palaeo-water depth deeper than the carbonate compensation depth (CCD). Sandstone beds commonly display sharp contact with underlying mudrocks, and are arranged in thicken- and coarsen-upward trends. Sedimentary structures of sandstone layers include normal grading, flute casts, ditch moulds, and slump structures, indicating deposition by turbidity currents. Slumping deposition with exotic blocks of conglomerate, sandstone, and carbonate is common throughout the succession, indicating an unstable setting (Wang et al. 2011; DeCelles et al. 2014). Provenance analysis indicated that volcaniclastic sandstones in the Sangdanlin and Zheya formations were derived from the Gangdese arc to the north. By contrast, the underlying strata (the Denagng Formation) consist of quartzose sandstones, silty sandstone and silty shale. Provenance study suggested an exclusive Indian source (Wang et al. 2011; Wu et al. 2014a, b; DeCelles et al. 2014; Hu et al. 2015). Arrival of Asian sediments onto the distal margin of Indian continent provides a solid constraint on the timing of Initial India-Asia collision. The age for provenance changes was precisely dated by radiolarian fossils, calcareous nanofossils and zircon U–Pb age of tuffs to be 59 ± 1 Ma (Hu et al. 2015).

In Gyangze area to the east, syncollisional sediments were represented by the Zongzhuo mélange (Figs. 9 and 11). The Zongzhuo mélange shows typical ‘blocks in matrix’ texture. The blocks are several centimeters to tens of meters in size, and include sandstone, chert, basalt, and basaltic conglomerate. The matrix is mainly black shale and siltstone. Provenance analysis indicated that clastic sediments of the mélange were derived from the Asian active margin (Wu et al. 2014a, b). It is suggested that the Zongzhuo mélange had been formed in the trench after the initial collision between Indian and Asian continents (Sun et al. 2011).

Syncolisional strata of the southern Tethyan Himalayan zone were documented in Tingri-Gamba areas (Figs. 9 and 10). Although initial India-Asia collision occurred as early as middle Paleocene (59 ± 1 Ma), carbonate platform (The Zongpu Fomration) continued to early Eocene (~50 Ma) in Tingri-Gamba area (Hu et al. 2012; Zhang et al. 2012; Li et al. 2015a, b). Notably, a suite of conglomerate occurs at the Paleocene-Eocene boundary. The clasts in the conglomerate are all carbonate rocks and were derived from underlying strata. Microfacies analysis indicates that Paleocene carbonates below the conglomerate were deposited in a carbonate mid-ramp environment, whereas the Eocene carbonates above the conglomerate were deposited in a restricted lagoon (Li et al. 2015a, b). Therefore, occurrence of the

conglomerate records a regression event. The conglomerate was interpreted by some scholars as a record of forebulge unconformity associated with India-Asia collision, but others suggested it is a response to the PETM event (Li et al. 2020a, b). The first appearance of Asian detritus occurs in the overlying Enba formation, which consists of calcareous shales and sandstones deposited in shelf to delta-front environments (Najman et al. 2010; Hu et al. 2012). The youngest strata in Tingri-Gamba areas are the fluvial Zhaguo Formation, deposition of which indicates the final retreat of seawater from this region.

1.5.2 Syn-Orogenic Conglomerates

Syn-orogenic conglomerate, also called as continental 'molasses' in some literature, is generally held to be a typical product of continental collision, documenting the stage of rapid topographic growth of a foreland fold-thrust belt. In the Himalayan orogen, typical molasses was deposited in the sub-Himalaya along the south frontier of the orogenic belt in Neogene time. This age is much later than initial continental collision as well as the final filling of the syncollisional basin. Syn-orogenic conglomerates had also been deposited and preserved along the Yarlung-Zangbo suture zone north of the Himalayan orogenic belt.

There are two syn-orogenic conglomerate belts along the Yarlung-Zangbo suture zone: one is the Kailas Conglomerate (or Gangrinboche Conglomerate), exposed along the southern foothills of the Gangdese arc; and the other is the Liuqu conglomerate, exposed to the south of the Kailas Conglomerate along the southern side of the Yarlung-Zangbo ophiolite (Figs. 9, 10, 11 and 12). The Kailas Conglomerate was deposited unconformably above the Gangdese magmatic rocks, and was commonly buried by the Great Counter Thrust with the Xigaze forearc strata in the hanging wall. The sedimentary environment of the Kailas Conglomerate evolved from lakes and meandering rivers at the base to braided rivers and alluvial fans at the top (DeCelles et al. 2011; Wang et al. 2013). Sediments of the base strata were derived entirely from the Gangdese arc in the north, whereas detritus from the Tethys Himalaya, Xigaze forearc basin strata, and Yarlung-Zangbo ophiolites in the south increase upward and become dominant at the top. The zircon ages of tuff layers and pollen constrain the age of the Kailas Conglomerate as late Oligocene-early Miocene (26–18 Ma; Aitchison et al. 2009; Li et al. 2010; DeCelles et al. 2011; Wang et al. 2013). Deposition of the Kailas Conglomerate was considered as a consequence of short-lived extension along the suture followed by the development of the Great Counter Thrust, which were geodynamically induced by the rollback and breakoff of the subducting Indian lithosphere (DeCelles et al. 2011).

The Liuqu Conglomerate was exposed between accretionary mélanges (to the south) and ophiolites, forearc deposits (to the north) along a central, 150-km-long segment of the India-Asia suture zone in southern Tibet. The age of the Liuqu conglomerate has been the object of a long-term controversy. Fossil plants indicated that it could be mid-late Eocene in age (Tao 1988; Fang et al. 2004), and sporopollen fossils indicated a late Eocene to Oligocene age (Wei et al. 2009). However, low

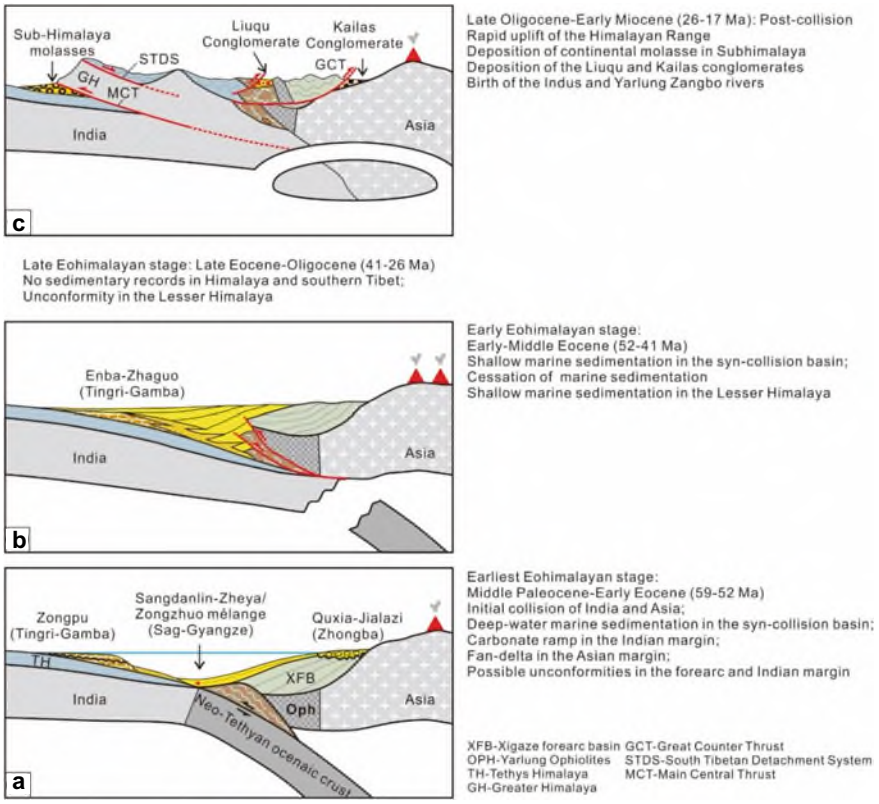

Fig. 11 Syncollisional to post-collisional basin evolution along the Indian-Asian collision belt (Hu et al. 2017)

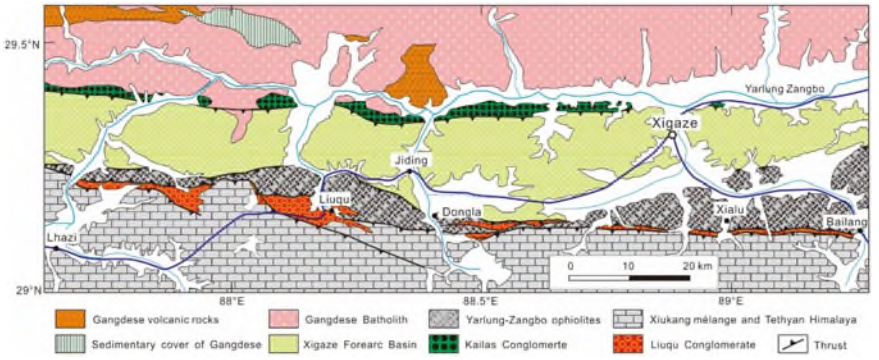

Fig. 12 Geological map shows the distribution of the Kailas Conglomerate and the Liuqu Conglomerate in the Xigaze area, southern Tibet (Hu et al. 2017)

temperature thermochronology data suggested instead that it is notably younger, probably during Late Oligocene-Early Miocene (Li et al. 2015a, b; Leary et al. 2016). Recent structural analysis indicates that the Liuqu Conglomerate was deposited in a contractional setting, probably associated with the development of the Great Counter Thrust system, thus supporting the Late Oligocene-Early Miocene depositional age. The Liuqu conglomerate was deposited mainly in an alluvial fan-braided river environment (Davis et al. 2002). Clasts of the Liuqu Conglomerate are of polymictic composition, varying among outcrops, and are dominantly quartz-arenite, litharenite, basalt, radiolarian chert, phyllite, and slate, along with minor quartzite, gabbro, and serpentinized ultramafic rocks. Paleocurrent and provenance data demonstrate that sediment was transported north-northwest from the hanging wall of a coeval thrust fault system along the southern limit of Liuqu outcrops. The Yarlung-Zangbo ophiolite, Xiukang Mélange, and Tethys Himalaya strata are potential source for the Liuqu Conglomerate (Davis et al. 2002; Wang et al. 2010; Leary et al. 2016).

Conglomerates deposited near the Yarlung-Zangbo suture zone during the late Oligocene to early Miocene (26–18 Ma) have about the same age as the initial stage of "molasse"-type sedimentation on the sub-Himalaya. During this time window, both the collisional suture zone and the Himalayan fold-thrust belt to the south were subjected to rapid uplift, erosion, and exhumation. Development of the Great Counter Thrust was associated with formation of a topographic depression (syn-orogenic basin) parallel to the suture zone between the Gangdese arc massif and the hanging wall of the Great Counter Thrust. This paleogeography created the conditions for the formation of the Yarlung-Zangbo and Indus rivers (Sinclair and Jaffey 2001; Wang et al. 2013).

1.6 Tethys Himalaya

The Tethys Himalaya is one of the major tectonic zones within the Himalaya Orogen (Gansser 1964). It is boarded by the Greater Himalaya Complex in the south and the Indus-Yarlung Zangbo Suture Zone in the north. The Tethys Himalaya (THS) has been located at the passive margin of Indian continent from the birth of Neo-Tethys Ocean till Indian-Asia collision, happened in the early Paleogene (Hu et al. 2015; An et al. 2021). The sedimentary succession in this area archives the tectonic and oceanographic evolution history of Neo-Tethys Ocean. Sedimentary rocks deposited in the Tethys Himalaya are exposed from Zanskar (NW India) to southern Tibet (SW China; Fig. 1; Sciunnach and Garzanti 2012), stretching for about 1500 km. In south Tibet, the hyper-extended THS margin is traditionally subdivided into the northern/outer (nTHS) and southern/inner (sTHS) subzones (Brookfield 1993; Liu and Einsele 1994; Yin and Harrison 2000; Yin 2006), separated by the Gyirong-Kangmar Thrust (Ratschbacher et al. 1994) or the Gamba-Tingri Fault (Wang et al. 1996). Lithologies of Mesozoic in nTHS are mainly deep-sea deposits. By contrast, in sTHS the Mesozoic sedimentary rocks were deposited on shallow marine environments consisting coastline to outer shelf.

The most widely spread sediments and spectacular outcrops in the Tethys Himalaya are of Jurassic to Eocene marine deposits (Fig. 13). Owing to few vegetation cover, the sediment successions are well cropped out along main roads in this area. In sTHS, the Jurassic succession is composed of carbonates in the Lower to Middle Jurassic, which is overlain by siliceous sediments, i.e., the black shales and quartz arenites of Menkadun Fm. The depositional environments of the carbonates were documented as tidal flats, reef rimed platform in the Hettangian-Pliensbachian and carbonate ramp in the Toarcian-Aalenian (Jadoul et al. 1998; Han et al. 2016). Between the carbonates and black shales, an interval of iron oolites developed, which is a few meters thick and is correspondence with global transgressive initiated in late Middle Jurassic. Black shales of the Menkadun Fm. are also called the 'Spiti Shale', which contains abundant well preserved ammonites. The Lower Cretaceous (?Berriasian-Aptian) in sTHS is characterized by volcanoclastic sandstones and black shales with clastic dykes, which recorded reactivation of the passive margin. From Albian to the latest Cretaceous the carbonate composition increased upward. The lithologies in this interval are mainly marl/limestone couplets and limestones deposited in ramp environments. A disconformity of ~10 Myr lies between early Campanian pelagic mudstones or foraminiferal wackstones and early Maastrichtian? intraclast packstones can be observed (Hu et al. 2012). This disconformity is interpreted as the regional uplift by the Deccan hotspot (Li et al. 2019a, b). Cretaceous in nTHS is composed mainly deep sea shales, turbidites and exotic blocks. The Early Cretaceous are volcanclastics and dark greenish gray shales overlain by Upper Cretaceous calcareous shales, radiolarian cherts, red shales with slumped limestones and olistostrome (Hu et al. 2008).

Recent years, the equivalent levels of global paleoceanographic events including Toarcian Oceanic Anoxic Event (T-OAE), Cretaceous OAEs, Paleocene-Eocene Thermal Maximum (PETM), and Cretaceous Oceanic Red Beds has been studied in detail. Moreover, the regional tectonic evolution, includes the reactivation of the passive margin in Early Cretaceous, the interaction between Deccan Trap and the Tethys Himalaya in Late Cretaceous, closure of Neo-Tethys Ocean revealed by latest marine horizon and provenance changes, have also been documented in last decades.

2 Schedule of the Field Trip

The field trip is mainly along the Yarlung Zangbo river in the south Tibet and the northside of the Himalaya. It takes 9 days to travel across four tectonic units of the Himalaya Orogen (Table 1), i.e., Gangdese Arc, Suture Zone, Xigaze Forearc Basin and Tethys Himalaya. We will investigate 27 typical outcrops (Fig. 14) related to closure history, the sedimentation process and paleoceanographic events in the Neo-Tethys Ocean. The field trip is mainly focused on the sediments of Jurassic to Paleogene. The igneous of Gangdese Arc and massif volcanic rocks of ophiolites will be observed as well. Additionally, one stop about the Permian–Triassic boundary event is involved. Therefore, the topics of the field trip are broad, which include not

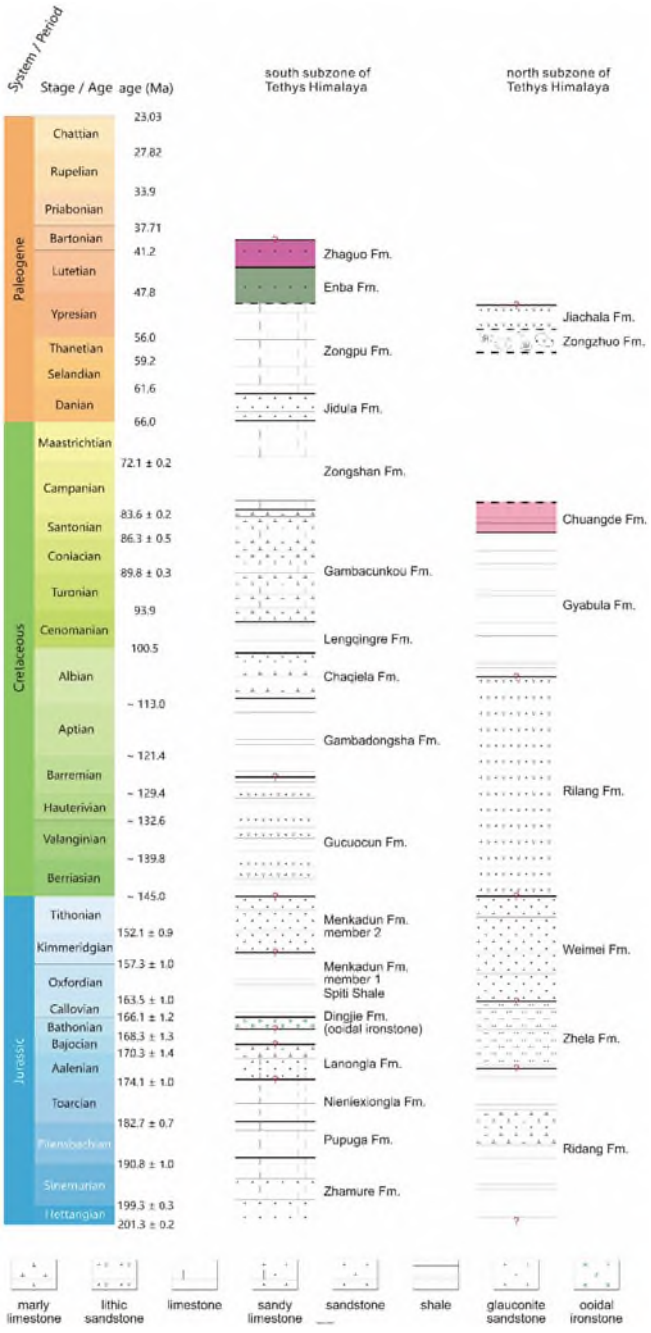

Fig. 13 Lithostratigraphy of Jurassic-Cretaceous in the south Tethys Himalaya and north Tethys Himalaya

Table 1 General schedule of the field trip

Date	Route	Stops	Observations
Day 1	Beijing to Lhasa		
Day 2	Lhasa to Xigaze	1–4	• Gangdese Batholith • Kailas Conglomerate • Channel conglomerate of the lower Nagmiring Formation in the Xigaze forearc basin
Day 3	Xigaze to Lhatse	5–9	• Sediments and tuff layer in Nagmiring Formation, Xigaze forearc basin • Liuqu Conglomerate • Sedimentary blocks of Xiukang Complex
Day 4	Lhatse to Old Tingri	10–12	• Upper Triassic deep-water sediments of northern subzone of Tethys Himalaya • Cretaceous-Paleogene shallow-water succession and hyperthermal events of southern subzone of Tethys Himalaya
Day 5	Old Tingri	13–17	• Latest marine horizon of Neo-Tethys • Early Cretaceous clastic dykes and cold seep carbonates • Lower Jurassic shallow-water succession and hyperthermal event • Triassic-Jurassic boundary sedimentation of southern subzone of Tethys Himalaya • Cenozoic N-S striking rift
Day 6	Old Tingri to Saga	18–19	• Middle-Upper Jurassic succession: transition from carbonate platform to siliceous clastic shelf • Permian–Triassic boundary sedimentation of south Tethys Himalaya
Day 7	Saga	20–21	• Late Cretaceous trench sediments of Neo-Tethys, Luogangcuo Formation • Cretaceous-Paleocene abyssal Sangdanlin section
Day 8	Saga to Xigaze	22–23	• Indian Asian provenance reversal recorded in Mubala section • Tectonic contact between the Xigaze forearc basin and Yarlung Zangbo Suture Zone
Day 9	Xigaze to Gyangze	24–26	• Ophiolites of Yarlung Zangbo Suture Zone • Sedimentary contact between the Xigaze forearc basin and Yarlung Zangbo Suture Zone
Day 10	Gyangze to Lhasa	27–29	• Cretaceous succession in north Tethys Himalaya • Triassic deep-water Langjiexue group
Day 11	Lhasa to Beijing		

only the tectonic sedimentation, but also the sedimentation of carbonate factory, submarine canyon, slope apron and of hyperthermal events. Most of the scheduled outcrops have been well studied and distributed in the last decades.

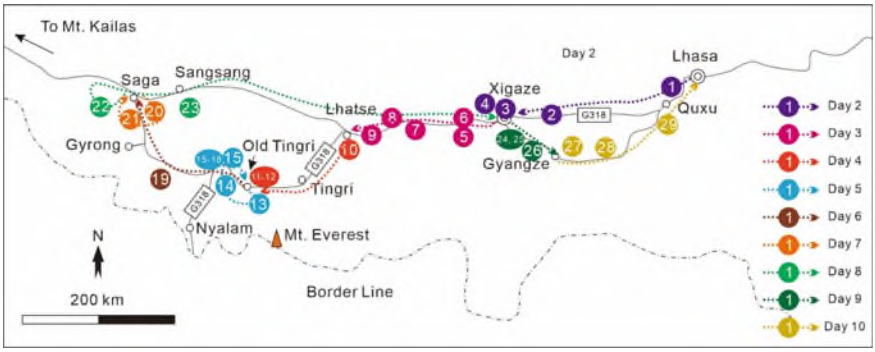

Fig. 14 Sketch shows the localities of the visiting stops

3 Description of Stops

Stop 1 Gangdese Batholith Near the Nietang Village, Quxu County (GPS: 29°29′57″N, 90°56′19″E)

This is a typical outcrop of the Gangdese batholith, and in literature it was called Quxu Batholith. Porphyritic monzogranite and coarse-grained granodiorite contain large amount of fine-grained gabbroic–dioritic enclaves (Fig. 15). Zircon U–Pb geochronology indicates the granitic hosts and the mafic microgranular enclaves have a same age of ~51 Ma (Ji et al. 2009). Co-occurrence of felsic and mafic rocks indicate significant magma mixing during emplacement of these intrusions. Hf isotopes from both the host rocks and the enclaves are also the same, with εHf(t) values of 11.0 ± 0.5 (Ji et al. 2009). Consistent Hf isotopic signatures indicate the mantle-derived gabbro and diorite and crustal-derived granitoids had become isotopically homogeneous during magma mixing, or they share a common isotopic source.

Emplacement of the Quxu pluton corresponds to the Paleocene- Eocene (~65–41 Ma) magmatic flare-up in the Gangdese arc. It is suggested that this magmatic active period was caused by rollback of the subducting Neotethyan oceanic slab and then culminated by the slab break-off that occurred around 50–45 Ma (Chung et al. 2005; Zhu et al. 2015). The intrusive and volcanic rocks (i.e., the Linzizong Volcanic Successions) formed during this period make up the main part of the present Gangdese arc.

On this outcrop, we can also see a Miocene (16.8 ± 0.4 Ma) granodioritic dyke intruded into the Eocene pluton (Fig. 15). The dyke show clear chilled margins and is characterized by lots of potassium feldspar phenocryst. These porphyry intrusions record an important post-collisional magmatic stage in the Gangdese arc, and are related to the formation of the Gangdese porphyry copper belt (Hou et al. 2009).

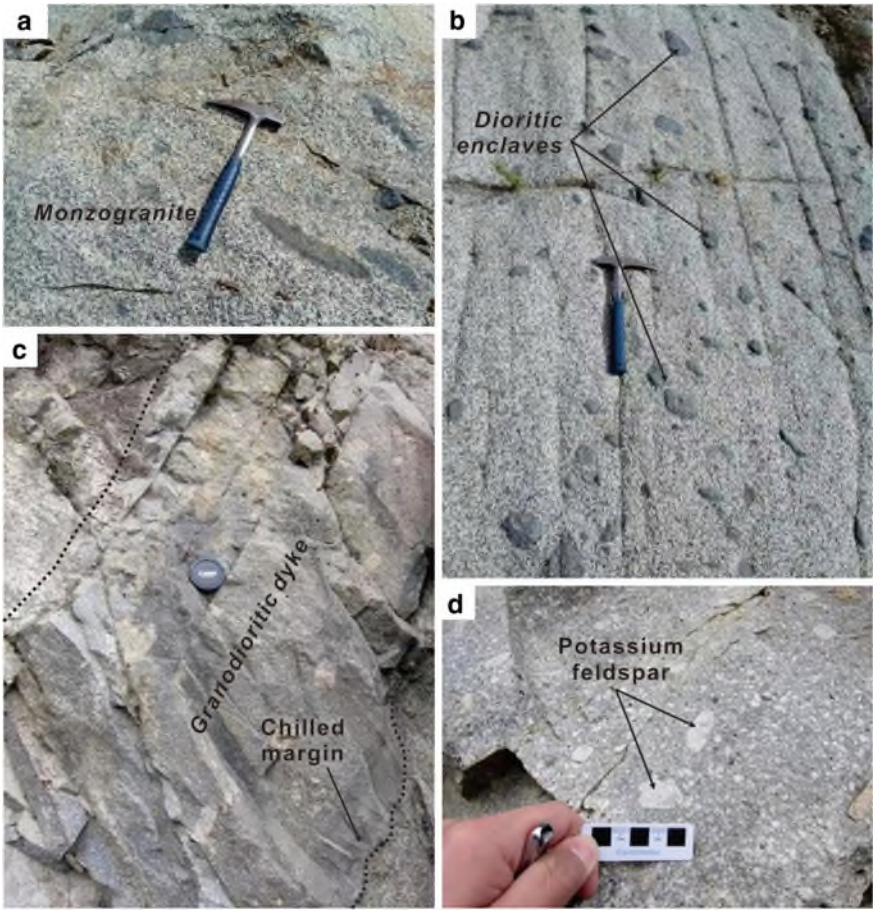

Fig. 15 Eocene monzogranite with dioritic enclaves (**a**, **b**); Miocene granodioritic dyke with potassium feldspar phenocryst (**c**, **d**). Photos are provided by Wei-Qiang Ji

Stop 2 Kailas Conglomerate at Dazhuka Bridge (GPS: 29°17′30.1″N, 89°47′54.4″E)

An exposure of the Kailas Conglomerate is observed. The conglomerate consists of gravels of various size and sandy matrix. Clasts are subangular to well rounded, poorly sorted. Rude normal grading and cross bedding are occasionally observed. Sedimentary textures indicate a braided river environment (Fig. 16). Gravel clasts are of polymictic composition, including chert, mafic and ultra-mafic rocks, sandstones, etc. The Yarlung-zangbo ophiolites and the accretionary mélange are the main source of the sediments.

Interlayer of felsic tuffs have been reported from nearby outcrops. $^{40}Ar/^{39}Ar$ dating of biotite and plagioclase separates from the tuffs gave ages of 20–22 Ma (Aitchison et al. 2009).

Fig. 16 Field photos of the Kailas Conglomerate in Dazhuka. Photos are provided by Jian-Gang Wang

Stop 3 Channelized Conglomerates of the Ngamring Formation in Xigaze Forearc Basin, Xigaze City (GPS: 29°16′01.4″N, 88°51′49.5″E)

At west of the Tashilhunpo Monastery in Xigaze city, five set of channel systems were identified within a west–east oriented zone extending 120 km long, interpreted to be channeled submarine fan megasequence (Fig. 17). In the Xigaze area, the submarine fan was outcropped 10–20 km west and east of the town. Five sandstone–conglomerate bodies as high, steep relief in the field were identified west of the Xigaze town: Quarry Ridge, Minor Ridge, Castle Ridge, Monastery Ridge, and West Ridge (Wang et al. 2012). These strata were developed during Cenomanian based on benthic foraminifera from siltstone along strike (Wan et al. 1998), with detritus mainly derived from the Gangdese magmatic arc, the central Lhasa terrane to the north and the underlying Sangzugang Formation (Wu et al. 2010; An et al. 2014).

At this stop, the Monastery Ridge system is composed by superimposed channel fills and overlying overbank/slope sediments, with a thickness of > 200 m. Channel fills are represented by conglomerates fining upwards to massive turbiditic sandstones with lenses of conglomerate and mudstone while overbank/slope sediments are characterized by mudstone intercalated with thin-bedded sandstone. Clastic-supported conglomerates contain well-rounded pebbles to cobbles of volcanics, granites, limestone, mudstone and chert. Bouma sequence Ta-c, scoured bases and shale intraclasts

Fig. 17 Panoramic view of the Monastery Rigde system of the Ngamring Formation. Photo by Wei An

were developed in sandstone beds (Wang et al. 2012). One rhyolitic cobble from its counterpart west of the Xigaze town was dated at ~95 Ma and one andesitic cobble from the southern limb of the forearc basin was dated at ~105 Ma (Dai et al. 2015).

Stop 4 Thrust Contact of the Kailas Conglomerate with the Ngamring Fm. At Tunqiong Village (GPS: 29°19′41.2″N, 88°47′35.5″E)

The top of the Kailas Conglomerate and its fault contact with the Xigaze forearc strata are observed (Fig. 18). The Kailas Conglomerate consists of purple-red, massive or laminated mudrock with carbonate nodules, and thin-bedded to massive siltstone, sandstone and fine-grained conglomerate. The red mudrocks were deposited in a floodplain, whereas sandstones and conglomerates represent braided river channels. Clasts are mainly various colored chert, with subordinate quartz sandstone, litharenite, mafic and ultramafic rocks, granite, and volcanic rocks. These sediments were derived from both sides of the basin, including the Gangdese arc to the north and the Xigaze forearc basin, the Yarlung-Zangbo ophiolite, the accretionary mélange and even the Tethyan Himalayan strata to the south. Deposition of the Kailas Conglomerate indicates a paleo-Yarlung-Zangbo River was established at the very start of the Miocene (Wang et al. 2013). On this outcrop, we can also see a lamprophyre dyke (~18 Ma; Yin et al. 1994) cross-cutting the stratigraphic beds of the Kailas Conglomerate. To the south, the Xigaze forearc strata (the Ngamring Formation turbidites) thrust northward over the Kailas Conglomerate by the Great Counter Thrust (Fig. 18).

Stop 5 Cold Seep Carbonates and Turbidites of the Ngamring Fm. Of the Xigaze Forearc Basin at Kadui Village (GPS: 29°09′06″N, 88°37′56″E)

This outcrop is located at the Kardoi village, which is ~20 km west to the Xigaze city and ~500 m south to the China-Nepal road. Nodular concretions are developed within the sandstone and shale intercalations of the Nagmiring Formation in Kardoi area (Fig. 19). Their sizes are much variable from a few centimeters to tens of centimeter.

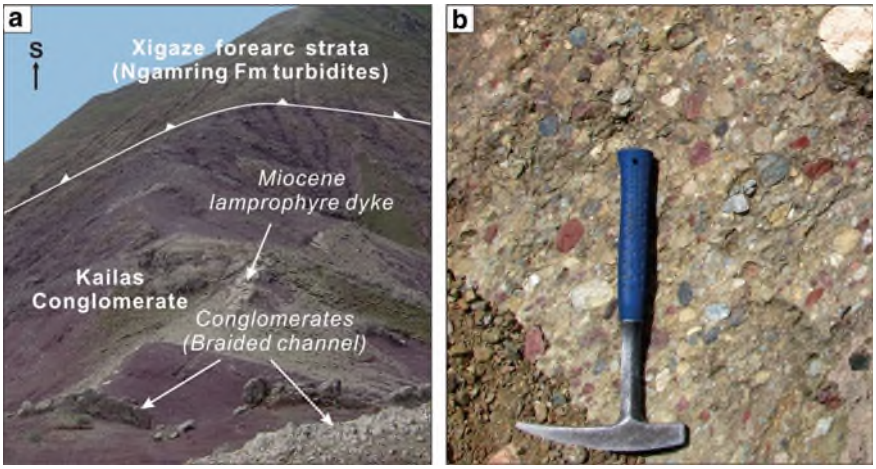

Fig. 18 Field photos of the Kailas Conglomerate in Tunqiong area, Xigaze. Photos are provided by Jian-Gang Wang

TOC content (0.05–0.31%) in the concretion is less than their host sediments (0.10–1.00%). The $\delta^{13}C$ values range from –26.68‰ to –6.07‰ (PDB) (Liang et al. 2016). Within the nodular concretions, the $\delta^{13}C$ values show a gradual decrease from the periphery to the center (Liang et al. 2016). These systematic variations reflect the diagenetic changes that occurred in the host sediment and indicate that the growth of the nodular concretions was sequential, from an early formed center to a later-formed periphery. The carbon source of the nodular concretions was derived from a mixture of anaerobic methane oxidation, methanogenic CO_2, and seawater-dissolved inorganic carbon (Liang et al. 2016).

At this stop, the sediments of submarine fan system can be observed (Fig. 20). The succession belongs to the megasequence 3, which is dominated by middle-outer fan to basin facies, e.g., gravity-flow sandstones, lobe and interchannel sandstone-shale couplets and basinal/pelagic limestones (Wang et al. 2012). It represents an assemblage of interchannel, overbank and channel sediments, which are clearly shown in the Fig. 20. At the base of sandstone unit, flute casts of ~0.5 m in size developed and indicat the sediments sourced from north (Fig. 21).

Stop 6 Tuff Layer in the Ngamring Formation of Xigaze Forearc Basin (GPS: 29°09′05″N, 88°37′13″E)

This stop will observe one tuff layer within the Ngamring Formation near the Kadui village. This tuff layer with a thickness of ~ 0.2 m was discovered within the upper Ngamring Formation (Fig. 22a, b) and one sample (ART01) was collected from this tuff layer. Zircons from this sample show relatively large size with a length of 100–200 μm, and a width of 80–120 μm. They show sector and oscillatory zoning and euhedral, long-prismatic shape. Their Th/U ratios are between 0.71 and 1.54. Fifteen zircon grains yield a weighted mean age of 91.3 ± 0.9 Ma (MSWD = 2.7; Fig. 22c, d;

Fig. 19 The cold seep carbonates, which are nodular concretions enclosed by dark gray shales and fine sandstones of the Nagmiring Formation in Kardoi area. Professor Chengshan Wang (left) and Qiyu Huang (Right) were standing in front of the outcrop. Photo by Xi Chen

Fig. 20 The submarine fan deposits of the Cretaceous Nagmiring Formation. The scour surface between the sandstone and the turbidites is clearly shown. At the base of the sandstone unit, flute casts were developed. Photo by Xi Chen

Fig. 21 Enlarged view of the flute casts show the paleo-current orientated from right (north) to left (south). The flute casts are of ~ a half meter in size. Photo by Xi Chen

Dai et al. 2015). This age provides more precise constraints on the deposition timing of the Ngamring Formation. Given that the tuff layer is conformably interbedded with the flysch, this age represents the timing of the air fall tuff and thus the age of deposition for the Ngamring Formation. Twenty analyses of tuff sample ART01 yield initial $^{176}Hf/^{177}Hf$ ratios of 0.282890–0.283005. These analyses show positive $\varepsilon_{Hf}(t)$ values of + 6.0 to + 10.2 and young $T_{DM}{}^{C}$ ages of 472–716 Ma, implying that they were also associated with an origin of juvenile crust. This interpretation is consistent with the extensive granitoid magmatism with large positive $\varepsilon_{Hf}(t)$ values in the Gangdese arc (e.g., Ji et al. 2009).

Stop 7 Liuqu Conglomerate Near Liuqu Village (GPS: 29°8′34.7″N, 88°9′25.1″E)

Exposure of the Liuqu Conglomerate and its structure relationship with surrounding tectonic domains are observed. The Liuqu Conglomerate here is folded into a several-kilometer-wide syncline by movement of faults along both its northern and southern boundaries. Along its northern outcrop boundary, the Liuqu Conglomerate is overthrust by ophiolitic rocks, whereas to the south, it is overthrust by the Xiukang Complex (Leary et al. 2016) (Fig. 23).

Lithofacies of the Liuqu Conglomerate are mainly clast-supported, massive or horizontally stratified, pebble-cobble conglomerate; red or green, massive mudstones; and massive and horizontally laminated siltstone. Massive, horizontally stratified, or trough cross-bedded sandstone; Matrix-supported, boulder conglomerate are occasionally presented. Sedimentological analysis shows the Liuqu Conglomerate is composed of mixed fluvial and sediment-gravity flow lithofacies assemblages locally interbedded with mature paleosols, suggesting a

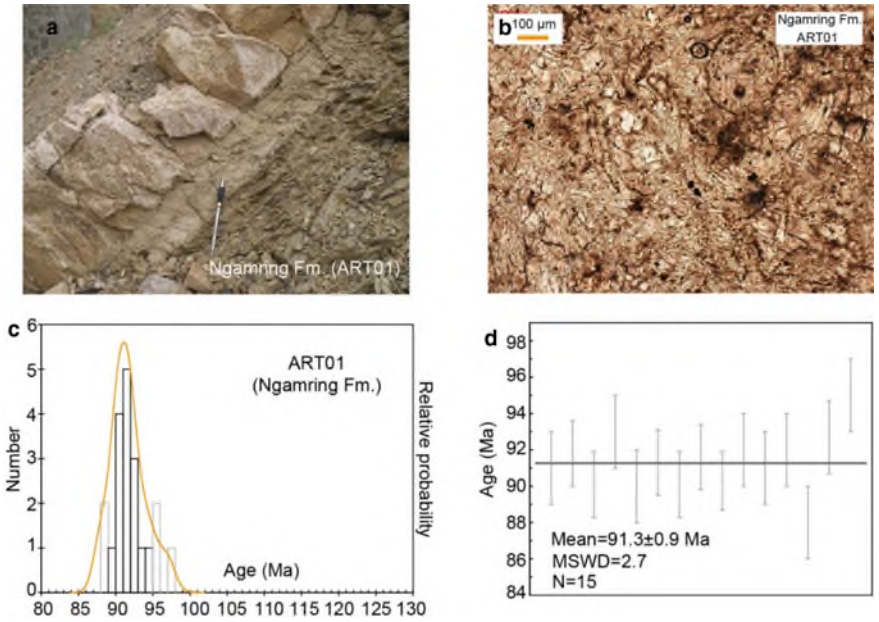

Fig. 22 Field photographs (**a**) and microstructure photomicrographs (**b**) of the Tuff in the Chongdoi Formation. Probability and weighted average of $^{206}Pb/^{238}U$ ages for sample ART01. Gray box in the probability diagram represents samples that plot outside of a Gaussian distribution or the highly discordant analyses, and they were excluded from the weighted mean age calculation (After Dai et al. 2015). Abbreviations: Fm., Formation

stream-dominated alluvial-fan environment (Davis et al. 2002; Leary et al. 2016) (Fig. 23).

Lithofacies and sedimentary texture indicate the Liuqu Conglomerate was deposited proximal to the source. Paleocurrent measured from clast imbrications suggests northeastward-northwestward sediment transport, indicating detritus were derived mainly from source terranes to the south. Basalt and serpentinized clasts were derived from the ophiolites; Green lithic sandstone and slate were most likely derived from the mélange complex; quartz sandstone, quartzite, and limestone were also likely derived from the mélange, with a probable ultimate origin in the Tethys Himalayan; chert clasts could be derived either from the ophiolites or from the mélange (Wang et al. 2010). Erosion of ophiolites and mélange could be a result of development of the Great Counter Thrust (Leary et al. 2016).

Stop 8 Xiukang Complex with Permian Exotic Limestone Blocks Near Quxia Village (GPS: 29°7′2.8″N, 88°2′57″E)

This stop is located at south of Quxia village to the west of G318 Road near the 5000 km milestone in Lhatse county.

The sedimentary-matrix mélange is composed of exotic limestone, sandstone, basalt and chert blocks within strongly deformed phyllitic matrix in the Zhongbei

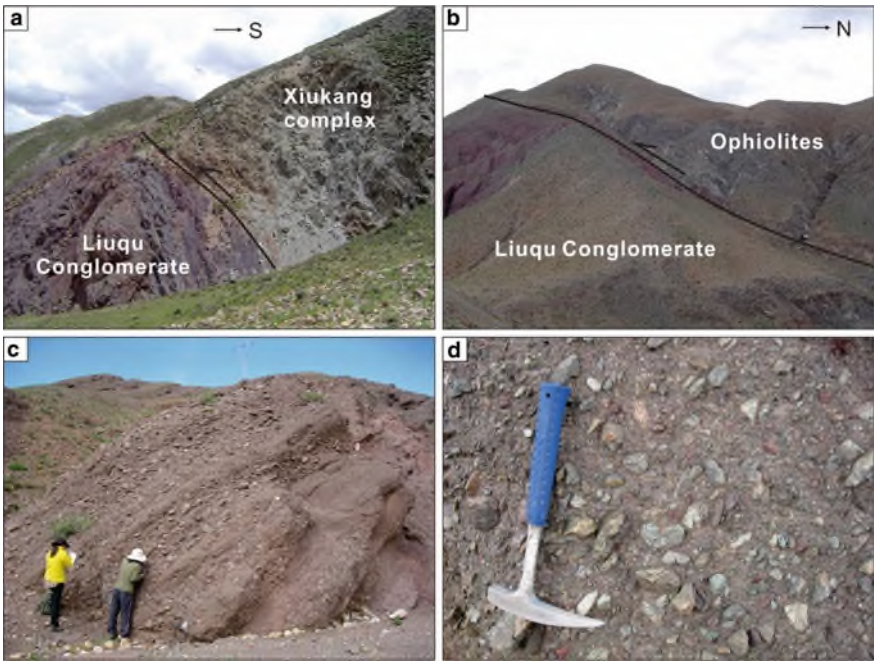

Fig. 23 Field photos of the Liuqu Conglomerate. Photos are provided by Jian-Gang Wang

area, Lhatse county. Numerous limestone blocks size from meter to kilometer, among which large ones form ridges of mountains and small ones often half buried or floating within matrix (Shen et al. 2003b; Jin et al. 2015). At this stop, the limestone blocks extend up to 3 km and for about 1 km along the road, in a wavy contact with the phyllitic matrix (Fig. 24). Brown, purplish red and greenish gray bioclastic limestones are intercalated with thin-bedded mudstone (Fig. 25). Fragments of crinoid and bryozoan, brachiopod shells and corals with peri-Gondwanan and cathaysian affinity are reported, indicating a middle-late Guadalupian age (Jin et al. 2015). The bioclastic limestone generally contains terrigenous clasts and/or intercalated with mudstone, suggesting a proximal depositional environment. Generally, these blocks are considered as dismembered units of middle Permian carbonate successions broken during the rifting process in the Late Triassic (Shen et al. 2003b; Jin et al. 2015).

Stop 9 The Xiukang Complex with Sandstone Blocks at Colha Pass Along G318 in Lhatse County (GPS 29°04′08.0″N, 87°59′29.7″E)

Small sandstone blocks and peridotite blocks are preserved within mudstone matrix at this stop (Figs. 26 and 27). Quartoze sandstones (Fig. 27c) are outcropped up to

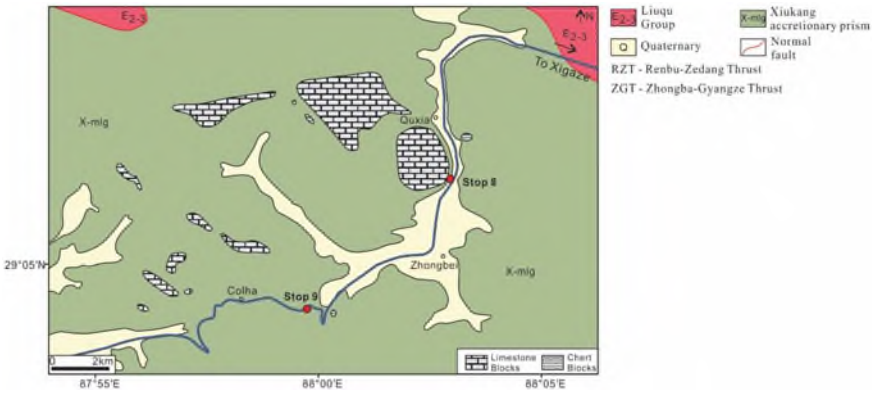

Fig. 24 Geological map of the Zhongbei area, Lhatse county (After An et al. 2017)

Fig. 25 Limestone blocks at Stop 9 (left: red bioclastic limestone intercalated with marls; right: bioclastic limestone). Photo by Wei An

a few kilometers in size, consist of thick-bedded or lenticular quartzarenite intercalated with thin-bedded gray siliceous mudstone. These blocks were derived from the Indian craton, deposited as Indian passive margin strata and incorporated into the accretionary prism during India-Asia collision (Fig. 28). Meanwhile, feldspatholitho-quartzose volcaniclastic sandstones are Late Cretaceous (Fig. 27d) or Paleogene (Fig. 27e, f) based on the youngest detrital zircon U–Pb ages and sourced from the Lhasa terrane (Fig. 28). The Late Cretaceous ones are rhythmically-interbedded with mudstone in m-size outcrops while the Paleogene ones are exposed sparsely along the G318. Therefore, these blocks were interpreted as deposited in trench/trench-slope basin accreted into the Xiukang Complex during Neo-tethyan subduction or syn-collisional basin and dismembered during the India-Asia collision (An et al. 2017). Also, a panoramic view of the Xiukang Complex will be observed at this stop (Fig. 26).

Fig. 26 Outcrops of Stop 8 (left: sandstone blocks; right: limestone blocks as ridges). Photo by Wei An

Stop 10 Upper Triassic Deep-Water Nieru Formation of the Northern Subzone of Tethyan Himalaya Near Lhatse County (GPS 29°00′15.8″N, 87°39′14.4″E)

The Nieru Formation consists slate and quartzo-sandstone with occasionally thin-bedded limestone and chert deposited in a deep marine environment on the Indian passive margin. The depositional age of Carnian-Norian is indicated by bivalve fossils (Yu and Zhen, 1979). Provenance studies indicate a continental block source from the Indian continent (Cai et al. 2016). In the Lhatse area, the Nieru Formation was intruded by Early Cretaceous bimodal suite of mafic and felsic rocks as part of the Tethyan Himalaya igneous province occurring across the whole Tethyan Himalaya (Chen et al. 2018). We will observe grey slate intruded by mafic dikes at this stop (Fig. 29), which display porphyritic textures with phenocrysts of olivine, augite and plagioclase, yielding a zircon age of 117–118 Ma (Chen et al. 2018).

Stop 11 The Cretaceous Nirang Section of Southern Tethys Himalaya Near Old Tingri (GPS: 28°39′56″N, 87°02′10.14″E)

At this stop we will observe the Cretaceous succession (Albian-Maastrichtian) at Nirang section in the Tingri area, which is ~40 km west of the city of Tingri and is located on the southern slope of the Zhepure mountain (Fig. 30).

In the Tingri area, the Cretaceous to Paleogene are mainly exposed in the Zhepure Mountain and form a syncline, which extends ~50 km from the New Tingri City in the east to the Old Tingri City in the west. Previous studies on the Cretaceous are mainly focused on the north flank of the syncline, e.g., Tingri section (Willems et al. 1996) and Gongzha section (Hao and Wan, 1985; Li et al. 2006; Hu et al. 2012). However, the strata before middle Cenomanian are not exposed in the north of Zhepure Mountain. Therefore, the Albian strata has not been identified in the Tingri area before. In last two years, we found a new section, namely Nirang section located in the south flank of the Zhepure Mountain, which contains Cretaceous of ~1,200 m thick (Fig. 31, Zhang et al. in review). The succession of the Upper Cretaceous in the upper half of the Nirang section is quite similar to the published

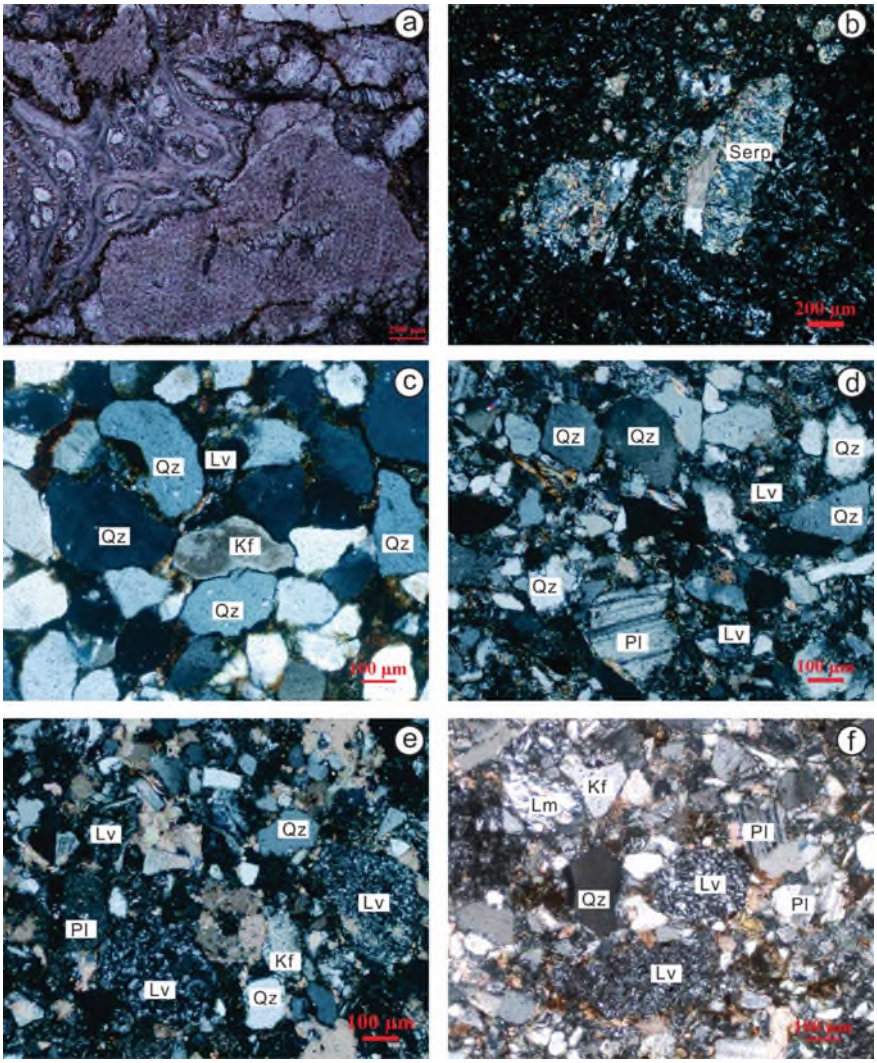

Fig. 27 Microphotographs from An et al. (2017): **a** bioclastic limestone with crinoids and bryozoans (limestone block at Stop 8); **b** serpentinized peridotite (near Stop 9); **c** Group 1 quartzarenite; **d** Group 2 volcaniclastic sandstone; **e** and **f** Group 3 volcaniclastic sandstone. (Qz = quartz; Kf = K-feldspar; Pl = plagioclase; Lm = metamorphic lithic fragments; Lv = volcanic lithic fragments)

Tingri and Gongzha sections. In this section, we can investigate the most complete succession of Albian-Campanian in the Tingri area: Albian fine siliciclastic rocks and marls with glauconitic sandstones in the top (Chaqiela Fm.), Cenomanian gray shales (Lengqingre Fm.), late Cenomanian to Santonian marls and marly limestone couplets (Gamba Cunkou Fm.), and limestones of Campanian to ?Maastrichtian

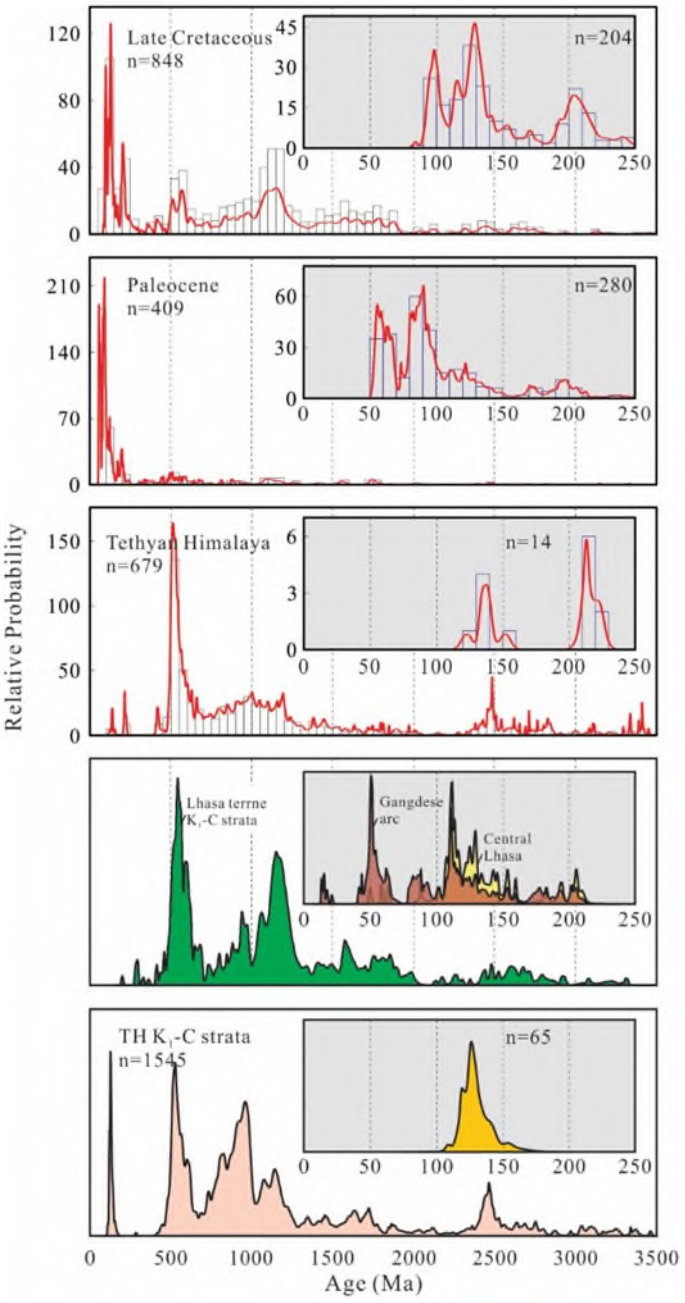

Fig. 28 U–Pb age spectra of detrital zircons in Group 1–3 sandstone blocks from the Cola pass, data from An et al. (2017) and Metcalf and Kapp (2019). Shown for comparison are data from Gangdese arc (Ji et al. 2009 and references therein), the Lhasa block (Leier et al. 2007a, b), Tethyan Himalaya successions (Zhu et al. 2011; Wu et al. 2014a, b)

Fig. 29 Outcrop of Stop 10 (left: slate with lens of limestone; right: diabase block within the Nieru Formation). Photo by Wei An

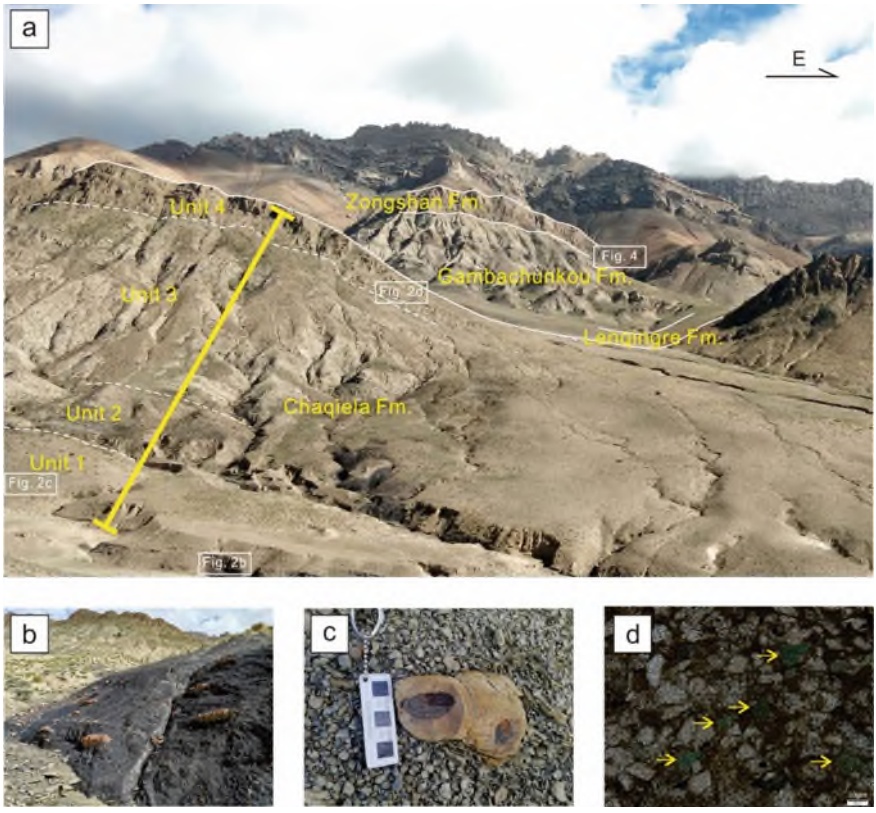

Fig. 30 Field photo of the Nirang section (**a**), underlying black shales of Gamba Dongshan Formation (**b**), seep carbonate concretions in the unit 1 of the Albian (**c**) and Glauconitic sandstone in thin section (**d**), glauconites are indicated by yellow arrows (Liu et al. in review)

(Zongshan Fm.) (Fig. 30, Liu et al. in review). Abundant trace fossils including *Zoophycos*, and other fossils e.g., shark teeth, can be found in the Albian glauconitic sandstones. Moreover, seep carbonate concretions were developed in the silts in the lower ~80 m of the section. Nannofossil biostratigraphy and chemostratigraphy studies have been submitted to international journals. Carbon isotope curve of Albian can be well correlated with the presentative sections in east Pacific, western Tethys and other areas. Furthermore, spectral analysis on the carbon isotope curve, magnetic susceptibility and TOC contents revealed that orbital-paced regional hydrological processes caused changes in terrigenous inputs and organic matter burial, which are responsible for periodically fluctuations of carbon isotope values (Liu et al. in review). Oceanic Anoxic Event 1b, 1c and 2 are identified in this section with biostratigraphy, lithostratigraphy and chemostratigraphy studies. OAE 1b and 1c is identified with the chemostratigrpahy (Liu et al. in review). Disconformity in the Late Cretaceous limestonesbetween Jiubao Fm. and Zhepure Shanpo Fm. in the north slope of the Zhepure Mountain were identified by the biostratigraphy and petrology observation (Fig. 31, Hu et al. 2012), which is inferred to be related to the uplift of Tethys Himalaya by Deccan hotspot (Li et al. 2019b, a). This disconformity is also found within the Zongshan Fm. of Nirang section. According to study of calcareous nannofossils, the spanning of this disconformity is less than 10 myr (Figs. 31 and 32.

Stop 12 Paleocene-Eocene Thermal Maximum (PETM) in Shallow-Water Carbonate Platform Environment in the Tethys Himalaya at Shenkezha Section in Old Tingri (GPS 28°26′39.1″N, 86°40′22.5″).

At this stop, we will observe the Paleocene-Eocene boundary section in shallow-water carbonate platform environment. The PE boundary here was located in the upper part of Zongpu Formation. The Zongpu Formation can be subdivided into four members, from bottom to top: Member 1 are dominated by thin- to medium-bedded yellowish-grey limestones and marly limestones with green algae and foraminifera; Member 2 to 3 is a dark grey nodular limestone with marly interbeds, the marly is increasing up-section; Member 4 is comprised by grey massive and thick-bedded limestones. The PE boundary interval was located in the boundary between member 3 and member 4, it is dominated by 18 m-thick nodular limestone and marly nodular limestone in the lower to middle part, and 6 m -thick massive limestone in the upper part (Fig. 33).

Detailed sedimentological, paleontological, and geochemical analysis indicates that a relative rise in sea level coincided with PETM onset, continued through PETM core, and terminated with a regression at PETM recovery (Fig. 34). At PETM onset, corresponding to the SBZ4/SBZ5 boundary, no obvious impact on biota and specifically on larger benthic foraminifera (LBF) is observed. The major biotic change occurs later on at PETM recovery, corresponding to the SBZ5/SBZ6 boundary. Our data suggest that relative sea level, rather than temperature, exerted the main control on benthic biota during the PETM. The $\delta^{13}C_{carb}$ value of bulk carbonates are significantly ^{13}C-depleted, which we attribute to environmental change driven by relative sea-level fluctuations.

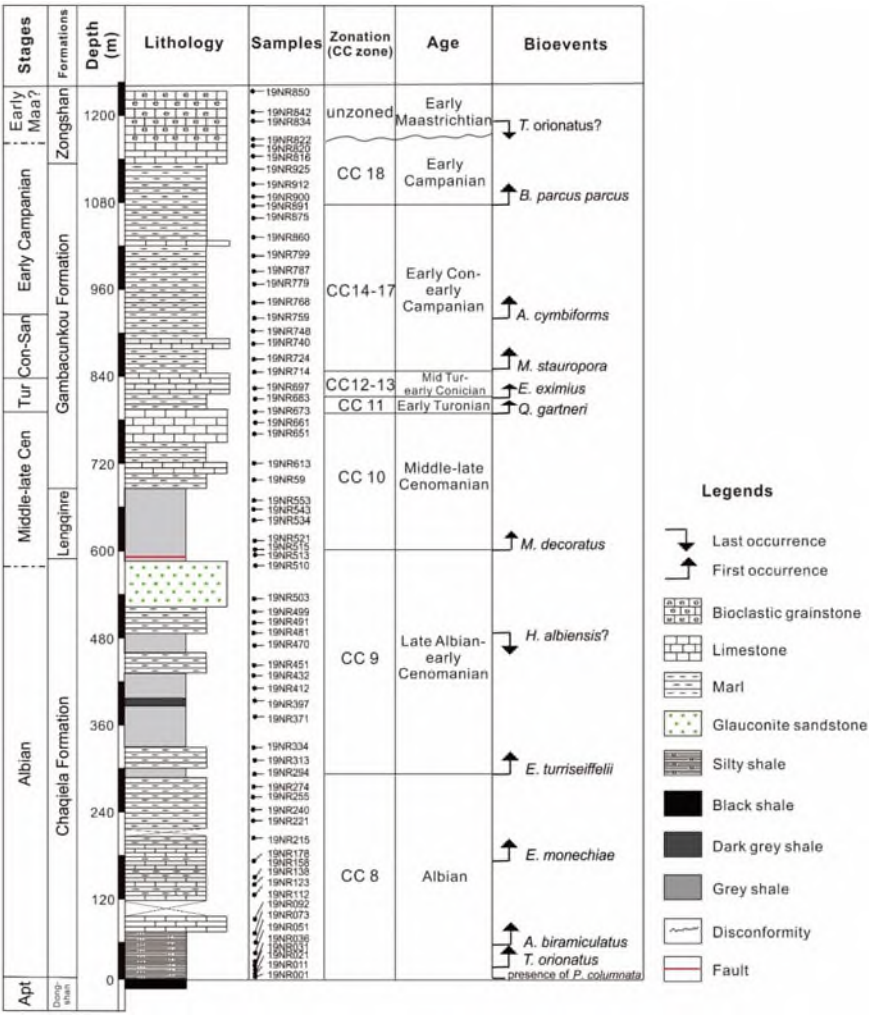

Fig. 31 Calcareous nannofossils biostratigraphy of the Nirang section (Zhang et al. in review)

Stop 13 Early Cenozoic Succession and Latest Marine Horizon in the Tethys Himalaya at Longjiang Section Near Old Tingri (GPS 28°26′39.1″N, 86°40′22.5″)

The Paleogene Zongpu, Enba and Zago formations are well exposed in the Longjiang section, about 5 km on the eastern side of the Old Tingri to Rungbulk monastery. At this location, the Upper Cretaceous gray marl (Gambacunkou Formation) transitions upward into sandy marl and marl with unequal thickness, and then upward into a marl layer (Zhepureshanpo Formation). The Palaeogene foraminifer-rich Zongpu Formation is sitting on top of the Zhepureshanpo Formation with fault contact which

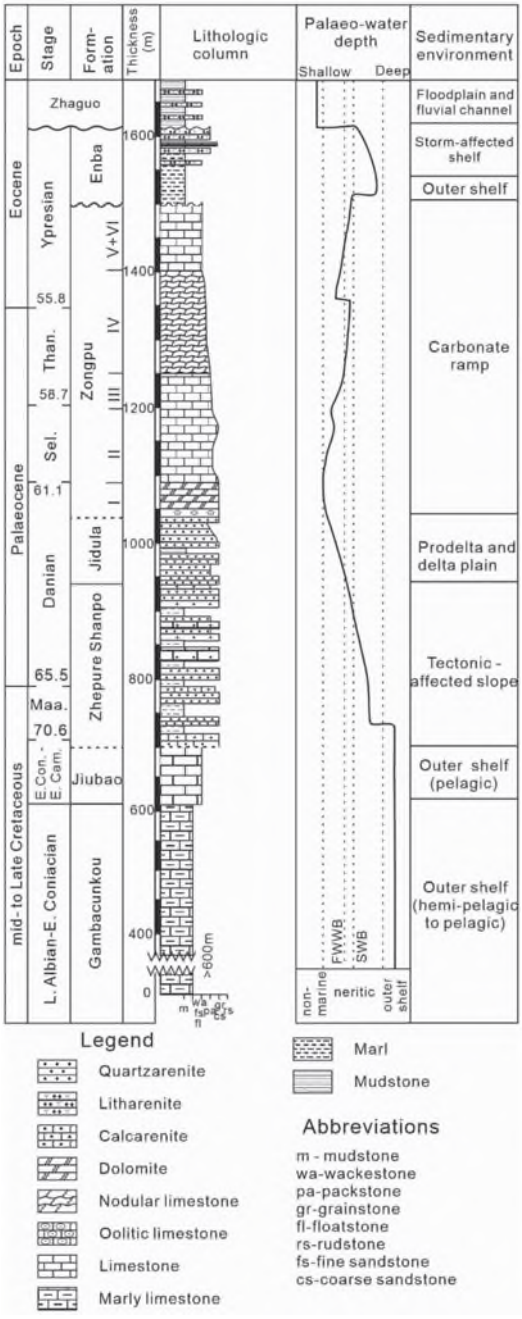

Fig. 32 Composite stratigraphic log of the Cretaceous—Palaeogene strata at the Zhepure Mountain area showing interpreted palaeo-water depth trend and sedimentary environments (Hu et al. 2012 and references there in). FWWB–fare weather wave base; SWB–storm wave base

Fig. 33 Outcrop photographs of PE boundary interval in the Shenkezha section (**a**) showing: (**b**) Member3 nodular limestone in the lower and middle part; and, (**c**) Member4 thick-bedded to massive limestone in the upper part (Li et al. 2020a, b)

is thrusted from north to south dipping to the north. The uppermost of the Zongpu Formation and the overlying Enba and Zhaguo formations are nicely exposed in the Longjiang section representing the latest marine deposits in the Himalayan area (Fig. 35) (Wang et al. 2002; Hu et al. 2012).

Larger benthic foraminifers were distributed in the limestones of the Zongpu Formation indicating Eocene SBZ7-SBZ12 (Fig. 36). The PETM record in shallow-marine carbonates of the Zongpu Formation (Li et al. 2021) reported in the Zhepure Mountain is not outcropped due to the thrusting. There is an erosional interface on the top of the Zongpu Formation, which is in parallel or slightly angular unconformity with the overlying Enba Formation. The main body of the Enba Formation is dark gray calcareous shale sandwiched by thin lithic sandstone, with a visible thickness greater than 40 m. The Enba Formation is in sedimentary contact with the Zhaguo Formation. The main body of the Zhaguo Formation is purple-red shale with a few

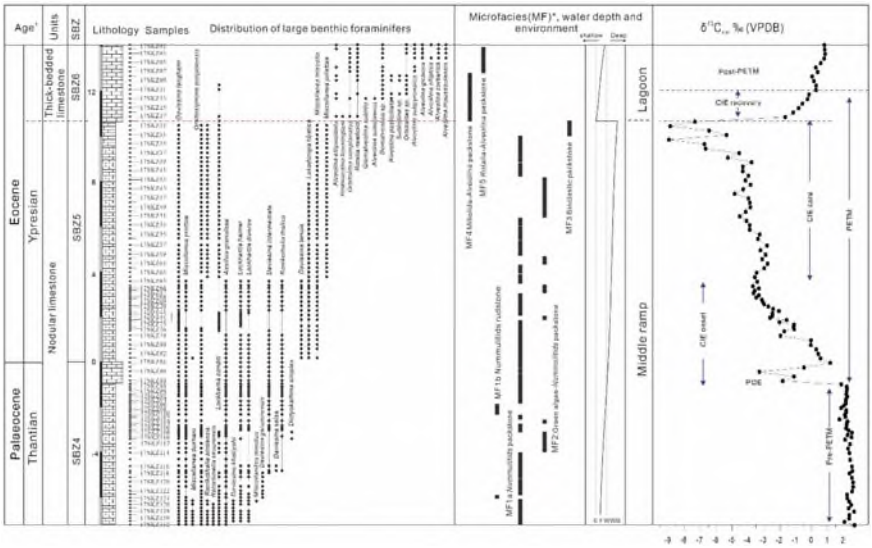

Fig. 34 Lithological log of the Shenkezha section (Tibet) showing the distribution of large benthic foraminifera, carbonate microfacies, interpreted paleowater depths, sedimentary environments and carbon-isotopes across PETM (Li et al. 2020a, b)

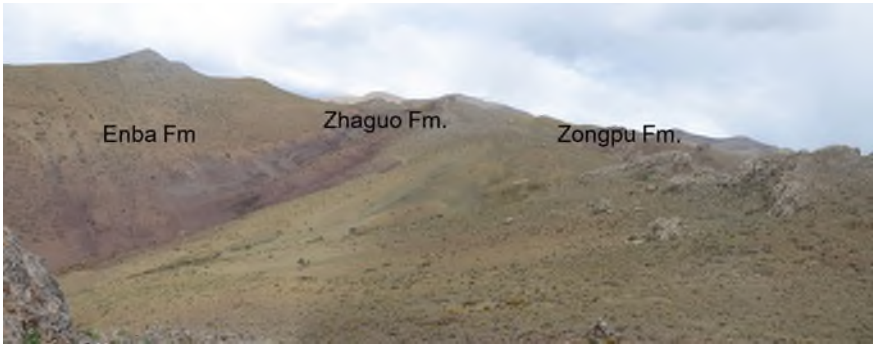

Fig. 35 Panoramic photo of the Longjiang section (southeast of the camera, photo by Xiumian Hu)

sandstone layers. Green nodular conglomerate is seen in the red sandstone, all of which are carbonate nodules, formed by the redeposition of palaeosoil nodules.

Provenance analysis from the sandstones in the Enba and Zhaguo formations including detrital modal, detrital zircon U–Pb age dating and Hf isotopes indicated that the sedimentary rocks of both the Enba and Zhaguo formations have similar provenance, with the main sources being rocks of the Lhasa terrane (Fig. 37). The Enba Formation records the first appearance of detritus from the Asian margin (Wang

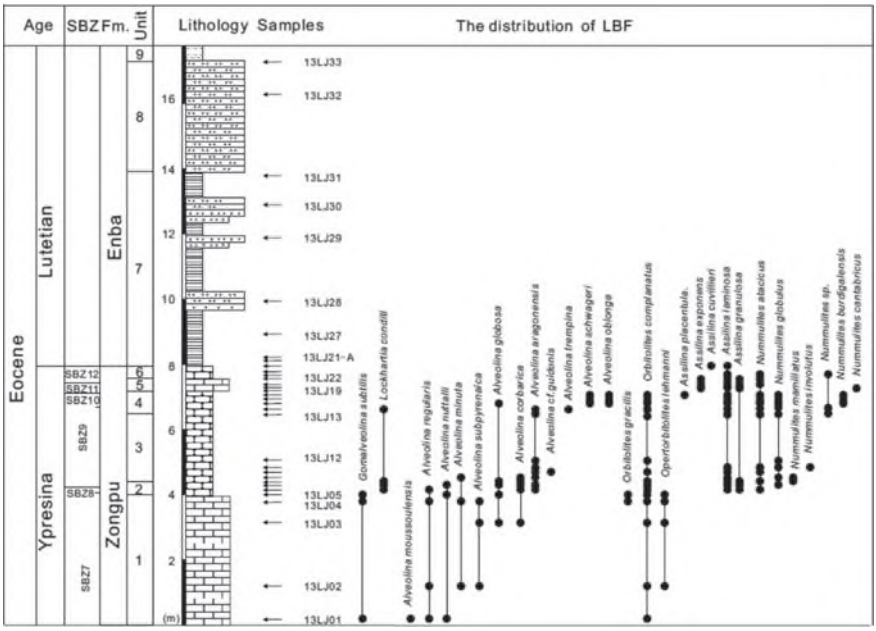

Fig. 36 The larger benthic foraminiferal distribution in the Longjiang section. Foraminiferal identification by Prof. Dr. Marcelle BouDagher-Fadel from University College London

et al. 2002; Zhu et al. 2005; Najman et al. 2010; Hu et al. 2012) in the southern Tethyan Himalaya in shallow-water environment in the northern Indian margin.

Stop 14 Lower Cretaceous Clastic Dykes and Cold Seep Carbonates Near Gucuo Village (GPS: 28°44′58″N, 86°18′38″E)

We will investigate field characteristics of Lower Cretaceous clastic dykes and cold seep carbonates in the southern Tethys Himalaya. This outcrop is located approximately 30 km northwest of Old Tingri and approximately 5 km south of the village of Gucuo. The clastic dykes and cold seep carbonates are logged at two sections positioned next to each other: Gucuo East (GPS: 28°44′36″N, 86°18′39″E) and Gucuo II (GPS: 28°44′58″N, 86°18′38″E) (Fig. 38). These two sections, which have a total thickness of approximately 480 m, correspond to Gucuo Formation and Gamba Dongshan Formation. Both sections consist largely of dark grey shales intercalated with volcaniclastic (Chen et al. 2017; Guo et al. 2021).

Clastic dykes composed of lithic-rich volcaniclastic sandstone are widely exposed in the lower Aptian shales. Most clastic dykes are subvertical. The length and width of clastic dykes range from 5 to 50 m and from 20 to 150 cm, respectively. The dykes exhibit sharp and undeformed contacts with the surrounding shales. The majority of the dykes display a sheet-like geometry and generally they do not thicken or thin significantly. Many dykes are distributed along a series of normal faults, and some display cross-cutting and drag relationships with each other (Fig. 39). The U–Pb age

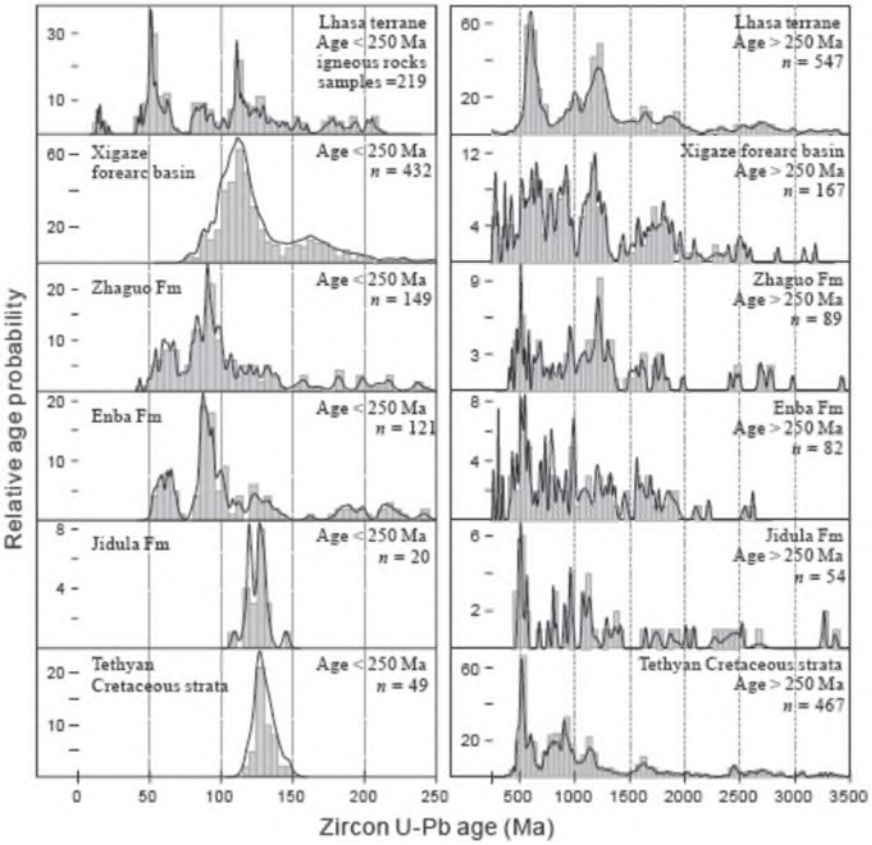

Fig. 37 Relative probability plots of analysed U–Pb data in Enba and Zhaguo formations (Hu et al. 2012)

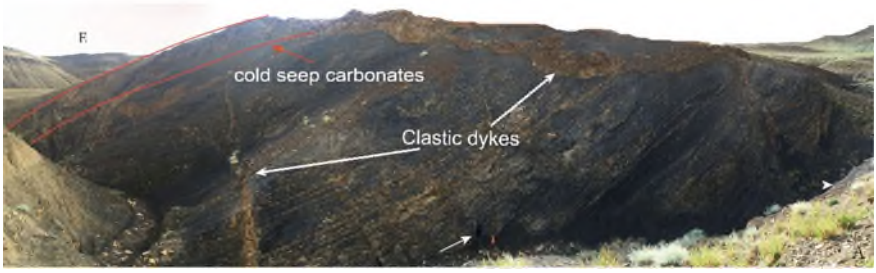

Fig. 38 Outcrop of Gucuo II section showing clastic dykes and cold seep carbonates (Chen et al. 2017)

spectra of zircon grains contained in clastic dykes display a youngest peak at 124.3 ± 2 Ma. Petrographic analyses show that the dykes were derived from underlying strata. The liquefaction of underlying strata was induced by earthquakes associated with the extensive magmatic activities and regional extension that affected the Indian passive margin of Neotethys during the Early Cretaceous (Guo et al. 2021).

A suite of carbonate nodules with a thickness of about 1.38 m developed under the oceanic anoxic events OAE1a of the Gucuocun Formation. The carbonate nodule layer can be subdivided into three layers: the lower layer is small pipe-shaped nodules

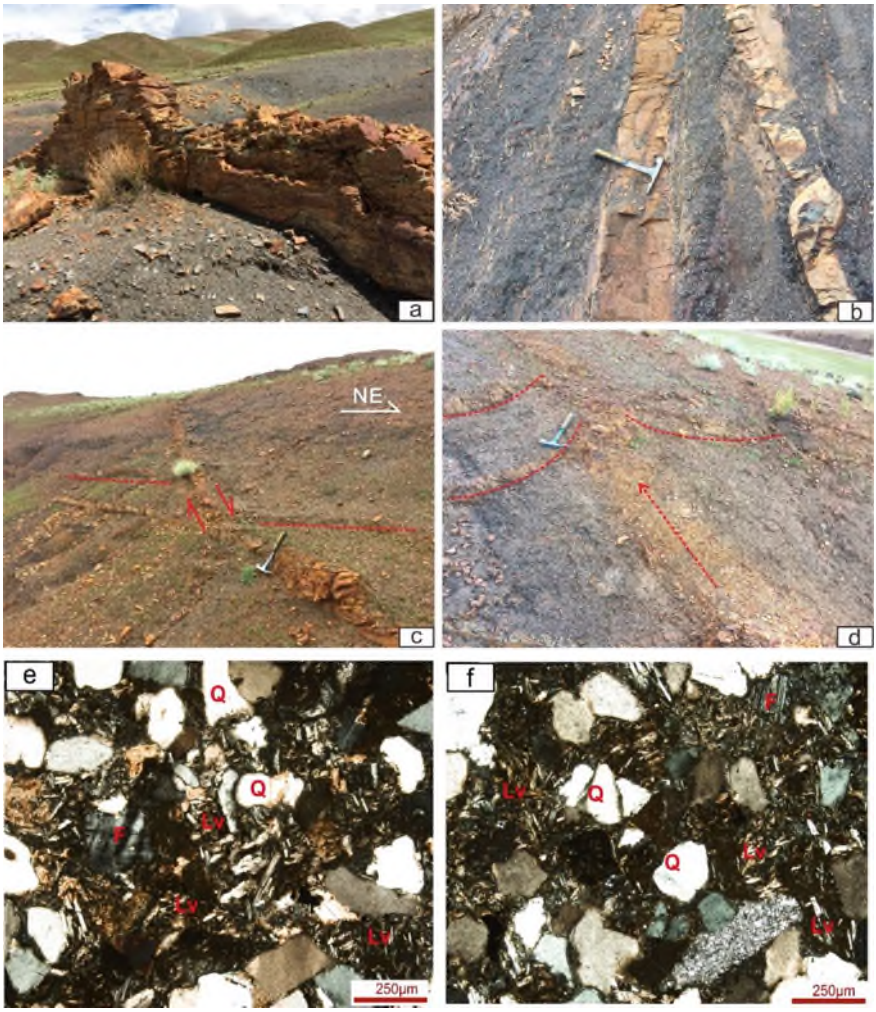

Fig. 39 Clastic dykes in outcrops and photomicrographs. (**a**, **b**) sharp undeformed contacts; (**c**) dykes distributed along normal faults; (**d**) drag relationship between clastic dykes; (**e**–**f**) sandstones within underlying volcaniclastic sandstones clastic dykes (Guo et al. 2021)

with a length-to-width ratio of 2.4 cm/1.8 cm, which are produced in parallel or obliquely across the layers. and the middle layer is composed of ellipsoidal and plate-shaped nodules. The length-to-width ratio of nodules is 17 cm/11.5 cm. The upper layer is breccia, and the breccia is composed of limestone. It is a sandy composition, and the nodules are mainly composed of authigenic carbonate minerals and detrital materials, with the development of banded and botryoidal cements (bbc), framboidal pyrite and other common sedimentary fabrics of modern cold spring carbonate rocks (Fig. 40, Fan, 2021)). The nodules contain trace fossils, foraminifera, cephalopods, bivalves and other biological fossils. The $\delta^{13}C$ value of carbonate rocks is −23.26–−7.14‰ (Fan, 2021). Sulfur isotope values of carbonate associated sulfates are 17.3–19.0‰ (Chen unpublished data). The morphological, mineralogical and geochemical analysis of the carbonate nodules all show that the nodules are cold seep carbonate rocks, indicating the occurrence of cold spring leakage under the sediment–water interface. The underlying clastic dykes provide a channel for upward seepage.

Stop 15 Kung Cuo Half Graben in Tingri (a Far View from the Location of GPS: 28°46′11.3″N, 86°20′53.1″E)

The formation of the Cenozoic N-S striking rifts in the Tibetan Plateau is the consequence of continuous contraction after the India-Asia collision. Its formation and evolution are of great significance for understanding the growth of the Tibetan Plateau. The main extension period of the N-S striking rifts in the Himalaya-Tibet Plateau is Miocene. Garzione et al. (2003) did a comprehensive study on the sediments in the Thakkhola graben, central Nepal and showed east–west extension and environmental change at that time in southern Tibet.

The Kung Co half graben is bounded by an active N–S normal fault with a minimum vertical offset of 1600 m. Mahéo et al. (2007) estimated the onset of normal faulting by combining high and medium temperature (U–Pb, Ar/Ar) and low temperature ((U–Th)/He) thermochronometry of the Kung Co pluton, a two-mica granite of the northern Himalayan granitic belt that outcrop in the footwall of the fault. Biotite and muscovite Ar/Ar ages, are close from each other [∼16 ± 0. Ma 2 (Ms) and ∼15 ± 0.4 Ma (Bt)], which is typical of fast cooling. The zircon and apatite (U–Th)/He ages range from 11.3 to 9.6 Ma and 9.9 to 3.7 Ma respectively. These He ages are indicative of (1) fast initial cooling, from 11.3 to ∼9 Ma, gradually decreasing with time and (2) a high geothermal gradient (∼400 °C/km), close to the surface at ∼10 Ma. The Kung Co pluton was emplaced at about 22 Ma (U–Pb on zircon) at less than 10 km depth and 520–545 °C. Subsequent to its shallow emplacement, the pluton underwent fast thermal re-equilibration ending around 7.5 Ma, followed by a period of slow cooling caused either by the end of the thermal re-equilibration or by very slow exhumation (0.02–0.03 mm/yr) from ∼7.5 Ma to at least 4 Ma. In either case the data suggest that the exhumation rate increased after 4 Ma, in which this increase was interpreted to be related to the initiation of the Kung Co normal fault.

Looking northward into the distance from Kung Co village, we have a view of Quaternary landforms and distribution features of recently active normal faults (Fig. 41). A series of triangular facets truncate the ridges between U-shaped glacial valleys. The lower part of each facet is hard and composed of shattered granite

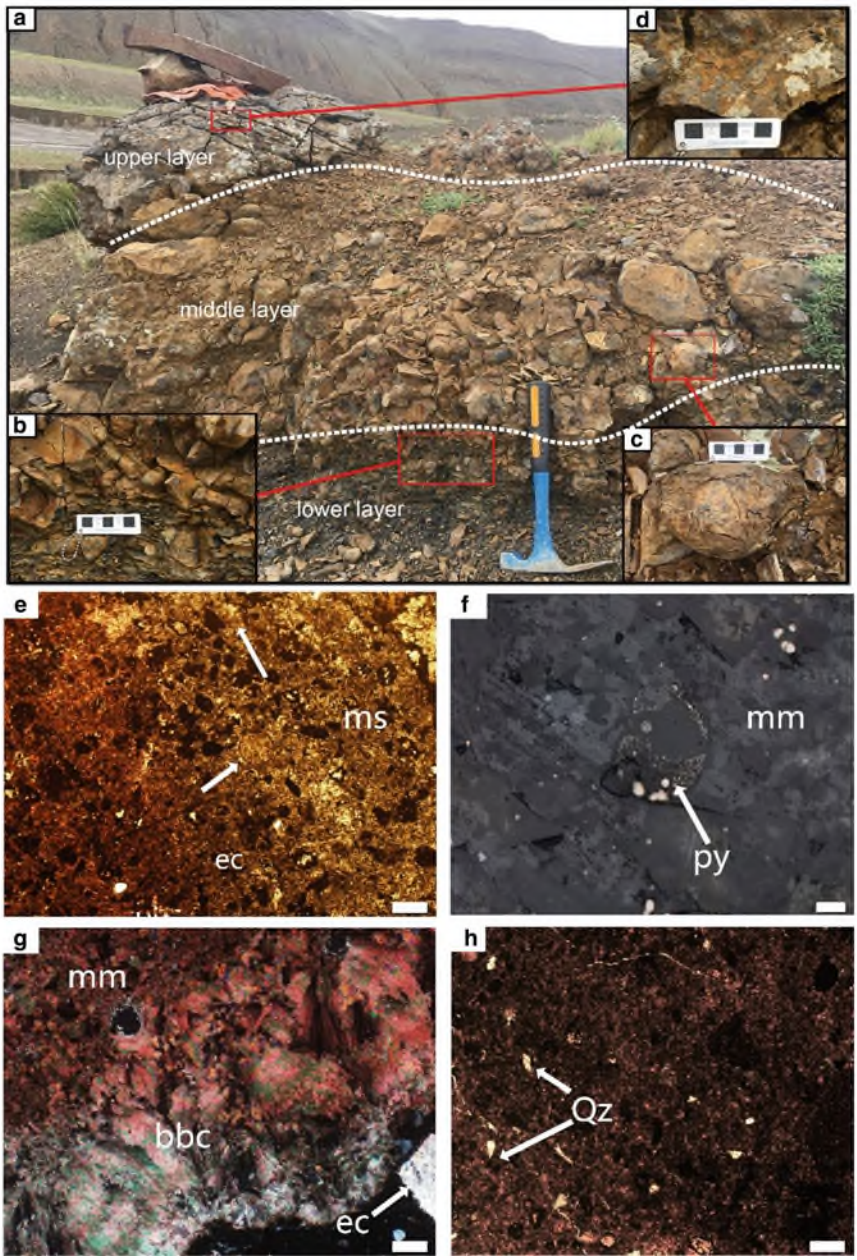

Fig. 40 Field photographs and photomicrographs of the cold seep carbonate (Fan, 2021). **a** the morphology of nodules in section (**b**) pipe-shaped nodules in the lower layer (**c**) ellipsoidal and plate-shaped nodules in the middle layer (**d**) breccia in the upper layer (**e**–**h**) thin section micrographs of representative authigenic carbonates. py: pyrite; mm: carbonate with matrix micrite; bbc: banded and botryoidal calcite; ec: equant calcite; ms: microspar

containing striations. The glacial valleys are "hanging" and horizontal breaks in slope are clearly displayed across the range front. Total vertical displacement on the major normal fault is larger than the relief of the bedrock landform which is more than 800 m.

Stop 16 Triassic-Jurassic Boundary Sedimentation at Gemig Section (GPS: 28°42.179′N, 86°08.623′E)

The Gemig section (Fig. 42) in the Nyalam area is located at the 5259 milestone of the Tingri–Nyalam Highway, about 2 km south of the small village of Gemig. The section provides a continuous exposure of ammonoid-bearing, uppermost Triassic and basal Jurassic strata. In total 11 lithological units have been recognized in this section which is composed of the Menkadun formation (unit 0), Zhamure formation (unit 1) and the Germig formation (units 2–10) and the overlying quartz-sandstone series (Fig. 43) (Yin et al. 1999).

The T-J boundary falls within the the Germig formation, which consists of alternations of fine calcareous sandstones and subordinate siltstones. In thin section the sandstones are seen to be well sorted, calcite-cemented quartz arenites. The highest bed contains abundant grains of glauconite. In the T-J boundary beds pyrite aggregates become locally highly abundant. This is stratigraphically close to the earliest recorded *Psiloceras* (Hallam et al. 2000).

Stop 17 Lower Jurassic Carbonate Succession and Outcrop of the Toarcian Oceanic Anoxic Event at Nianduo Section (GPS: 28°40′52″N, 86°08′7″E)

The Nianduo section is located near Nianduo village between the 5263 and 5264 km milepost on the Tingri–Nyalam Highway in the Nyalam County. This section preserves the shallow-water carbonate deposits on the so-called Kioto Platform which extensively developed during the Pliensbachian to Toarcian interval in the southern zone of the Tethys Himalaya. The lithostratigraphic unit has been traditionally subdivided into the Pupuga and Nieniexiongla Formations from the bottom to top and well studied in the Nianduo (Nyalam County) and the Wölong (Tingri County) sections (Jadoul et al. 1998; Han et al. 2016, 2021a, 2021b, 2022). The Pupuga Formation represents shallow-water carbonate platform, dominated by bioclastic grainstones/packstones and yielding *Lithiotis* bivalves. The overlying Nieniexiongla Formation represents a deeper water carbonate ramp and is mainly composed of micrites alternating with coarser grained storm-generated layers. The larger benthic foraminifera, the occurrence of *Lithiotis* bivalves and carbon-isotope chemostratigraphy date the Pupuga Formation as the Pliensbachian to lowest Toarcian (Jadoul et al. 1998; Han et al. 2016, 2021a, b; Jiang et al. 2020). The T-OAE records has been placed at the Pupuga–Nieniexiongla transitional interval, characterized by the occurrence of the characteristic negative CIE, significant sea-level rise, carbonate-platform crisis, and abundant storm-generated layers (Han et al. 2016, 2021a, b).

In the field, the Pupuga Formation is dominated by thick- and medium-bedded, offwhite grainstones (Fig. 44a–g), whereas the Nieniexiongla Formation is characterized by thin-bedded, dark grey micrites (Fig. 44a, d, i, j) (Han et al. 2016).

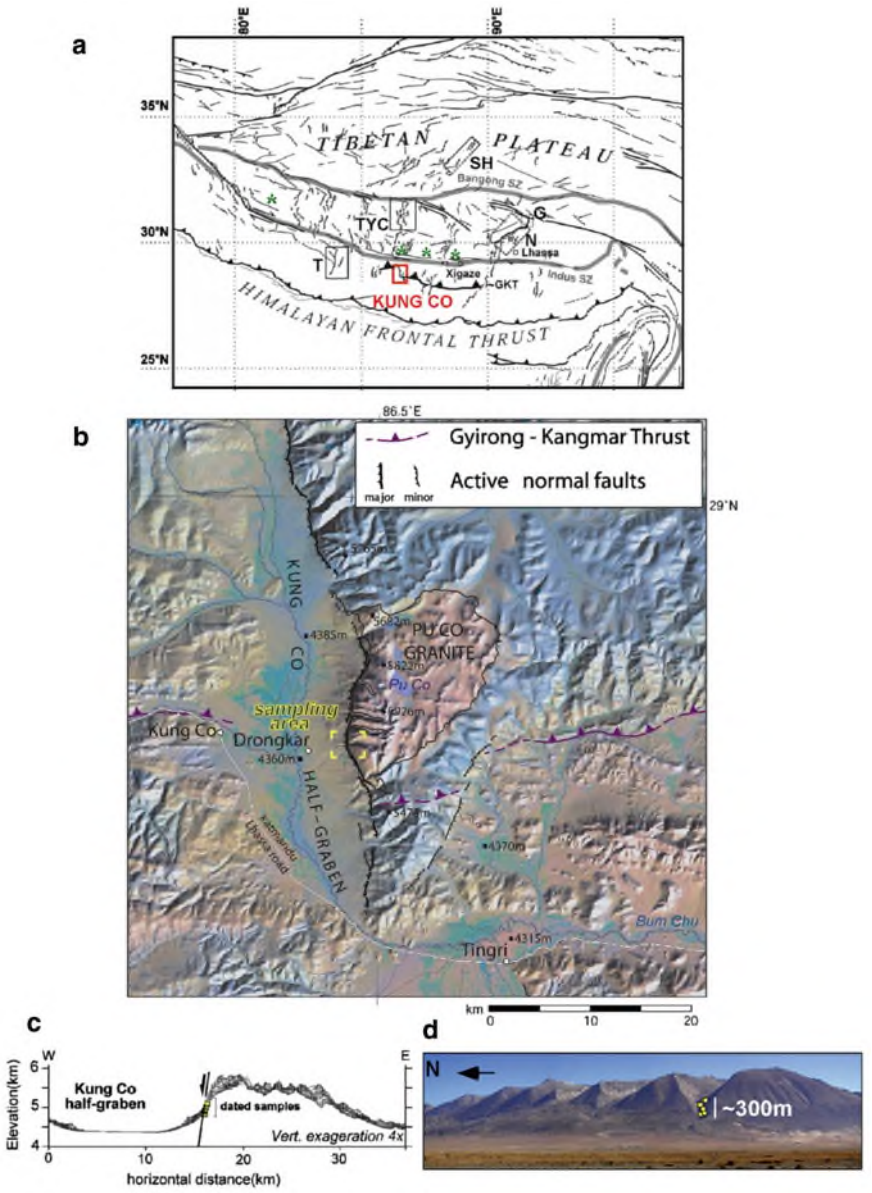

Fig. 41 Structural setting of the Kung Co half graben and sample location (Mahéo et al. 2007). **a** Main active faults (black) and suture zones (grey) of the India–Asia collision zone. Green *: N–S trending andesitic dykes. G: Gulu rift, N: Nyainqentangla graben, T: Thakkhola graben, TYC: Tangra Yum Co rift, SH: Shuang Hu graben, y: Yangbajing. **b** Landsat satellite image and Digital Elevation Model (SRTM data) of Kung Co area and main tectonic features (Giyrong–Kangmar Thrust location). **c** E–W topographic profiles across Kung Co half graben and normal fault (SRTM data) and sampling locations. **d** Photograph of Kung Co normal fault and sampling location. View towards the east from valley floor

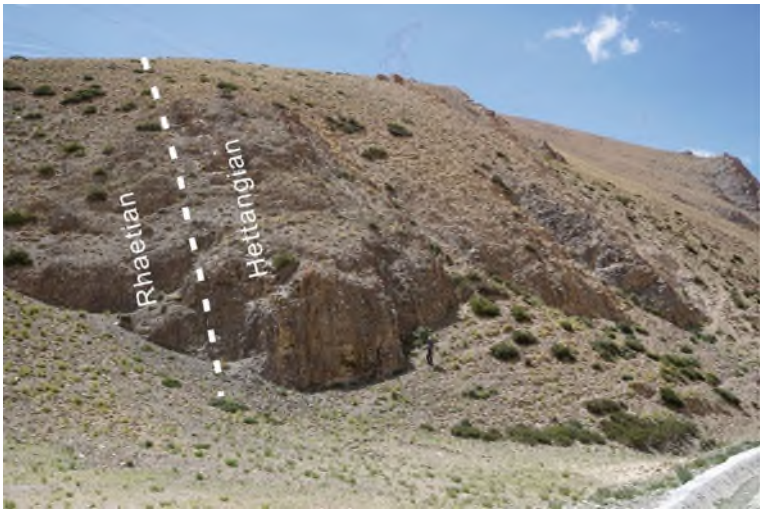

Fig. 42 Field photo of the Gemig section. Photo by Zhong Han

The formation boundary is obvious and shown in Fig. 2a. Based on the biostratigraphy, the negative excursion of ~–2.5‰ recorded in organic matter (–2.6 to 28.4 m) was confirmed to be the T-OAE CIE (Fig. 45). The microfacies analysis show that the platform-top grainstones deposited under high-energy conditions of the Pupuga Formation are abruptly overlain by middle/outer ramp micrites reflecting low-energy conditions of the Nieniexiongla Formation during the onset of the T-OAE CIE (Fig. 3; Han et al. 2016). This change also records the early Toarcian global sea-level rise, as envisaged in other sites (Hallam, 1981; Hesselbo and Jenkyns 1998; Han et al. 2016). The Kioto Carbonate Platform suffered the carbonate productivity crisis, which is directly illustrated by biotic extinction and obvious reduction of carbonate content. Based on the data recently obtained from the Kioto Platform, the foraminiferal diversity severely decreased and the *Lithiotis* bivalves, prominent framework builders in reef systems at that time, disappeared during the negative phase of the T-OAE CIE (Fig. 45; Han et al. 2021a, b; Jiang et al. 2020).

Notably, abundant storm-generated coarse-grained interlayers, including carbonate, e.g. ooid (Fig. 45i), peloid (Fig. 45f, h) and clastic grains (Fig. 45g), occurred in the micrites formed in the bottom Nieniexiongla Formation, corresponding to the negative phase of the T-OAE CIE (Han et al. 2016). The associated sedimentary structures are dominated by hummocky and swaley cross-stratification (HCS and SCS; Fig. 45a), U/V-shaped gutter casts (Fig. 45b), parallel laminations (Fig. 45c), climbing ripples (Fig. 45d), current ripple (Fig. 45e), graded bedding (Fig. 45c) and sharp erosive bases (Fig. 45f) in field and microfacies.

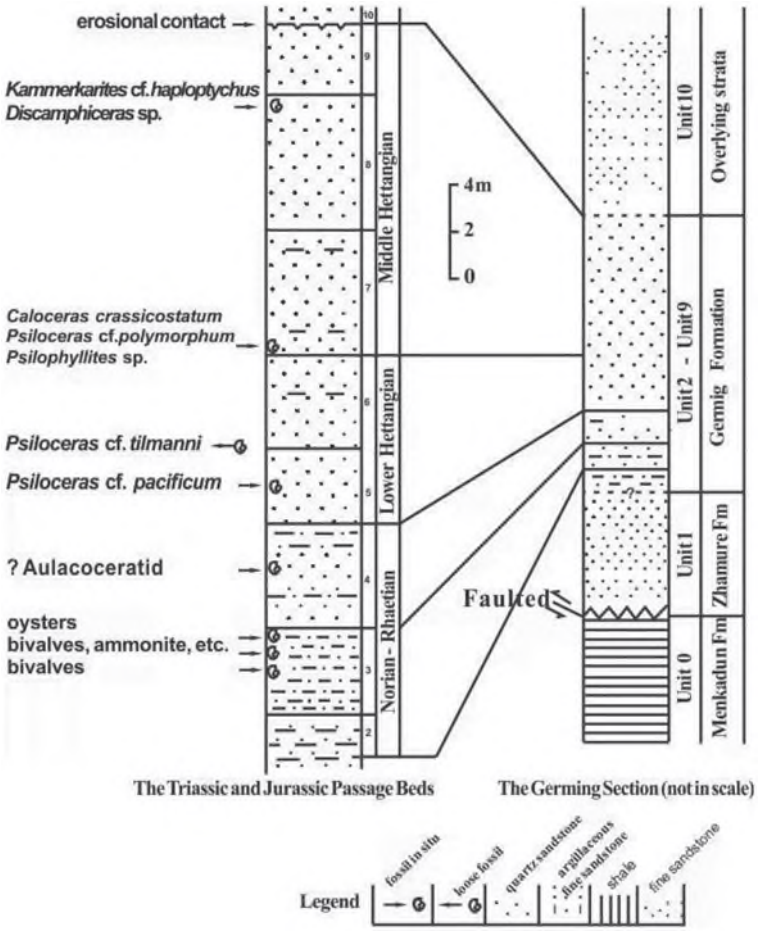

Fig. 43 The Triassic and Jurassic boundary passage beds in the Germig section (Yin et al. 1999)

Stop 18 Middle Jurassic Iron Oolites and Late Jurassic Spiti Shales at Kongcuo Section (GPS: 28°29′56″N, 87°06′32″E)

The Kongcuo section is in a valley of the Menbu area, near the Nylam county in the south subzone of the Tethyan Himalaya (Fig. 46). At this section, the Bajocian-Callovian Ferruginous Oolite Formation (FOF) (Dingjie Fm.) (Yin, 2010) and Callovian black shales (member 1 of Menkadun Fm.) are well exposed. The member 1 of the Menkadun Fm. is equivalent to "Spiti Shale", which is described across the Tethyan Himalaya from west to east: Zanskar, Lahaul, western Spiti (Losar area),

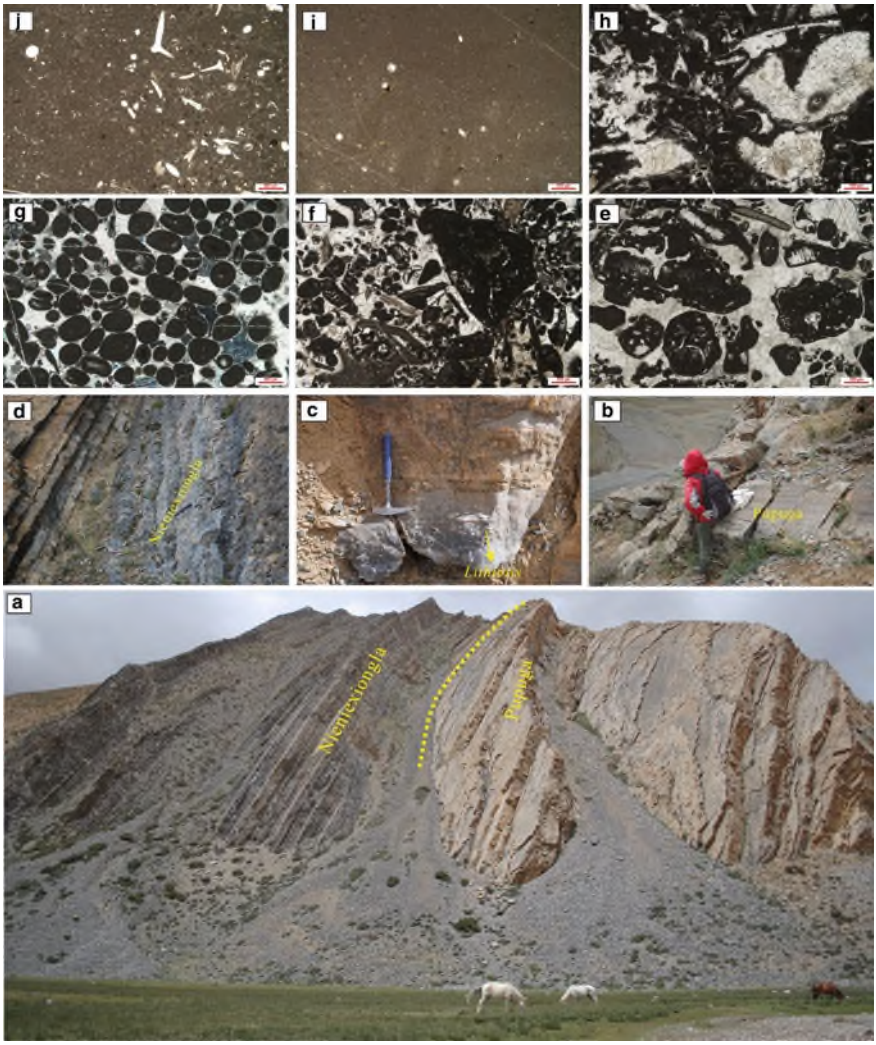

Fig. 44 Field (**a**–**d**) and carbonate microfacies (**b**–**j**) photographs of the Nianduo section. The Pupuga Formation is dominated by thick- and medium grainstone/packstone (**a**–**c** and **e**–**h**) with *Lithiotis* bivalve (**c**). The Nieniexiongla mainly consists of thin-bedded micrites (**a**, **d**, **i** and **j**) intercalated with abundant storm-generated coarse-grained beds (Fig. 38). **e**: Lump grainstone; **f**: Bioclastic grainstone; **g**: Ooid grainstone; **h**: Bioclastic packstone; **i**: Micrite; **j**: Spiculitic micrite. Figure 4b, d are from Han et al. (2022) and others from Zhong Han

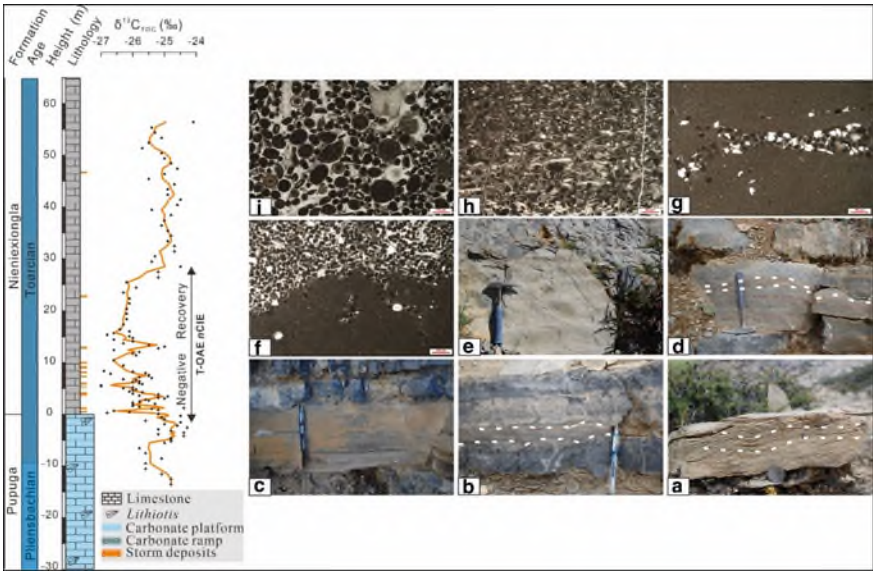

Fig. 45 Photographs of storm-generated deposits and associated sedimentary structures in the field and microfacies. **a** Storm beds with HCS/SCS; **b** V-shaped gutter casts filled with mixed coarse carbonate and terrestrial grains showing HCS/SCS; **c** Storm beds with parallel lamination; **d** Sandy beds within micrite. **e** Current ripple marks; **g** Micrites with an intercalated lamina enriched in siliciclastic minerals; **h** Intraclastic bioclastic packstone with graded bedding; **i** Ooid grainstone within the micrites. Figure 4a–e, h are from Han et al. (2016) and others from Zhong Han

central Spiti (Pin Valley), Dolpo, Thakkhola, Manang, and south Tibet (Everest-Shishapangma area) (Sciunnach and Garzanti, 2012). The Kongcuo section starts at the middle of the Lalongla Fm. and ends in the black shales of the Menkadun Fm. (Fig. 46a). The measured succession is ~55 m thick (Fig. 47). From 0 to ~27 m, the sediments consist mainly of marl and marly limestone couplets with a few medium bedded bioclastic limestones in the top, which belongs to the Lanongla Fm. The contact between FOF and the Lalongla Fm. is an erosive base (Fig. 46b). FOF spans from ~27 m to 32 m (Fig. 47). The ooidal ironstone of FOF macroscopically shows reddish to yellow, some parts are disseminated by Fe through weathering, and thus it was described as "Fe-cap" in previous studies (Fig. 46a). The FOF can be divided into two lithology units based on the content of bioclasts. Unit A is from the bottom to 1.4 m of FOF. It is composed of medium bedded ironstones with abundant fossils including corals, bivalves, foraminifera and echinoderms (Fig. 46b). At ~1 m of the FOF, abundant belemnites arranged parallel to the bedding surface were found (Fig. 46c). An ammonite rich layer was found at ~1.3 m from the base of FOF (Fig. 46d). Unit B, from 1.4 m to the top of the FOF, is characterized by ooidal ironstones, which consist of a large amount of ferruginous ooids and fine quartz grains cemented by brown ferruginous minerals. Only few fossils can be observed in this unit. The ferruginous ooids are green colored. However, the color of cements is dark

brown resulting in the brown color of the weathered surface. The deposit of ooidal ironstone was coincided with the onset of a global transgression. Upwards, FOF is overlain by dark shales of the Menkadun Fm. (Han et al. under review), where abundant well-preserved ammonites can be found.

Stop 19 Permian–Triassic Boundary Sedimentation at Selong Xishan Section, Nyalam County (GPS: 28°40′15″N 85°49′36″E)

The Selong Xishan section (Fig. 48a) is located ~1 km northwest of Selong village by the road from Nyalam to Gyirong, with an altitude of ~4500 m. In the Selong area, the uppermost Selong Group was subdivided into two parts: the lower is dominated by bioclastic rudstone intercalated with dark grey silty shale and the upper mainly consist of massive crinoid grainstone (Fig. 48B-E; Shen et al. 2000; An et al.

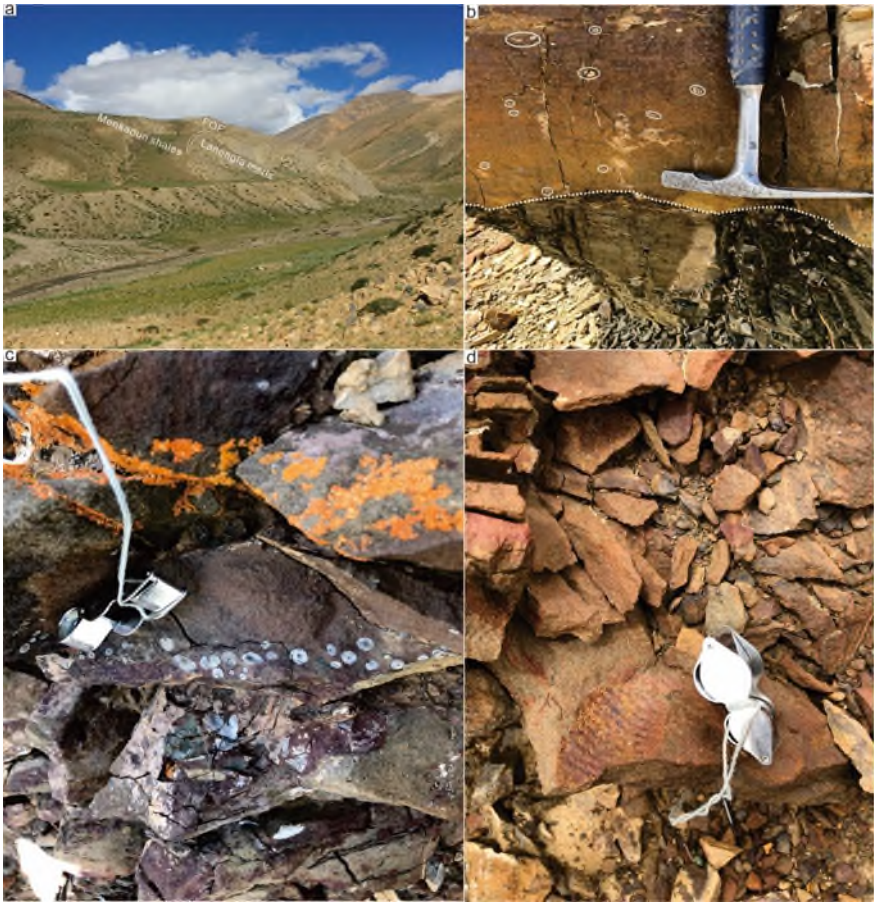

Fig. 46 **a** Photo of the Kongcuo section. **b** The erosive base between FOF and the Lalongla Fm., fossils are marked by white circles. **c** Abundant belemnites arranged parallel to the bedding surface. **d** The ammonite rich layer (Han et al. under review)

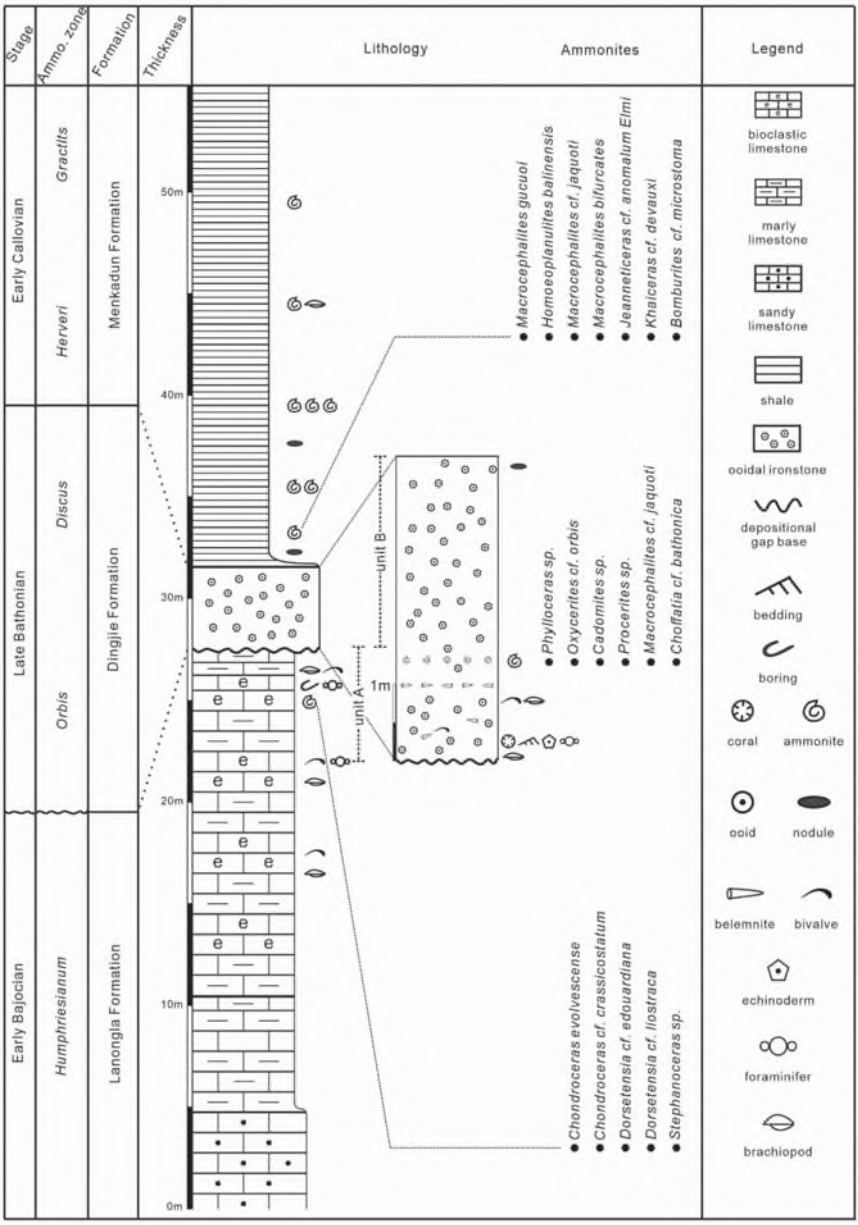

Fig. 47 Lithologic log of the Kongcuo section (Han et al. under review)

2018a, b; Li et al. 2019a, b). The brachiopod and conodont biostratigraphy suggest a Wuchiapingian of the lower part and latest Changhsingian age of the upper part, respectively, and therefore a Lopingian age for the uppermost Selong Group (Shen et al. 2000; Orchard et al. 1994; Wang et al. 2017a, b; Yuan et al. 2018). The overlying Kangshare Formation is in conformable contact with the uppermost Selong Group (Fig. 48a), and characterized by thin-bedded bioclastic packstone/wackestone (Shen et al. 2000; An et al. 2018a, b). The conodont and ammonite biostratigraphy indicate an Induan age for this unit (Shen et al. 2006; An et al. 2018a, b).

For the PTB, the demise of low-latitude carbonate platforms widely occurred where the reef-building corals and symbiotic calcareous algae and fusulinid completely lost during this biotic crisis (Stanley and Yang, 1994; Wang and Sugiyama, 2000). Notably, the Selong Xishan section is absent of large mounds/reefs but yields carbonate producers of metazoan community including bryozoans, echinoderms and brachiopods during the Late Permian, which suggest a cool-water carbonate factory at that time (Shen et al. 2006; Li et al. 2019a, b). The Uppermost Permian Selong Group consists of four microfacies (Fig. 49; Li et al. 2019a, b): the lower part is dominated by bioclastic wackestone/floatstone (MF6); the upper part consists of calcrete (MF1; Fig. 49A), crinoid grainstone (MF2; Fig. 49B) and coral-bearing grainstone (MF3; Fig. 49C). By contrast, the lower Kangshare Formation develops densely packed bivalve grainstone with micritic intraclasts (MF4; Fig. 49D), bioclastic packstone with diverse fossils (MF5; Fig. 49E), bioclastic wackestone/floatstone (MF6; Fig. 49F) and lime-mudstone (MF11). The temporal microfacies changes suggest: (1) a sedimentary environmental change from lower outer ramp to upper inner ramp beneath the PTB, marked by the dolostone bed; (2) subsequently, the inner ramp was abruptly succeeded by a middle ramp setting. The microfacies results also show that the loss of most cold-water carbonate-producing assemblage of bryozoans, brachiopods and echinoderms across the PTB biotic crisis led to collapse of the Late Permian carbonate factory, which was followed by benthic automicrite factory with only minor amounts of calcifying metazoans (Li et al. 2019a, b).

Stop 20 Late Cretaceous Trench Sediments at Luogangcuo Section in Saga County (GPS 29°15′40.8″N, 85°20′35.8″E)

The Luogangcuo section is located at about 12 km southeast of Saga county, at the south bank of the Yarlung Zangbo river (Fig. 50). The Luogangcuo Formation at this section is composed of thick-bedded or amalgamated conglomerates with minor sandstone in the lower part and massive conglomerate in the upper part (Fig. 51). Graded bedding and oblique lamination occur in the section. The conglomerates are poorly sorted, with blocks of chert, sandstone, and limestone. Granules to cobbles consist of radiolarian chert (70%–85%), subordinate shale (3%–23%), sandstone (1%–20%), and minor limestone, indicating a proximal provenance from the adjacent accretionary prism. Meanwhile, the lateral limited sandstone beds are feldspatho-quartzo-lithic volcaniclastic sourced from the Gangdese magmatic arc and the central Lhasa terrane. The depositional age was constrained as ca. 88–81 Ma by youngest detrital zircon ages. Therefore, the section was interpreted to

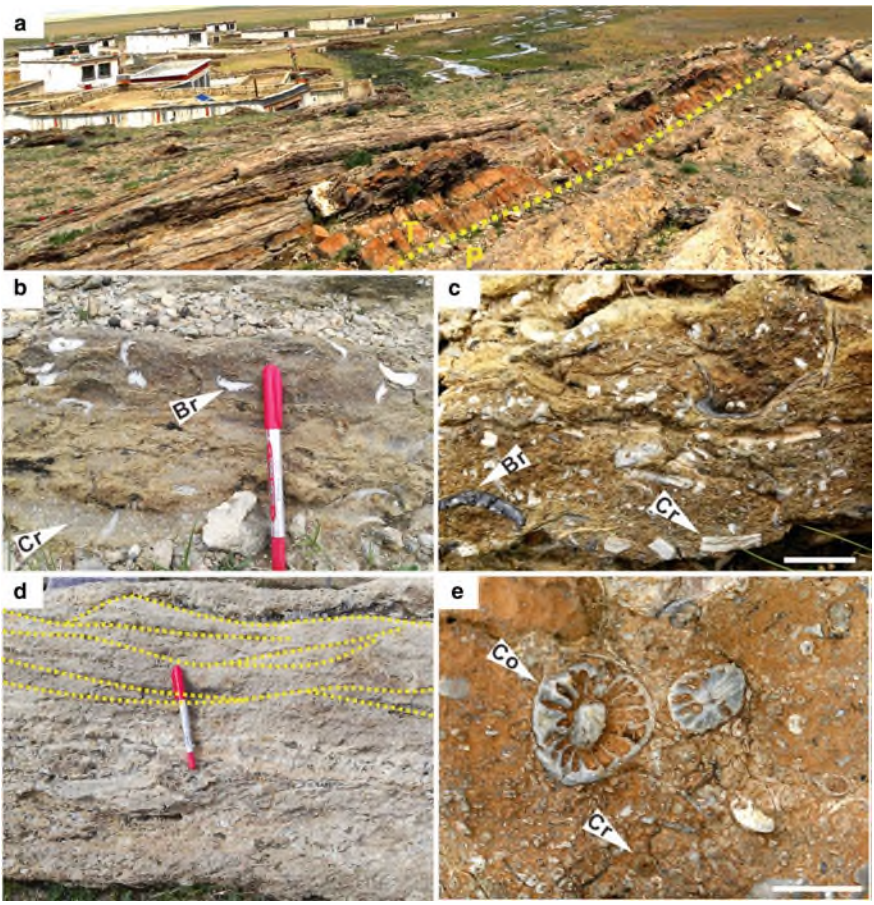

Fig. 48 Field photographs of the Selong Xishan section, showing the feature of the Permian–Triassic Boundary (yellow dashed line). Field of view is *ca* 2.5 m. **b** Thin-bedded, fossiliferous limestone containing abundant fragments of crinoids (Cr) and brachiopods (Br), −5.9 m. **c** Bryozoan–echinoderm rudstone containing abundant fragments of bryozoans, crinoids (Cr) and brachiopods (Br), −4.5 m. Scale bar = 1 cm. **d** Crinoid grainstone showing cross-stratification (denoted by dashed yellow lines), −1.5 m. **e** Coral-bearing grainstone that contains occasional corals (Co) floating in crinoid (Cr) grainstone, −0.25 m. Scale bar = 1 cm. Photographs and descriptions are from Li et al. (2019a, b)

be deposited by proximal submarine fan in the Neo-tethyan trench during Late Cretaceous.

Stop 21 The Sangdanlin Section, Near Sangdanlin Village (GPS 29°15′28N″, 85°14′52″E), About 5 km South to the Saga. Near the Highway from Saga to Gyirong

The Sangdanlin section (Fig. 52) preserves the most complete succession of Cretaceous-Paleocene abyssal strata documented so far in the Himalayas, and has been consequently the focus of research to date.

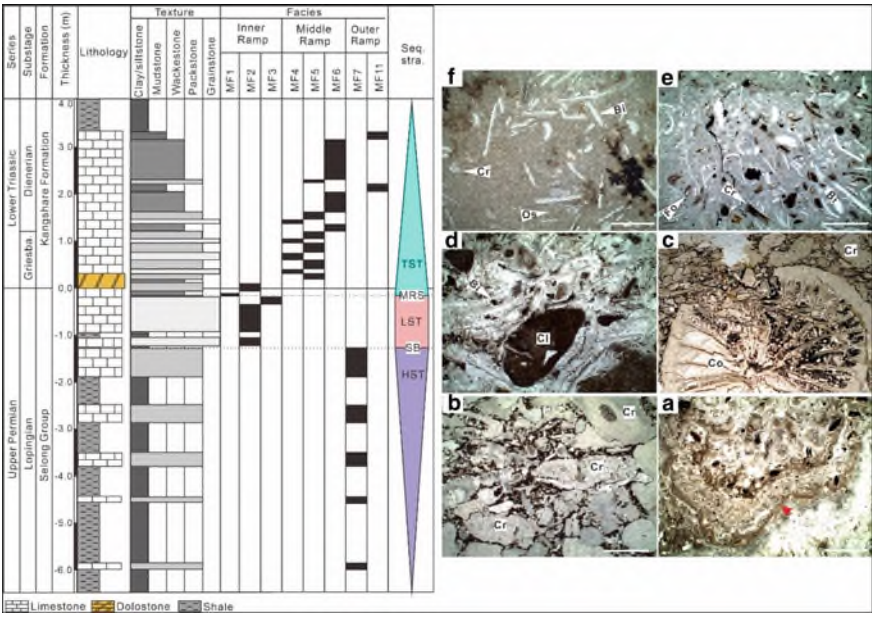

Fig. 49 Microfacies distribution (left) and photographs (right) of the Selong Xishan section during the Permian–Triassic boundary. A. Calcrete (MF1) withdownward-growing, crust-like structure (red arrow) containing amorphous brown pigments, −0.15 m; B. Crinoid grainstone (MF2) exhibiting densely packed crinoid (Cr) fragments, −0.70 m; C. Coral-bearing grainstone containing slightly abraded rugose corals (Co) and abundant crinoid (Cr) fragments, −0.25 m; D. Shelly tempestite (MF4) consisting of densely packed bivalve shells (Bi) with rounded micritic intraclasts (Cl), + 0.30 m; E. Bioclastic packstone (MF5) containing abundant crinoid (Cr) and occasional bivalve (Bi) fragments and foraminifera (Fo), +1.25 m; F. Bioclastic wackestone containing diverse fossils (MF6), including bivalves (Bi), crinoids (Cr) and ostracods (Os), +1.8 m. Note that the scale bar = 1 mm. except for the Fig. 3 C with scale bar = 1 cm. Photographs and descriptions are from Li et al. (2019a, b)

The Sangdanlin section can be divided into three units from base to top (Fig. 53): the Denggang, Sangdanlin and Zheya formations (Wang et al. 2011; DeCelles et al. 2014). The Denggang Formation (units 1–10) is approximately 105 m thick and composed of light yellow fine to coarse quartzose sandstones interbedded with grey-green (weathering to light yellow) silty sandstone and silty shale. It is capped by a 60 cm-thick, green volcaniclastic sandstone bed (unit 10). The overlying Sangdanlin Formation (units 11–21) is approximately 95 m thick, and composed of purple-red siliceous shale, chert, quartzose sandstone, and feldspatho-litho-quartzose volcaniclastic sandstone. Quartzose sandstones are found in unit 13, lower part of units 16, 17, and 19. Volcaniclastic sandstones are found in units 14 and 15, upper part of units 16, 18 and 22. The alternating quartzose and volcaniclastic sandstones are unique of the Sangdanlin Formation. The overlying Zheya Formation (units 22–49) is more than 500 m-thick and composed of grey-black silty shale, thick to massive layers of

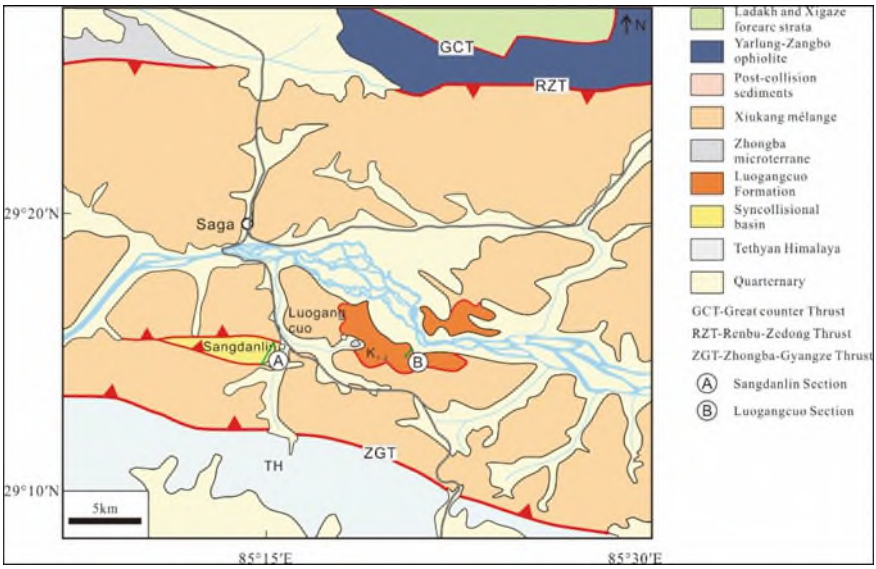

Fig. 50 Geological map of the Sangdanlin and Luogangcuo sections near Saga

Fig. 51 Luogangcuo section at Stop 19 (left: Panorama of the Luogangcuo section; right: sandstone and chert blocks within conglomerate). Photo by Xiumian Hu

grey-green feldspatho-litho-quartzose volcaniclastic sandstone and a few intervals of mottled chert.

The thickness of sandstone beds in the Denggang Formation varies from several centimetres to several metres, and the layers exhibit sharp contact with the underlying and overlying mudrocks. Sedimentary structures include cross-lamination, parallel-lamination, normal grading, and flute casts. The Denggang Formation is interpreted as deposited at the toe of the Indian continental slope, and thicker sandstone beds as deposited by high-density turbidity currents (Wang et al. 2011; DeCelles et al. 2014). The appearance of purple-red siliceous shale in the Sangdanlin Formation indicates

Fig. 52 Field photographs of the Sangdanlin section (Hu et al. 2017). **a** Panorama of the section, looking to the northwest; stratigraphic units are indicated; **b** sandstone bed of unit 8 (Denggang Formation); **c** boundary between quartzose sandstone of unit 17 and volcaniclastic sandstone of unit 18 (Sangdanlin Formation); **d** mudrocks of unit 26 yielding calcareous nannofossils; **e** turbiditic volcaniclastic sandstones of unit 27 (Zheya Formation); **f** sedimentary olistoliths in unit 30; **g** interbeded tuff in unit 47 (Zheya Formation)

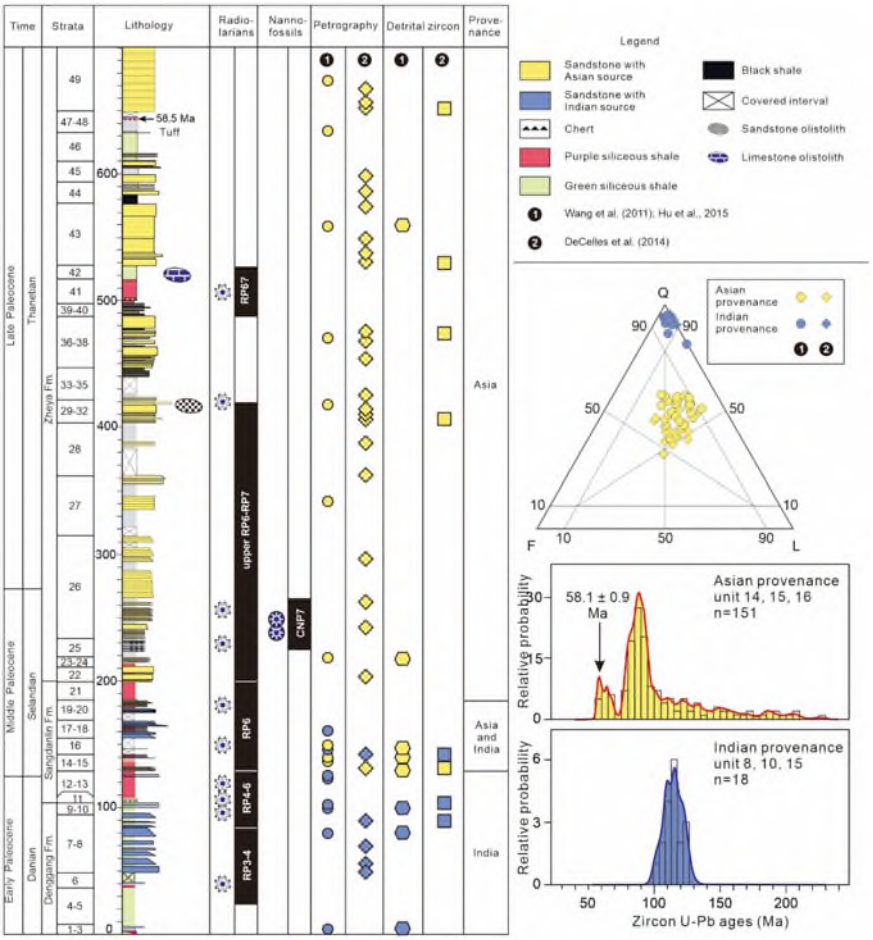

Fig. 53 Integrated bio- and chrono-stratigraphy, sandstone petrography, detrital-zircon chronostratigraphy and provenance change in the Sangdanlin section. Detrital-zircon U–Pb age patterns highlight the sharp difference between Indian-derived quartzose turbiditic sandstones and Asian-derived volcano-plutonic turbiditic sandstones. After Hu et al. (2016)

a palaeo-water depth deeper than the carbonate compensation depth (CCD). Volcaniclastic sandstones in the Sangdanlin Formation mostly display lenticular shape and sharp contact with underlying mudrocks. Slump the Zheya Formation sedimentary structures of sandstone layers include normal grading, flute casts, ditch moulds, and slump structures, indicating deposition by turbidity currents. Background sedimentation is represented by siliceous shale deposited in abyssal environment (Wang et al. 2011; DeCelles et al. 2014). Exotic blocks of conglomerate, sandstone, and carbonate in silty shale are common in the upper part of the Zheya Formation.

The quartz content of the Denggang Formation exceeds 98%, and most particles are well rounded. The U–Pb ages of detrital zircons are mainly Early Palaeozoic to Precambrian, with an Early Cretaceous age peak (approximately 140–120 Ma). These characteristics indicates provenance from the northern Indian continent (Wang et al. 2011; DeCelles et al. 2014; Hu et al. 2015). Volcaniclastic sandstones in the Sangdanlin and Zheya formations have drastically different petrologic characteristics from the underlying Denggang Formation. The average detrital composition is Qm:F:Lt = 41:9:50 (Wang et al. 2011) or 44:25:31 (DeCelles et al. 2014). Textures of lithic fragments indicate origin from intermediate to felsic volcanic rocks. Embayed monocrystalline quartz was derived from felsic volcanic rocks (Wang et al. 2011). Ages of detrital zircons cluster at ~196–180 Ma, ~125–80 Ma, and ~70–54 Ma (Wang et al. 2011; DeCelles et al. 2014), which correspond to the three main periods of magmatic activity in the Gangdese arc. In addition, most of these Mesozoic and Cenozoic zircon grains yield positive εHf(t) values (Hu et al. 2016) as Gangdese zircons. These data conclusively indicate that volcaniclastic sandstones in the Sangdanlin and Zheya formations were derived from the Gangdese magmatic arc on the southern margin of the Asian continent (Wang et al. 2011; DeCelles et al. 2014; Hu et al. 2016).

Provenance analysis indicates that detritus from the Asian continent first appears in unit 14 (Wang et al. 2011; Hu et al. 2016). Alternating turbidite beds with sharply contrasting composition in the Sangdanlin Formation indicates that the sedimentary basin was synchronously receiving clastic materials from both Indian and Asian continental margins during this time period. Accumulation was thus taking place in the topographic trough that separated the two continents, which cannot be anything else than the trench where India began to underthrust Asia (Hu et al. 2016b).

The siliceous shales in the Sangdanlin and Zheya formations contain abundant radiolaria, but their stratigraphic age is debated. Ding (2003) proposed a Palaeocene age (radiolarian zones RP1-RP7), whereas Li et al. (2007) found a Campanian radiolarian assemblage in unit 11 and an early Eocene radiolarian in unit 16. Chan (2006) found RP5 radiolaria in layer S4 (equivalent to units 11, 12), a mid-Cretaceous radiolarian assemblage in layers S5 (equivalent to units 31, 32) and S7 (equivalent to unit 41), and Palaeocene radiolaria of zones RP6 and RP7 near unit 29. They concluded that the Sangdanlin section may contain multiple structural repetitions. A careful biostratigraphic study was carried by Prof. Ted Moore on the Sangdanlin section (Hu et al. 2015), where radiolarian fossils are rare and not well preserved. Moreover, radiolarian assemblages include species of different age in the same sample. Depositional ages have thus to be inferred from the youngest fossils of the assemblage, whereas older fossils, representing more than half of the assemblage in most samples, are interpreted as redeposited (Hu et al. 2015). With the limitations posed by extensive recycling, poor preservation and imperfect definition of the Paleogene radiolaria time scale, we concluded that (Hu et al. 2015): radiolaria in the siliceous shales of the Sangdanlin Formation (units 11–20) are Palaeocene in age (RP4-RP6 zones), while radiolaria in the lower part of the Zheya Formation (units 25 and 32) may extend to zone RP7. Calcareous nanofossils were also found for the first time

at the base of the Zheya Formation (unit 26), indicating an age corresponding to calcareous nannozone CNP7 (Hu et al. 2015).

DeCelles et al. (2014) found a tuff layer at the top of the Zheya Formation (unit 48). The weighted average of 38 U–Pb ages obtained by LA-MC-ICPMS on zircon crystals is 58.5 ± 0.6 Ma (2σ), which provides a precise age constraint for this layer, located more than 500 m above unit 14 recording the first appearance of Asian derived detritus. Combined with evidence mentioned above this supports rapid sedimentation in the trench during the very first stage of the India-Asia collision.

Stop 22 The Mubala Section, About 60 km West to the Saga (GPS 29°19′41N″, 84°41′26″E)

The Mubala section, ~60 km west of the Sangdanlin section (Fig. 54) is a newly discovered, ~2 km-thick siliciclastic succession that conformably overlies interbedded chert and dark grey siliceous shale equivalent to the Cretaceous Zhela Formation deposited on the distal part of the Indian shelf within the Tethyan Himalaya (An et al. 2021). The Mubala section preserves the same stratigraphy as the Sangdanlin section, from Denggang Formation to Zheya Formation (An et al. 2021). However, the name of Formations has been revised according to the recent biostratigraphic work (Li et al. 2022). The Seven Formations preserved in the Mubala section are now called Zhela, Weimei, Rilang, Duobeng, Chuangde, Sangdanlin and Zheya (Fig. 55, Li et al. 2022).

The c. 300 m thick Zhela Formation are quartzose and sedimentary structures indicate a submarine lobe environment. The overlying Rilang Formation is sublitharenite and sedimentary structures also indicate a submarine lobe environment. Then Rilang Formation is capped by a sand injection complex intruding into a chert dominated interval. The lithology of the sandstone is glaucony-bearing feldspatho-quartzose. Immediate above the sand injection interval is a red shale dominated interval, with folded chert layers, folded carbonate layers, chert blocks and quartzose blocks, indicating a mass transport deposit (MTD I). Then another mass transport deposit (namely MTD II), with folded and shingled sandstone, immediately sitting above MTD I (Liu

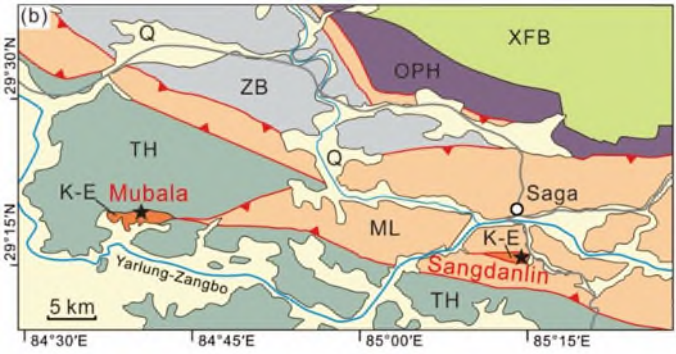

Fig. 54 Geological map of the Sangdanlin and Mubala sections near Saga

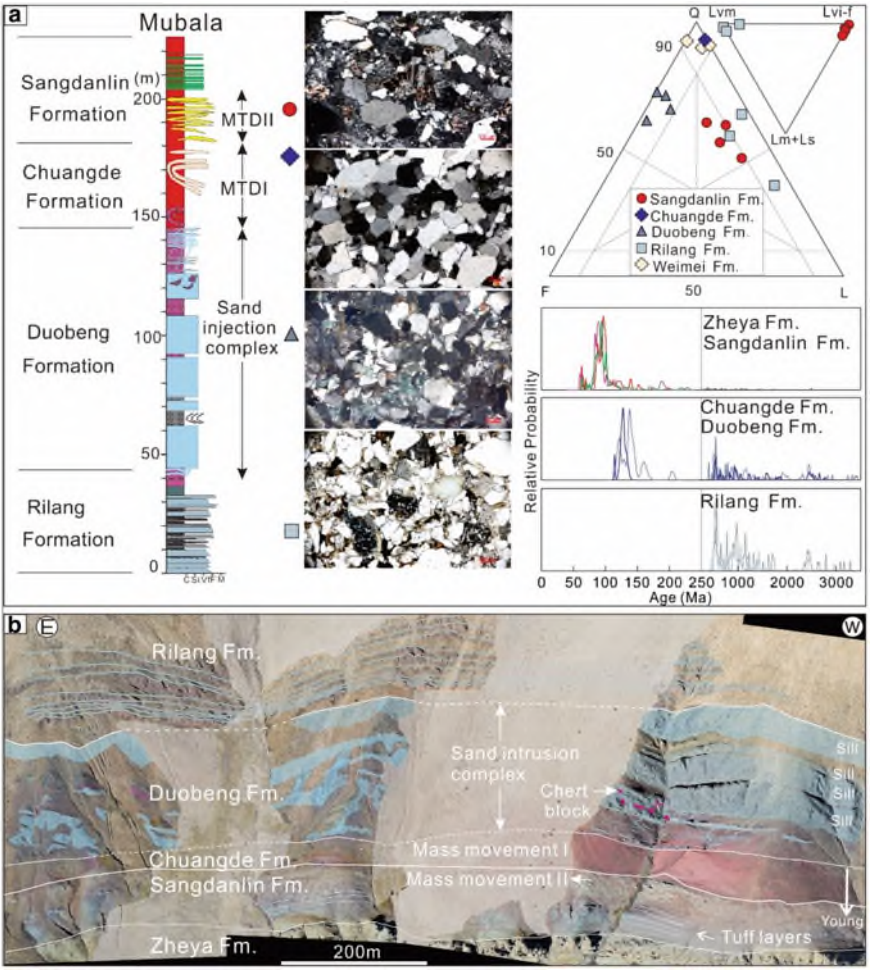

Fig. 55 The **a** Sedimentary column of Mubala section (left), lithology of Rilang to Sangdanlin Formations (middle), provenance data of the Mubala section (right); **b** Outcrop interpretation of Mubala section

et al. 2021). The lithology of this sandstone is volcaniclastic sublitharenite. By provenance study, the Sangdanlin sandstone is the first Asia derived sandstone, and before which the sandstones are all coming from Indian (An et al. 2021). Zheya Formation is represented by sheet sandstone with two giant mass transport deposits, the sediments are all from Indian. Thus, the Chuangde and Sangdanlin Formation represent an abrupt Indian to Asia provenance reversal.

This Indian to Asian provenance reversal (IAPR) is dated by a tuff layer immediately above it at 61 ± 0.3 Ma (zircon U–Pb age using Secondary Ion Mass Spectrometry; Fig. 56, An et al. 2021). Also, radiolarian fossils identified from the same layers give an age of around 61 Ma (Fig. 56, Li et al. 2022). Thus, the Indian to Asian provenance reversal has been tightly constrained at 61 ± 0.3 Ma, and the well exposed outcrop offer a great opportunity to disclose the sedimentary processes occurring before and during continental collision.

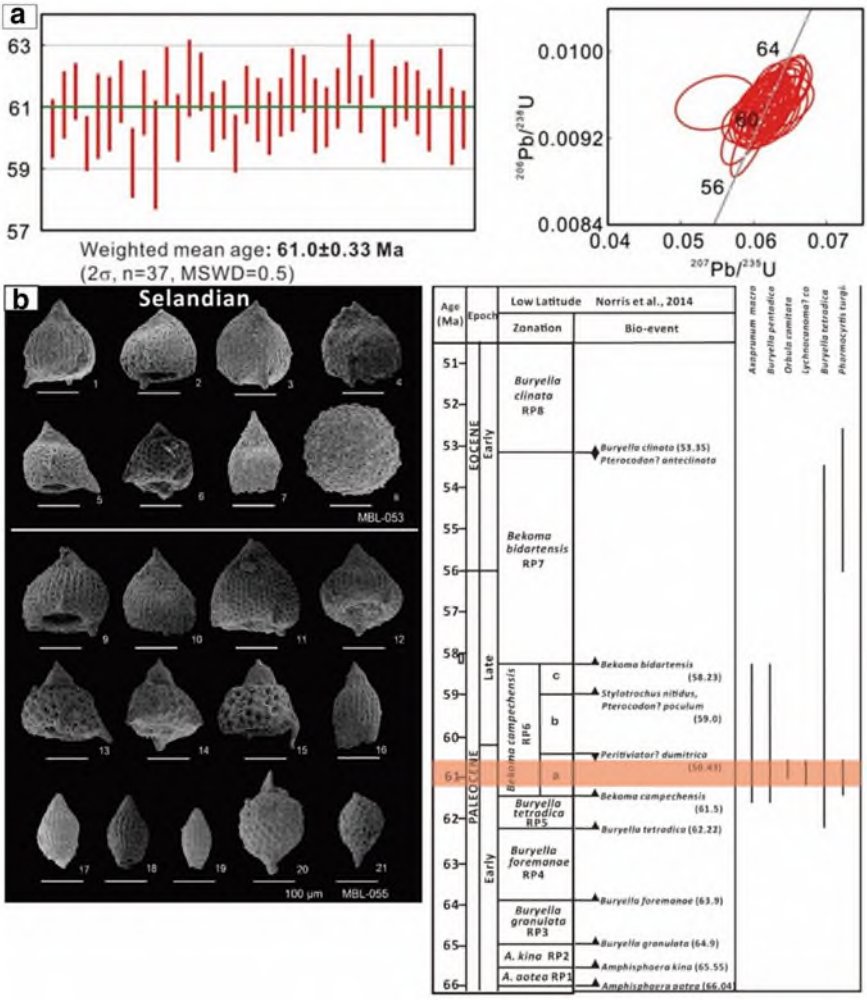

Fig. 56 The **a** Age plots for the tuff immediately above the IAPR; **b** Radiolarian fossil identified from the chert layer immediately above the IAPR with an indicative age

Fig. 57 Outcrops of Stop 21 (left: purple mudstone interbedded within thin-bedded sandstone) and Stop 19b (right: the fault contact between the Padana Formation and the Xigaze ophiolite). Photo by Wei An

Stop 23: Tectonic Contact Between the Xigaze Forearc Basin and the Ophiolite of Yarlung Zangbo Suture Zone at Riwuqi in Sangsang Area (GPS: 29°20′37.6″N, 86°36′59.6″E)

The Xigaze ophiolite lies under a southward thrust with the Padana Formation deposited in a deltaic-fluvial environment in the Xigaze forearc basin. In the Sangsang area, the depositional age of the Padana Formation is constrained between ca. 83–76 Ma by the youngest detrital zircon ages (An et al. 2014). Provenance studies suggests the sandstone were derived from the Lhasa terrane in the north (An et al. 2014; Huang et al. 2015). This stop was interpreted to a direct contact between the Ngamring Formation with highly sheared ophiolitic mantle or ophiolitic mélange (Huang et al. 2015; Maffione et al. 2015). However, the red sandstone interbedded within purple and grey mudstone represents part of the fluvial-deltaic Padana Formation (Wang et al. 2017a, b). Therefore, this stop was reinterpreted to be a tectonic contact between the Xigaze forearc basin and the ophiolite consisting of serpentinized peridotites (Fig. 57). Red sandstone of the Padana Formation, the fault gouge and fractured serpentinites can be found at this stop.

Stop 24 Qunrang Pillow-Lava Basalt (GPS: 29°09′17.7″N, 89°02′40.2″E)

The volcanic rocks of the top crustal section are mainly massive and pillow basalts (Fig. 58a, b). Secondary veins and amygdules of carbonate, quartz, and chlorite are observed in the pillow basalt. The intrusive section in the crust consisting of gabbro, diabase and sheeted sill (Fig. 58c) is cut by basaltic and diabase dikes (Fig. 58d). Basaltic dikes are porphyritic with clinopyroxene and plagioclase phenocrysts.

Most Xigaze Ophiolite pillow basalts display LREE depleted patterns similar to that of N–MORB (Fig. 59a). In the plots of Zr/Yb versus Sm/Yb and Zr versus Y, all our and published basalts from the Xigaze Ophiolite plot in the “MORB array” (Fig. 59d) and overlap with global MORB (Fig. 59c). However, pillow basalts and other published basalts display pronounced depletion of Nb and Ta, and some enrichment of LILE, resembling those of IBM FABs (Fig. 60a, b). In this context, the generation mechanism of the Xigaze Ophiolite basalts is similar to IBM FABs, that

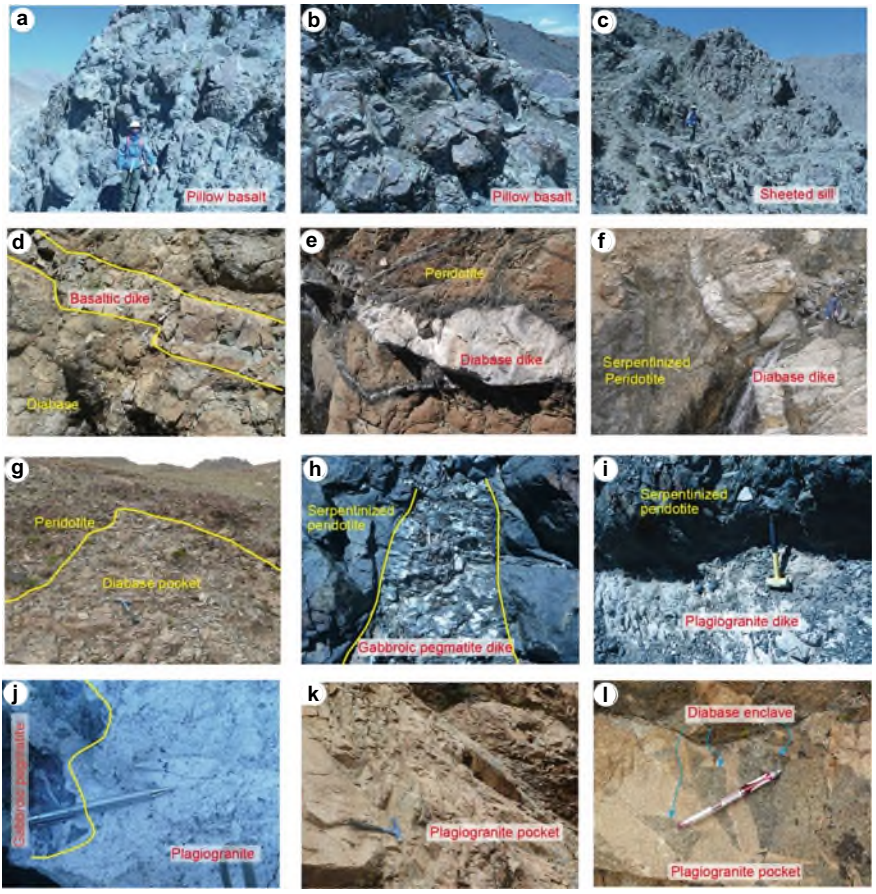

Fig. 58 Field photographs of the Xigaze Ophiolite showing pillow basalt, sheeted sill and basaltic dike in the crust section, and various mafic and felsic dikes in the mantle. Pillow basalt (**a**, **b**), sheeted sill (**c**), basaltic dike (**d**) in the crust; various dikes including diabase dike/pocket (**e**–**g**), gabbroic pegmatite (**h**), plagiogranite (**i**–**k**) in the mantle, and the association of gabbroic pegmatite and plagiogranite (**j**), diabase enclave in the plagiogranite pocket (**m**)

is, the partial melting was mainly caused by decompression as the contribution of fluids derived from the sinking slab during this stage was limited. Xigaze Ophiolite basalts have higher Zr/Y and Zr/Yb ratios than those of IBM FABs, indicating that they may have been generated from a more fertile mantle source compared to IBM FABs (Fig. 59c, d).

Stop 25 Luqu Ophiolite Massif (Mantle Rocks and Various Dikes, GPS: 29°09′09.28″N, 88°53′35.12″E)

The mantle peridotite is dominated in the XO, and it is mainly composed of variably serpentinized harzburgite associated with dunite and lherzolite (Girardeau et al.

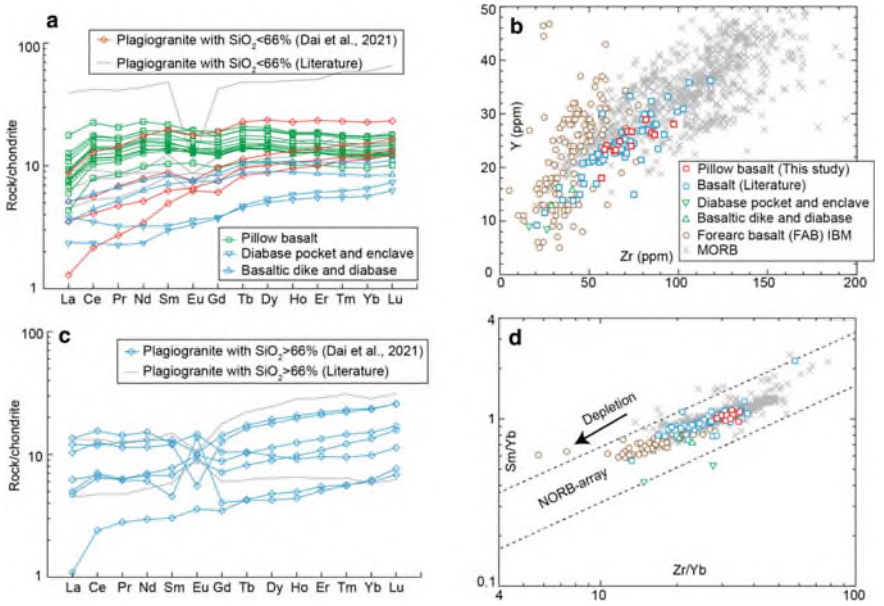

Fig. 59 Chondrite–normalized REE patterns of pillow basalts (**a**), basaltic and diabase dikes (**a**), plagiogranites (**a**, **b**) in the Xigaze Ophiolite. The normalizing values are from Sun and McDonough, 1989. Compared data sources for plagiogranites are from Zhang et al. 2016a, b. Variations of (**c**) Zr versus Y, (**d**) Zr/Yb versus Sm/Yb for basalt and diabase. Note that Zr/Y and Zr/Yb ratios for Xigaze Ophiolite basalts are higher than IBM forearc basalts, but similar to MORB, indicating derivation from a more fertile mantle source. Basalts of the XO from Bao et al. 2013; Chen and Xia, 2008; Dubois–Côté et al. 2005; Malpas et al. 2003; Li et al. 2012; Niu et al. 2006; Zhang et al. 2016a, b. FABs from Ishizuka et al. 2011, 2018; Reagan et al. 2010, 2017; global MORBs from Gale et al. 2013

1985a; Hébert et al. 2003; Nicolas et al. 1981). These mantle rocks are crosscut by abundant mafic dikes and sporadic plagiogranite dikes (Dai et al. 2013, 2021). Diabase dikes/pockets (for brevity, in some places we use dikes for both) are widespread in the peridotite and are 0.3–4.5 m wide (Fig. 58e–g). They are composed of plagioclase and clinopyroxene and sometimes are intensely altered. Gabbroic pegmatites occur as 3–4–m–wide pods or 0.1–0.3–m–wide dikes (Fig. 58h). Gabbroic pegmatites are dominated by clinopyroxene megacrysts with coarse–grained plagioclase and amphibole. Plagiogranite usually occurs as dikes from 0.3 m to 1 m wide (Fig. 58i), or pockets with an area of ~40 × 45 m (Fig. 58h, i; Location C in Fig. 6). At Location A in Fig. 6, an association of gabbroic pegmatites and plagiogranite was observed, and their contact is diffuse (Fig. 58J). Most diabase enclaves present sharp contacts with the host plagiogranite (Fig. 58m). One sample (DJ12–20) was collected from these enclaves. The plagiogranite is medium–grained, and mainly consists of plagioclase and quartz, with minor amphibole, biotite and orthopyroxene, as well as common accessory minerals such as zircon, titanite. It is traversed by pumpellyite veins. Plagioclase is subhedral to euhedral and is partly altered into secondary

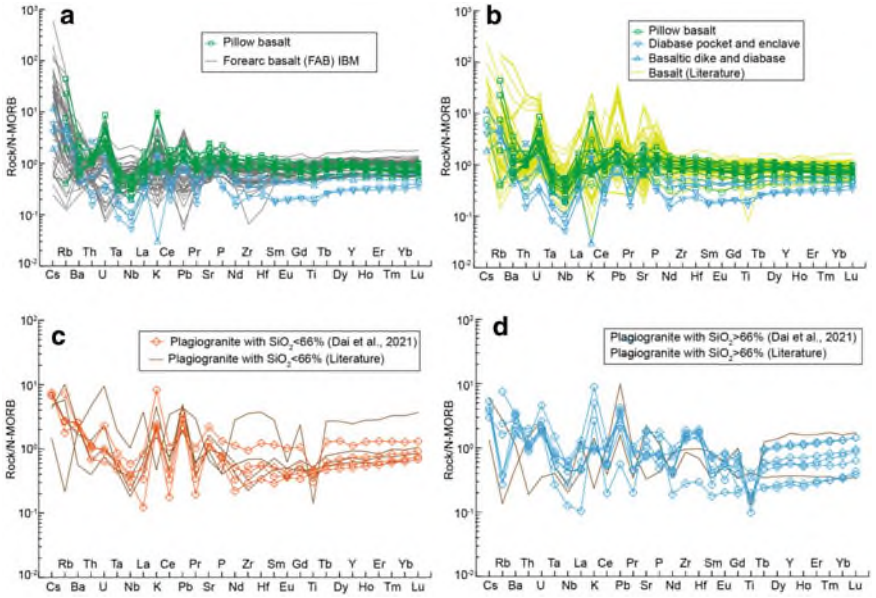

Fig. 60 N–MORB normalized trace element diagrams for pillow basalts (**a**, **b**), basaltic and diabase dikes (**a**, **b**) plagiogranites (**c**, **d**). N–MORB normalizing values are from Sun and McDonough (1989). Plagiogranites from Zhang et al. 2016a, b; basalts from Bao et al. 2013; Chen and Xia, 2008; Dubois–Côté et al. 2005; Malpas et al. 2003; Li et al. 2012; Niu et al. 2006; Zhang et al. 2016a, b

minerals, mainly epidote and sericite. Amphibole is euhedral and ranges in color from brown to green. Orthopyroxene occurs both as megacrysts and as small grains. Quartz is commonly medium– and fine–grained, anhedral to subhedral.

Basaltic dike and diabase enclave/pocket samples are characterized by LILE enrichment and significant HFSE depletion, especially negative Nb and Ta anomalies (Fig. 60b), suggesting that they reflect flux melting of a depleted mantle. Their depleted mantle source is also supported by low Zr and Y contents (Fig. 59c).

Stop 26 Chongdui Formation of the Xigaze Forearc Basin at Qunrang Village (GPS: 29°09′17.7″N, 89°02′40.2″E)

Base strata of the Xigaze forearc basin (the Chongdui Formation) are observed in this section (Fig. 61). The Chongdui Formation here consists of ~95 m thick, steeply north-dipping strata, deposited on top of pillow basalts of the Xigaze ophiolite. The strata could be subdivided into two members: a lower member comprising purplish red chert (6.4 m thick) overlain by siliceous mudrocks (12.6 m thick), and a conformably overlying upper member dominated by sandstones and shales (76 m thick). The top of the succession is faulted against a different sliver of ophiolitic basalt to the north (Wang et al. 2017a, b).

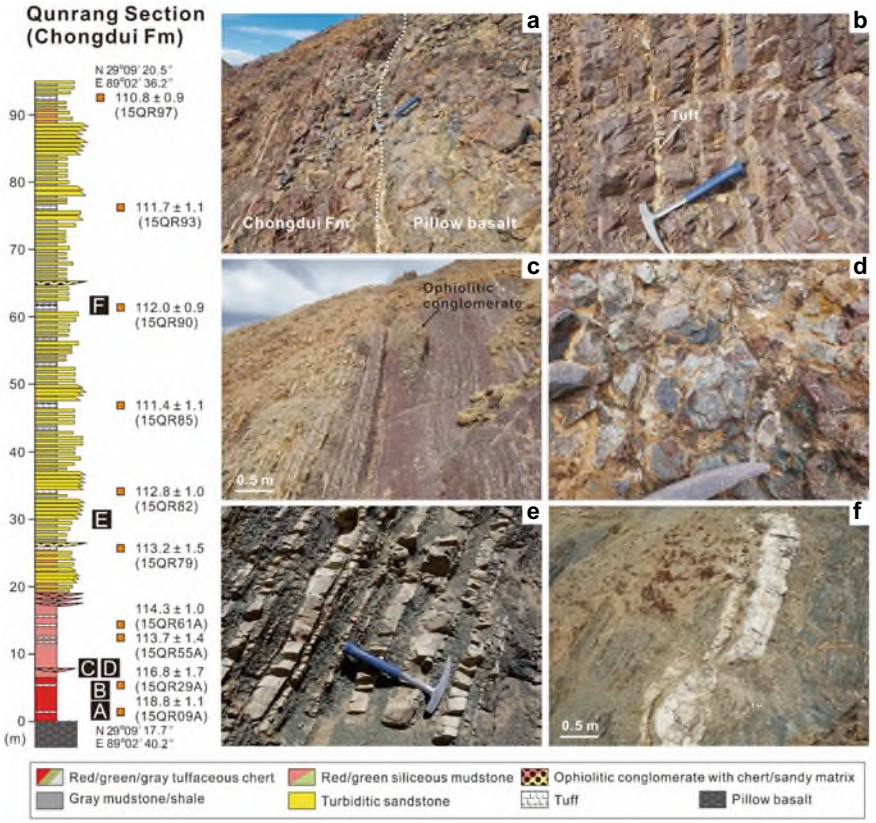

Fig. 61 Stratigraphy (left) and field photos (right) of the Chongdui Formation in the Qunrang section (After Wang et al. 2017a, b). **a**, Boundary between the Chongdui Formation and pillow basalts of the Yaarlung-Zangbo ophiolites; **b**, Chert from the lower member; **c**, conformably contact between the lower and upper members, also show a lenticular conglomerate bed in the lower member; **d**, Ophiolitic conglomerate; **e**, turbidites; **f**, white tuff layer in the upper member

Chert beds in the lower member are commonly 5–10 cm thick and rich in radiolarian fossils, whereas siliceous mudrocks are massive. Tuffaceous laminaes and thin tuff layers (0.5–3 cm) are common throughout the lower member, increasing in frequency and thickness (up to 10 cm) up-section. The upper member comprises thin-bedded, fine-grained sandstones, greenish gray shales, minor purplish radiolarian mudrocks, and medium to thick-bedded (10–60 cm) white tuffs. Sandstone beds, commonly 5–20 cm thick, laterally continuousand arranged in thickening-upward cycles, include massive, plane-parallel-laminated and rippled sandstones. Four lenticular conglomerate beds with siliceous matrix are intercalated in the siliceous mudrocks of the lower member, and two conglomerate beds with sandy-mud matrix occur in the upper member. Conglomerate clasts are mostly subangular to an-gular basalt and minor diabase, gabbro and serpentinite. Radiolarian chert,

siliceous shale and interbedded tuffs of the lower member represent abyssal sediments deposited onto oceanic crust with in-tercalated fallout tephra. Sandstones of the upper member were deposited by low-density turbiditic flows on a lower deep-marine fan, whereas the conglomerates with mafic and ultramafic gravel were deposited by submarine debris flows sourced from nearby ophiolitic highs (Wang et al. 2017a, b).

Radiolarian faunas and Zircon SIMS U–Pb ages of tuffs gave accurate constraints on the depositional age of the Chong-dui Formation (Ziabrev et al. 2003; Wang et al. 2017a, b). Chronostratigraphic results suggested that initial deposition of the Chongdui Formation at late Barremian, immediately after the formation of the Yarlang-Zangbo ophiolite (~131–124 Ma). Deposition of turbidites started at ~113 Ma. Detritus of turbiditic rocks are from the Gangdese arc.

Stratigraphy of the Chongdui Formation indicates (1) The Yarlung-Zangbo ophiolite were formed adjacent to the Lhasa terrane, in the Gangdese forearc; (2) The Xigaze forearc basin had experienced a starved stage of ~10–15 Ma before turbiditic filling; (3) The Asian active margin of Neotethys was fully established only after Early Cretaceous.

Stop 27 Upper Cretaceous Oceanic Red Beds of the North Tethys Himalaya at Chuangde Section, Gyangze County (GPS 28°58′00″N, 89°44′05″E)

The Cretaceous marine strata of north Tethys Himalaya can be observed in the Chuangde section in Gyangze area (Fig. 62). The volcanoclastics of Rilang Fm., shales of Gyabula Fm., red shale with exotic limestones of Chuangde Fm. and olistostrome of Zongzhuo Fm. are well exposed in this section. The Chuangde section is one of the representatives for Cretaceous Oceanic Red Beds (CORBs), which is considered as a major change of the Cretaceous oceanic condition from anoxic to oxic in deep-sea environments (Wang et al. 2005a, b). The CORBs in the Gyangze basin mainly consist of shales, thin-bedded marls, re-sedimented limestones and clasts supported conglomerates-breccias (e.g., Chen et al. 2011).

CORBs in Chuangde section is mainly composed of ca. 30 m thick red siliceous shales intercalated with thin bedded marls, caused by turbidites (Hu et al. 2006). Medium to thick bedded variegated limestones were found at the base and in the upper part of the CORB succession. The limestone beds are commonly deformed and in sharp contact with the shales. At the base of the succession, a single limestone bed (limestone unit of Chuangde 1, Lc1; Chen et al. 2011) is out-cropping with an average thickness of 0.5 m. The thickness of the bed varies laterally from tens of centimeters to about 1.5 m. In contrast, the medium bedded limestones are interbedded with shales and are discrete laterally in the middle part of the succession (Lc2; Chen et al. 2011). Mudstone fragments paralleling the dip of the sequence are distributed widely in the limestone beds. The upper 10 m of the formation is characterized by the occurrence of lenticular and round limestone olistoliths enclosed by red shales (Lc3; Chen et al. 2011). The limestones are mainly gray in color. The planktonic foraminiferal result indicates that the onset of the Chuangde CORBs of early Campanian age (Chen et al. 2011), which may be slightly younger than previously documented (Li et al. 2005; Wan et al. 2005).

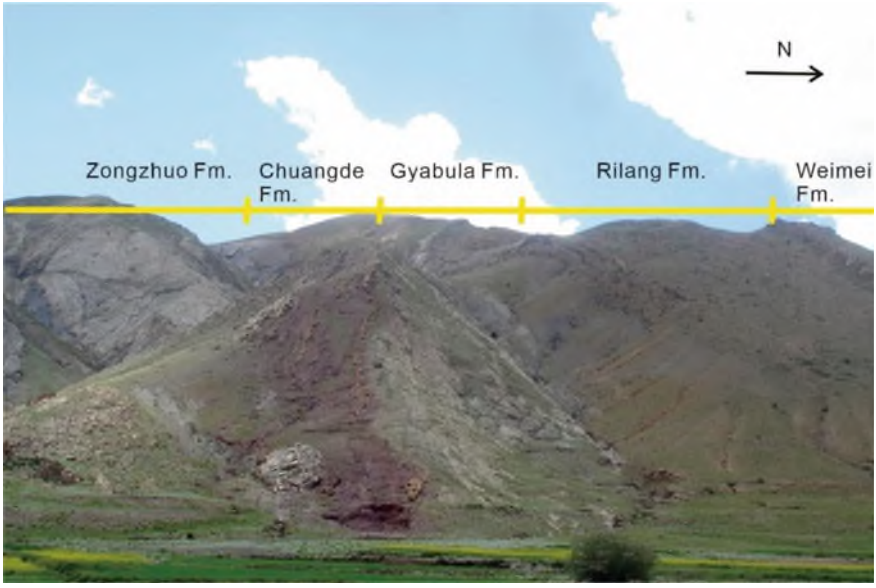

Fig. 62 Field photo of the Chuangde section showing the quartz arenites of latest Jurassic Weimei Fm., volcanoclastics of Rilang Fm., shales of Gyabula Fm., red shale with exotic limestones of Chuangde Fm. and olistostrome of Zongzhuo Fm

Stop 28 Longma, Zongzhuo Mélange Aside the Main Road from Gyangze-Ngyangze (GPS: N28°57′47.0″, E89°44′14.0″)

Here near the Baisa village, the Zongzhuo mélange is comprised by exotic blocks and unmetamorphic shale and mudstone 'matrix' (Fig. 63). Exotic blocks are several centimeters to tens of meters in size, and comprise a variety of lithologies including sandstones, cherts, basalts, limestones and conglomerates. Detrital modes of the sandstones bocks are composed of dominantly volcaniclastic grains and subordinately quartzes and feldspars, similar to sandstones from the Xigaze forearc basin (Sun et al. 2011). Detrital zircon U–Pb ages from an exotic sandstone block are mainly clustered at ~77–129 Ma, with two peaks at ~90 Ma and 110 Ma. Occurrence of abundant volcanic detritus and Mesozoic detrital zircons suggest that the Zongzhuo mélange contain significant amount of materials originally derived from the Gangdese volcanic arc.

Stop 29 Triassic Langjiexue Group, Nanggarze Area (GPS: 29°13′42.7″N, 90°37′58.2″E)

The Upper Triassic (roughly Carnian to Norian) Langjiexue Group is a suite of turbidites exposed south of the Yarlung-Zangbo suture zone in the eastern Himalaya (Fig. 64). It tectonically belongs to the Tethys Himalayan zone, but its provenance signatures significantly different from those of other Tethys Himalayan sandstones. These features include: (1) Southward to southwestward paleocurrent direction; (2)

Fig. 63 Panoramic view on the Zongzhuo mélange near the Baisa village

'Recycled Orogen Provenance' detrital composition; (3) Depleted whole-rock Nd isotopes; (4) Late Paleozoic to early Mesozoic (400–200 Ma, mostly clustered at 280–220 Ma with peak at ~245 Ma) detrital zircons; and (5) Arc-basalt or mantle-peridotite-derived chrome spinels (Meng et al. 2019 and references therein). As the Langjiexue Group is everywhere in fault contact with Tethys Himalayan strata, its depositional setting and provenance had been for a long time. Some scholars proposed that the Langjiexue Group was part of an exotic terrane deposited in the forearc region of either the Lhasa block or an intra-oceanic arc, and accreted to the northern Indian margin during the convergence and collision between India and Asia, but others insist it was originally deposited on the distal Indian margin only with unique depositional process (see Wang et al. 2016a, b and Liu et al. 2020 for summary).

A recent study by Meng et al. (2019) found that the Qulonggongba Formation in the southern Tethyan Himalayan zone and the Langjiexue Group had similar sandstone petrography. The presence of Late Paleozoic to early Mesozoic detrital

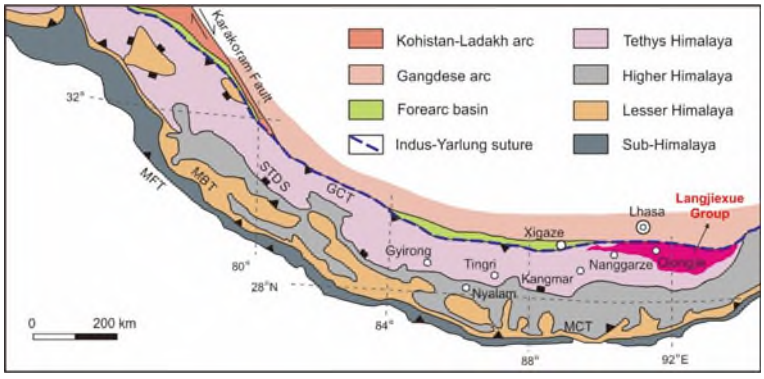

Fig. 64 Tectonic map shows distribution of the Langjixue Group

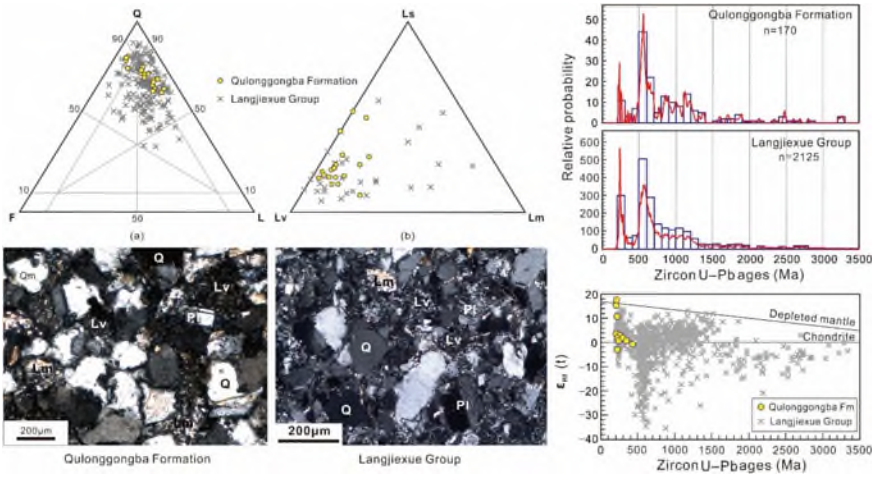

Fig. 65 A comparison of provenance feature between the Langjixue Group and the Qulonggongba Formation (Data are from Meng et al. 2019)

zircons in the Qulonggongba Fomration further proves that it has consistent provenance with the Langjiexue Group (Fig. 65). Because the Qulonggongba Formation certainly belongs to the Tethys Himalayan zone, the provenance similarity with the Langjiexue Group indicates that the latter is also an in situ Tethys Himalayan sedimentary sequence. That is to say, the Langjiexue Group is deep marine sediments of the north Indian margin.

Unique provenance features of the Langjiexue Group would be attributed to the special paleogeography during it was deposition. Wang et al. (2016a, b) suggested that Late Triassic rifting along the northwestern margin of astern Gondwana might have changed the original paleogeography. Thermal uplift rift would have formed a long relief that forced northwestward-draining river systems to be deflected southwestward, carrying detritus from the Gondwanide orogen to as far as the northern Indian margin and filling the huge turbiditic fan of the Langjiexue Group (Fig. 66). This model is somewhat analogous to the East African rift system, which forced the Nile River to flow northward along the strike of the rift to eventually reach the Mediterranean Sea. Although this working hypothesis still needs to be proven, discovery of syn-depositional bimodal volcanic rocks in the Langjiexue Group supports the model (Huang et al. 2018; Meng et al. 2021). Moreover, huge turbiditic fans are necessarily associated with big-river systems.

On this outcrop, turbiditic rocks of the Langjiexue Group are observed (Fig. 67).

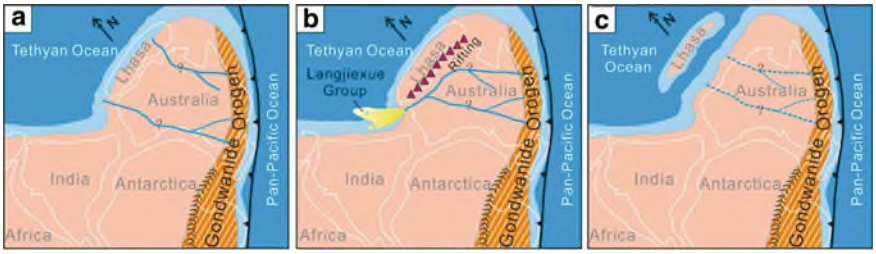

Fig. 66 Late Triassic paleogeographic evolution of northwestern margin of eastern Gondwana, showing depositional process of the Langjiexue Group (After Meng et al. 2019)

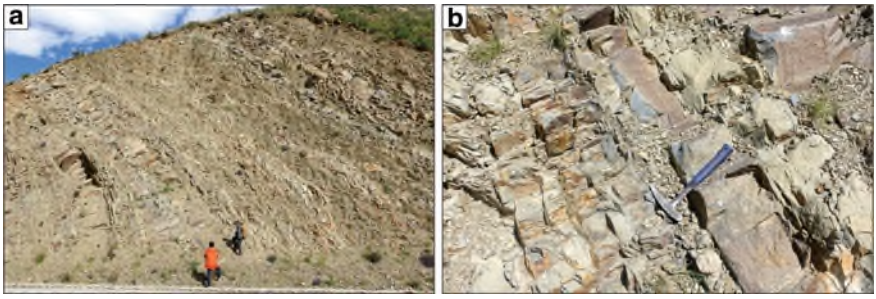

Fig. 67 Field photos of the Langjixue Group in Nanggarze area. Photos are provided by Jian-Gang Wang

References

Aitchison J, Badengzhu DA, Liu J, Luo H, Malpas J, McDermid I, Wu H, Ziabrev S, Zhou MF (2000) Remnants of a Cretaceous intra-oceanic subduction system within the Yarlung-Zangbo suture (southern Tibet). Earth Planet Sci Lett 183:231–244

Aitchison JC, Ali JR, Chan A, Davis AM, Lo CH (2009) Tectonic implications of felsic tuffs within the Lower Miocene Gangrinboche conglomerates, southern Tibet. J Asian Earth Sci 34:287–297

Allègre CJ, Courtillot V, Tapponnier P, Hirn A, Mattauer M, Coulon C, Jaeger JJ, Achache J, Schärer U, Marcoux J, Burg JP, Girardeau J, Armijo R, Gariépy C, Göpel C, Li TD, Xiao XC, Chang CF, Li GQ, Lin BY, Teng JW, Wang NW, Chen GM, Han TL, Wang XB, Den WM, Sheng HB, Cao YG, Zhou J, Qiu HR, Bao PS, Wang SC, Wang BX, Zhou YX, Xu RH (1984) Structure and evolution of the Himalaya-Tibet orogenic belt. Nature 307:17–22

An W, Hu X, Garzanti E, BouDagher-Fadel MK, Wang J, Sun G (2014) Xigaze forearc basin revisited (South Tibet): provenance changes and origin of the Xigaze Ophiolite. Geol Soc Am Bull 126(11–12):1595–1613

An W, Hu X, Garzanti E (2017) Sandstone provenance and tectonic evolution of the Xiukang Mélange from Neotethyan subduction to India–Asia collision (Yarlung-Zangbo suture, south Tibet). Gondwana Res 41:222–234

An W, Hu X, Garzanti E (2018a) Discovery of Upper Cretaceous Neo-Tethyan trench deposits in south Tibet (Luogangcuo Formation). Lithosphere 10(3):446–459

An X, Zhang Y, Zhu T, Zhang Y, Yuan D (2018b) Stable carbon isotope characteristics of Permian-Triassic boundary at the Selong Xishan Section. Earth Sci 43:2848–2857

An W, Hu X, Garzanti E, Wang JG, Liu Q (2021) New precise dating of the India–Asia collision in the Tibetan Himalaya at 61 Ma. Geophys Res Lett 48:e2020GL090641. https://doi.org/10.1029/2020GL090641

Bao PS, Su L, Wang J, Zhai QG (2013) Study on the Tectonic Setting for the Ophiolites in Xigaze, Tibet. Acta Geol Sin-Engl Ed 87(2):395–425

Bedard E, Hebert R, Guilmette C, Lesage G, Wang CS, Dostal J (2009) Petrology and geochemistry of the Saga and Sangsang ophiolitic massifs, Yarlung Zangbo Suture Zone, Southern Tibet: evidence for an arc-back-arc origin. Lithos 113:48–67

Brookfield M (1993) The Himalayan passive margin from Precambrian to Cretaceous Times. Sed Geol 84:1–35

Burg JP, Leyreloup A, Girardeau J, Chen GM (1987) Structure and Metamorphism of a Tectonically Thickened Continental Crust: the Yalu Tsangpo Suture Zone (Tibet): Philosophical Transactions of the Royal Society of London. Ser A, Math Phys Sci 321(1557):67–86

Cai F, Ding L, Leary RJ, Wang H, Xu Q, Zhang L, Yue Y (2012) Tectonostratigraphy and provenance of an accretionary complex within the Yarlung-Zangpo suture zone, southern Tibet: insights into subduction–accretion processes in the Neo-Tethys. Tectonophysics 574–575:181–192

Cai F, Ding L, Laskowski AK, Kapp P, Wang H, Xu Q, Zhang L (2016) Late Triassic paleogeographic reconstruction along the Neo-Tethyan Ocean margins, southern Tibet. Earth Planet Sci Lett 435:105–114

Carrapa B, Orme DA, DeCelles PG, Kapp P, Cosca MA, Waldrip R (2014) Miocene burial and exhumation of the India-Asia collision zone in southern Tibet: response to slab dynamics and erosion. Geology 42(5):443–446

Chauvel C, Marini JC, Plank T, Ludden JN (2009) Hf-Nd input flux in the Izu-Mariana subduction zone and recycling of subducted material in the mantle. Geochem Geophys Geosyst 10(1):Q01001

Chen GW, Xia B (2008) Platinum-group elemental geochemistry of mafic and ultramafic rocks from the Xigaze ophiolite, southern Tibet. J Asian Earth Sci 32(5–6):406–422

Chen X, Wang CS, Kuhnt W, Holbourn A, Huang YJ, Ma C (2011) Lithofacies, microfacies and depositional environments of Upper Cretaceous Oceanic red beds (Chuangde Formation) in southern Tibet. Sed Geol 235:100–110

Chen X, Idakieva V, Stoykova K, Liang H, Yao H, Wang C (2017) Ammonite biostratigraphy and organic carbon isotope chemostratigraphy of the Early Aptian oceanic anoxic event (OAE 1a) in the Tethyan Himalaya of southern Tibet. Palaeogeogr Palaeoclim Paleoecol 485:531–542

Chen SS, Fan WM, Shi RD, Liu XH, Zhou XJ (2018) 118–115 Ma magmatism in the Tethyan Himalaya igneous province: constraints on Early Cretaceous rifting of the northern margin of Greater India. Earth Planet Sci Lett 491:21–33

Chu MF, Chung SL, O'Reilly SY, Pearson NJ, Wu FY, Li XH, Liu D, Ji J, Chu CH, Lee HY (2011) India's hidden inputs to Tibetan orogeny revealed by Hf isotopes of Transhimalayan zircons and host rocks. Earth Planet Sci Lett 307(3–4):479–486

Chung SL, Liu D, Ji J, Chu MF, Lee HY, Wen DJ, Lo CH, Lee TY, Qian Q, Zhang Q (2003) Adakites from continental collision zones: Melting of thickened lower crust beneath southern Tibet. Geology 31:1021–1024

Chung SL, Chu MF, Zhang YQ, Xie YW, Lo CH, Lee TY, Lan CY, Li XH, Zhang Q, Wang YZ (2005) Tibetan tectonic evolution inferred from spatial and temporal variations in post-collisional magmatism. Earth-Sci Rev 68:173–196

Colleps CL, McKenzie NR, Horton BK, Webb AAG, Ng YW, Singh BP (2020) Sediment provenance of pre- and post-collisional Cretaceous-Paleogene strata from the frontal Himalaya of northwest India. Earth Planet Sci Lett 534:116079

Dai JG, Wang CS, Hébert R, Santosh M, Li YL, Xu JY (2011) Petrology and geochemistry of peridotites in the Zhongba ophiolite, Yarlung Zangbo Suture Zone: implications for the Early Cretaceous intra-oceanic subduction zone within the Neo-Tethys. Chem Geol 288(3–4):133–148

Dai J, Wang C, Li Y (2012) Relicts of the Early Cretaceous seamounts in the central-western Yarlung Zangbo Suture Zone, southern Tibet. J Asian Earth Sci 53:25–37

Dai J, Wang C, Polat A, Santosh M, Li Y, Ge Y (2013) Rapid forearc spreading between 130 and 120 Ma: evidence from geochronology and geochemistry of the Xigaze ophiolite, southern Tibet. Lithos 172–173:1–16

Dai JG, Wang CS, Zhu DC, Li YL, Zhong HT, Ge YK (2015) Multi-stage volcanic activities and geodynamic evolution of the Lhasa terrane during the Cretaceous: insights from the Xigaze forearc basin. Lithos 218:127–140

Dai JG, Wang CS, Stern RJ, Yang K, Shen J (2021) Forearc magmatic evolution during subduction initiation: insights from an Early Cretaceous Tibetan ophiolite and comparison with the Izu-Bonin-Mariana forearc. GSA Bull 133:753–776

Davis AM, Aitchison JC, Luo H, Zyabrev S (2002) Paleogene island arc collision-related conglomerates, Yarlung-Tsangpo suture zone, Tibet. Sedimentary Geology 150(3):247–273

DeCelles PG, Kapp P, Quade J, Gehrels GE (2011) Oligocene-Miocene Kailas basin, southwestern Tibet: record of postcollisional upper-plate extension in the Indus-Yarlung suture zone. Geol Soc Am Bull 123(7–8):1337–1362

DeCelles P, Kapp P, Gehrels G, Ding L (2014) Paleocene-Eocene foreland basin evolution in the Himalaya of southern Tibet and Nepal: implications for the age of initial India–Asia collision. Tectonics 33(5):824–849

Ding L, Xu Q, Yue YH, Wang HQ, Cai FL, Li S (2014) The Andean-type Gangdese Mountains: Paleoelevation record from the Paleocene-Eocene Linzhou Basin. Earth Planet Sci Lett 392:250–264

Ding L, Kapp P, Wan XQ (2005) Paleocene–Eocene record of ophiolite obduction and initial India-Asia collision, south central Tibet. Tectonics 24:TC3001

Ding L (2003) Paleocene deep-water sediments and radiolarian faunas: implications for evolution of Yarlung-Zangbo foreland basin, southern Tibet. Sci China Ser D: Earth Sci 46

Dubois-Côté V, Hébert R, Dupuis C, Wang CS, Li YL, Dostal J (2005) Petrological and geochemical evidence for the origin of the Yarlung Zangbo ophiolites, southern Tibet. Chem Geol 214(3–4):265–286

Dupuis C, Hébert R, Dubois-Côté V, Guilmette C, Wang CS, Li YL, Li ZJ (2005) The Yarlung Zangbo Suture Zone ophiolitic mélange (southern Tibet): new insights from geochemistry of ultramafic rocks. J Asian Earth Sci 25(6):937–960

Dürr SB (1996) Provenance of Xigaze fore-arc basin clastic rocks (Cretaceous, south Tibet). GSA Bull 108(6):669–684

Fan HH (2021) Early Cretaceous cold seep carbonates in Dingri, Southern Tibet: the feather and formation model. Master thesis, China University of Geosciences (Beijing) (in Chinese with English abstract)

Fang AM, Yan Z, Liu XH, Pan YS, Li JL, Yu LJ, Tao JR (2004) The age of the plant fossil assemblage in the Liuqu Conglomerate of southern Tibet and its tectonic significance (in Chinese with English abstract). Prog Nat Sci 14:1419–1427

Fu H, Hu X, Crouch EM, An W, Wang J, Garzanti E (2018) Upper Cretaceous trench deposits of the Neo-Tethyan subduction zone: Jiachala Formation from Yarlung Zangbo suture zone in Tibet, China. Sci China Earth Sci 61(9):1204–1220

Gale A, Dalton CA, Langmuir CH, Su Y, Schilling JG (2013) The mean composition of ocean ridge basalts. Geochem Geophys Geosyst 14(3):489–518

Gansser (1964) Geology of the Himalayas. Interscience Publishers John Wiley and Sons, New York, pp 1–289

Garzanti E, Van Haver T (1988) The Indus clastics: forearc basin sedimentation in the Ladakh Himalaya (India). Sed Geol 59(3):237–249

Garzione CN, DeCelles PG, Hodkinson DG, Ojha TP, Upreti BN (2003) East-west extension and Miocene environmental change in the southern Tibetan plateau: Thakkhola graben, central Nepal. Geol Soc Am Bull 115(1):3–20

Girardeau J, Marcoux J, Zao Y (1984) Lithologic and tectonic environment of the Xigaze ophiolite (Yarlung Zangbo suture zone, southern Tibet, China), and kinematics of its emplacement. Eclogae Geol Helv 77:153–170

Girardeau J, Mercier JCC, Xibin W (1985a) Petrology of the mafic rocks of the Xigaze ophiolite, Tibet: implications for the genesis of the oceanic lithosphere. Contrib Miner Petrol 90(4):309–321

Girardeau J, Mercier JCC, Yougong Z (1985b) Origin of the Xigaze ophiolite, Yarlung Zangbo suture zone, southern Tibet. Tectonophysics 119(1–4):407–433

Guilmette C, Hébert R, Wang C, Villeneuve M (2009) Geochemistry and geochronology of the metamorphic sole underlying the Xigaze Ophiolite, Yarlung Zangbo Suture Zone, South Tibet. Lithos 112(1–2):149–162

Guilmette C, Hebert R, Dostal J, Indares A, Ullrich T, Bedard E, Wang CS (2012) Discovery of a dismembered metamorphic sole in the Saga ophiolitic melange, South Tibet: assessing an early cretaceous disruption of the Neo-Tethyan suprasubduction zone and consequences on basin closing. Gondwana Res 22(2):398–414

Guo T, Liang DY, Zhang YZ, Zhao CH (1991) Geology of Nagri, Tibet (Xizang). China University of Geosciences Press, Wuhan, p 464

Guo H, Chen X, Yao H, Han K, Garzanti E, Liu X, Fan H (2021) Lower Cretaceous clastic dykes in southern Tibet: characteristics and palaeogeographic significance. Geol J 56:1726–1739

Hallam A (1981) A revised sea-level curve for the early Jurassic. J Geol Soc 138:735–743

Hallam A, Wignall PB, Yin J, Riding JB (2000) An investigation into possible facies changes across the triassic–jurassic boundary in southern tibet. Sed Geol 137:101–106

Hampel A, Adam J, Kukowski N (2004) Response of the tectonically erosive south Peruvian forearc to subduction of the Nazca Ridge: analysis of three-dimensional analogue experiments. Tectonics 23

Han Z, Hu X, Li J, Garzanti E (2016) Jurassic carbonate microfacies and relative sea-level changes in the Tethys Himalaya (southern Tibet). Palaeogeogr Palaeoclimatol Palaeoecol 456:1–20

Han Z, Hu X, BouDagher-Fadel M, Jenkyns HC, Franceschi M (2021a) Early Jurassic carbon-isotope perturbations in a shallow water succession from the Tethys Himalaya, southern hemisphere. Newsl Stratigr 54:461–481

Han Z, Hu X, Boudagher-Fadel MK, Jenkyns HC, Franceschi M (2021b) Early Jurassic carbon-isotope perturbations in a shallow-water succession from the Tethys Himalaya, southern hemisphere. Newsl Stratigr 54(4):461–481

Han Z, Hu X, He T, Newton RJ, Jenkyns HC, Jamieson RA, Franceschi M (2022) Early Jurassic long-term oceanic sulfur-cycle perturbations in the Tibetan Himalaya. Earth Planet Sci Lett 578:117261

Han Z, Hu X, Hu Z, Jenkyns H, Su T, Geochemical evidence from the Kioto Carbonate Platform (Tibet) reveals enhanced terrigenous input and deoxygenation during the early Toarcian. Glob Planet Chang, In review

Han KB, Chen X, Garzanti E, Yao HW, Guo HF, Liu X, Zhu SP, Formation process of the Mid-Jurassic oolitic ironstone in Nyalam area, southern Tibet: implications for the paleoceanography in eastern Tethys margin. Unpublished

Hao Y, Wan X (1985) The marine Cretaceous and Tertiary strata of Tingri, Xizang (Tibet). Contribution to the Geology of the Qinghai-Xizang (TIBET) Plateau 17:227–332 (in Chinese with English abstract)

Harrison TM, Copeland P, Kidd WSF, Yin A (1992) Raising Tibet. Science 255:1663–1670

Hébert R, Bezard R, Guilmette C, Dostal J, Wang CS, Liu ZF (2012) The Indus-Yarlung Zangbo ophiolites from Nanga Parbat to Namche Barwa syntaxes, southern Tibet: first synthesis of petrology, geochemistry, and geochronology with incidences on geodynamic reconstructions of Neo-Tethys. Gondwana Res 22(2):377–397

Hébert R, Huot F, Wang CS, Liu ZF (2003) Yarlung Zangbo ophiolites (Southern Tibet) revisited: geodynamic implications from the mineral record. In: Dilek Y, Robinson PT (eds) Ophiolites in earth history, vol 218. Geological Society, London, Special Publications, 165–190

Hesselbo S, Jenkyns H (1998) British Lower Jurassic Sequence Stratigraphy, pp 561–581

Hou ZQ, Gao YF, Qu XM, Rui ZY, Mo XX (2004) Origin of adakitic intrusives generated during mid-Miocene east-west extension in southern Tibet. Earth Planet Sci Lett 220:139–155

Hou ZQ, Yang ZM, Qu XM, Meng XJ, Li ZQ, Beaudoin G, Rui ZY, Gao YF, Zaw K (2009) The Miocene Gangdese Porphyry copper belt generated during post-collisional extension in the Tibetan orogeny. Ore Geol Rev 36:25–51

Hou ZQ, Duan LF, Lu YJ, Zheng YC, Zhu DC, Yang ZM, Yang ZS, Wang BD, Pei YR, Zhao ZD, McCuaig TC (2015) Lithospheric architecture of the Lhasa Terrane and its control on ore deposits in the Himalayan-Tibetan Orogen. Econ Geol 110:1541–1575

Hu H, Stern RJ (2020) Early Cretaceous subduction initiation beneath southern Tibet caused the northward flight of India. Geosci Front 11(4):1123–1131

Hu XM, Luba J, Sarti M (2006) Mid-Cretaceous oceanic red beds in the Umbria–Marche Basin, central Italy: constraints on paleoceanography and paleoclimate. Palaeogeogr Palaeoclimatol Palaeoecol 233:163–186

Hu XM, Jansa L, Wang CS (2008) Upper Jurassic-Lower Cretaceous stratigraphy in south-eastern Tibet: a comparison with the western Himalayas. Cretac Res 29:301–315

Hu XM, Sinclair HD, Wang JG, Jiang HH, Wu FY (2012) Late Cretaceous-Palaeogene stratigraphic and basin evolution in the Zhepure Mountain of southern Tibet: implications for the timing of India–Asia initial collision. Basin Res 24(5):520–543

Hu XM, Garzanti E, Moore T, Raffi I (2015) Direct stratigraphic dating of India-Asia collision onset at the Selandian (middle Paleocene, 59±1Ma). Geology 43(10):859–862

Hu XM, Wang JG, BouDagher-Fadel M, Garzanti E, An W (2016b) New insights into the timing of the India–Asia collision from the Paleogene Quxia and Jialazi Formations of the Xigaze forearc basin, South Tibet. Gondwana Res 32:76–92

Hu XM, An W, Garzanti E, Liu Q (2020) Recognition of trench basins in collisional orogens: Insights from the Yarlung Zangbo suture zone in southern Tibet. Sci China Earth Sci 63:2017–2028

Hu XM, Garzant IE, Wang JG, Huang WT, An W, Webb A (2016a) The timing of India–Asia collision onset—Facts, theories, controversies. Earth-Sci Rev 160:264–299

Hu X, Wang J, An W, Garzanti E, Li J (2017) Constraining the timing of the India–Asia continental collision by the sedimentary record. Sci China Earth Sci 60

Huang WT, van Hinsbergen DJJ, Maffione M, Orme DA, Dupont-Nivet G, Guilmette C, Ding L, Guo ZJ, Kapp P (2015) Lower Cretaceous Xigaze ophiolites formed in the Gangdese forearc: evidence from paleomagnetism, sediment provenance, and stratigraphy. Earth Planet Sci Lett 415:142–153

Huang Y, Cao HW, Li GM, Brueckner SM, Zhang Z, Dong L, Dai ZW, Lu L, Li YB (2018) Middle-Late Triassic bimodal intrusive rocks from the Tethyan Himalaya in South Tibet: geochronology, petrogenesis and tectonic implications. Lithos 318:78–90

Ishizuka O, Tani K, Reagan MK, Kanayama K, Umino S, Harigane Y, Sakamoto I, Miyajima Y, Yuasa M, Dunkley DJ (2011) The timescales of subduction initiation and subsequent evolution of an oceanic island arc. Earth Planet Sci Lett 306(3–4):229–240

Ishizuka O, Hickey-Vargas R, Arculus RJ, Yogodzinski GM, Savov IP, Kusano Y, McCarthy A, Brandl PA, Sudo M (2018) Age of Izu-BoninMariana arc basement. Earth Planet Sci Lett 481:80–90

Jadoul F, Berra F, Garzanti E (1998) The Tethys Himalayan passive margin from Late Triassic to Early Cretaceous (South Tibet). J Asian Earth Sci 16:173–194

Ji WQ, Wu FY, Chung SL, Li JX, Liu CZ (2009) Zircon U-Pb geochronology and Hf isotopic constraints on petrogenesis of the Gangdese batholith, southern Tibet. Chem Geol 262:229–245

Jiang S, Song H, Kemp DB, Dai X, Liu X (2020) Two pulses of extinction of larger benthic foraminifera during the Pliensbachian–Toarcian and early Toarcian environmental crises. Palaeogeogr Palaeoclimatol Palaeoecol 560:109998

Jiang JX, Hu XM, Li J, BouDagher-Fadel, Garzanti E (2021) Discovery of the Paleocene-Eocene thermal maximum in shallow-marine sediments of the Xigaze forearc basin, Tibet: a record of enhanced extreme precipitation and siliciclastic sediment flux. Palaeogeogr Palaeoclimatol Palaeoecol 562:110095

Jin X, Huang H, Shi Y, Zhan L (2015) Origin of Permian exotic limestone blocks in the Yarlung Zangbo Suture Zone, Southern Tibet, China: with biostratigraphic, sedimentary and regional geological constraints. J Asian Earth Sci 104:22–38

Kang ZQ, Xu JF, Wilde SA, Feng ZH, Chen JL, Wang BD, Fu WC, Pan HB (2014) Geochronology and geochemistry of the Sangri Group Volcanic Rocks, Southern Lhasa Terrane: implications for the early subduction history of the Neo-Tethys and Gangdese Magmatic Arc. Lithos 200–201:157–168

Kapp P, DeCelles PG, Leier AL, Fabijanic JM, He S, Pullen A, Gehrels GE (2007) The Gangdese retroarc thrust belt revealed. GSA Today 17(7):4–9

Leary RJ, DeCelles PG, Quade J, Gehrels G, Waanders G (2016) The Liuqu Conglomerate, southern Tibet: early Miocene basin development related to deformation within the Great Counter Thrust system. Lithosphere 8(5):427–450

Lee HY, Chung SL, Lo CH, Ji J, Lee TY, Qian Q, Zhang Q (2009) Eocene Neotethyan slab breakoff in southern Tibet inferred from the Linzizong volcanicrecord. Tectonophysics 477:20–35

Leier AL, DeCelles PG, Kapp P, Ding L (2007a) The Takena Formation of the Lhasa terrane, southern Tibet: the record of a Late Cretaceous retroarc foreland basin. Geol Soc Am Bull 119:31–48

Leier AL, DeCelles PG, Kapp P, Gehrels GE (2007b) Lower Cretaceous strata in the Lhasa Terrane, Tibet, with implications for understanding the early tectonic history of the Tibetan Plateau. J Sediment Res 77:809–825

Li XH, Wang CS, Hu XM (2005) Stratigraphy of deep-water Cretaceous deposits in Gyangze, southern Tibet, China. Cretac Res 26:33–41

Li XH, Jenkyns HC, Wang CS, Hu XM, Chen X, Wev Y, Huang YJ, Cui J (2006) Upper Cretaceous carbon- and oxygen-isotope stratigraphy of hemipelagic carbonate facies from southern Tibet, China. J Geol Soc 163:375–382

Li YL, Wang CS, Hu XM, Bak M, Wang JG, Chen L (2007) Characteristics of early Eocene radiolarian assemblages of the Saga area, southern Tibet and their constraint on the closure history of the Tethys. Chin Sci Bull 52:2108–2114

Li JF, Xia B, Liu LW, Xu LF, He GS, Wang H, Zhang YQ, Yang ZQ (2009) SHRIMP U-Pb dating for the gabbro in the Qunrang ophiolite, Tibet: the geochronology constraint for the development of eastern Tethys basin. Geotecton Metallog 33(2):294–298

Li JG, Guo Z, Batten DJ, Cai H, Zhang Y (2010) Palynological stratigraphy of the Late Cretaceous and Cenozoic collision-related conglomerates at Qiabulin, Xigaze, Xizang (Tibet) and its bearing on palaeoenvironmental development. J Asian Earth Sci 38:86–95

Li WX, Zhao ZD, Zhu DC, Dung GC, Zhou S, Mo XX, DePaolo D, Dilek Y (2012) Geochemical discrimination of tectonic environments of the Yarlung Zangpo ophiolite in southern Tibet. Acta Petrol Sin (Yanshi Xuebao) 28(5):1663–1673

Li GW, Kohn B, Sandiford M, Xu ZQ, Wei L (2015a) Constraining the age of Liuqu Conglomerate, southern Tibet: Implications for evolution of the India–Asia collision zone. Earth Planet Sci Lett 426:259–266

Li J, Hu X, Garzanti E, An W, Wang J (2015b) Paleogene carbonate microfacies and sandstone provenance (Gamba area, South Tibet): stratigraphic response to initial India–Asia continental collision. J Asian Earth Sci 104:39–54

Li M, Song H, Woods AD, Dai X, Wignall PB (2019b) Facies and evolution of the carbonate factory during the Permian-Triassic crisis in South Tibet, China. Sedimentology 66:3008–3028

Li J, Hu X, Garzanti E, Banerjee S, BouDagher-Fadel M (2020a) Late Cretaceous topographic doming caused by initial upwelling of Deccan magmas: Stratigraphic and sedimentological evidence. Geol Soc Am Bull 132:835–849

Li J, Hu X, Garzanti E, BouDagher-Fadel M (2021) Climate-driven hydrological change and carbonate platform demise induced by the Paleocene-Eocene thermal maximum (southern Pyrenees). Palaeogeogr Palaeoclimatol Palaeoecol 567:110250

Li J, Hu X, Garzanti E, Banerjee S, Boudagher-Fadel M (2019) Late cretaceous topographic doming caused by initial upwelling of deccan magmas: stratigraphic and sedimentological evidence. Geol Soc Am Bull 132(3–4)

Li J, Hu XM, Zachos JC, Garzanti E, BouDagher-Fadel M (2020) Sea level, biotic and carbon-isotope response to the Paleocene–Eocene thermal maximum in Tibetan Himalayan platform carbonates. Glob Planet Chang 103316

Li X, Hu X, An W, Liu Q, Garzanti E, Jun M (2022) From Neo-Tethyan convergence to India–Asia collision: radiolarian biostratigraphy of the Cretaceous to Paleocene deep-water Tethys Himalaya. Newsletters Strat

Liang H, Chen X, Wang C, Zhao D, Weissert H (2016) Methane-derived authigenic carbonates of mid-Cretaceous age in southern Tibet: types of carbonate concretions, carbon sources, and formation processes. J Asian Earth Sci 115:153–169

Liu G, Einsele G (1994) Sedimentary history of the Tethyan basin in the Tibetan Himalayas. Geol Rundsch 83(1):32–61

Liu CJ, Yin JX, Sun XX, Sun YY (1988) Marine Late Cretacous–early Tertiary sequences—the non-flysch deposits of the Xigaze Forearc Basin in the south Xizang. Mem Inst Geol, Acad Sin 3:130–157 (in Chinese)

Liu CZ, Zhang C, Yang LY, Zhang LL, Ji WQ, Wu FY (2014) Formation of gabbronorites in the Purang ophiolite (SW Tibet) through melting of hydrothermally altered mantle along a detachment fault. Lithos 205:127–141

Liu T, Wu FY, Zhang LL, Zhai QG, Liu CZ, Ji WB, Zhang C, Xu Y (2016) Zircon U-Pb geochronological constraints on rapid exhumation of the mantle peridotite of the Xigaze ophiolite, southern Tibet. Chem Geol 443:67–86

Liu T, Wu FY, Liu CZ, Tribuzio R, Ji WB, Zhang C, Xu Y, Zhang WQ (2018) Variably evolved gabbroic intrusions within the Xigaze ophiolite (Tibet): new insights into the origin of ophiolite diversity. Contrib Miner Petrol 173(11):91

Liu T, Wu FY, Liu CZ, Zhang C, Ji WB, Xu Y (2019) Reconsideration of Neo-Tethys evolution constrained from the nature of the Dazhuqu ophiolitic mantle, southern Tibet. Contrib Miner Petrol 174(3):23

Liu YM, Dai JG, Wang CS, Li HA, Wang Q, Zhang LL (2020) Provenance and tectonic setting of Upper Triassic turbidites in the eastern Tethyan Himalaya: Implications for early-stage evolution of the Neo-Tethys. Earth Sci Rev 200:103030

Liu Q, Kneller B, An W, Hu X (2021) Sedimentological responses to initial continental collision: triggering of sand injection and onset of mass movement in a syn-collisional trench basin, Saga, southern Tibet. J Geol Soc 178(6)

Liu X, Zhang Y, Han KB, Batenburg SJ, Guo HF, Ma C, Yao HW, Fan HH, Wu Q, Chen X, Chemo- and Cyclostratigraphic records of the Albian from the Tethyan Himalaya of southern Tibet, China. In review

Maffione M, van Hinsbergen DJJ, Koornneef LMT, Guilmette C, Hodges K, Borneman N, Huang W, Ding L, Kapp P (2015) Forearc hyperextension dismembered the south Tibetan ophiolites. Geology 43(6):475–478

Mahéo G, Leloup PH, Valli F, Lacassin R, Arnaud N, Paquette JL, Fernandez A, Haibing L, Farley KA, Tapponnier P (2007) Post 4 Ma initiation of normal faulting in southern Tibet. Constraints from the Kung Co half graben. Earth Planet Sci Lett 256(1):233–243

Malpas J, Zhou MF, Robinson PT, Reynolds PH (2003) Geochemical and geochronological constraints on the origin and emplacement of the Yarlung Zangbo ophiolites, southern Tibet. In Dilek Y, Robinson PT (eds) Ophiolites in Earth History: Geological Society [London] Special Publication, vol 218, pp 191–206

Meng ZY, Wang JG, Ji WQ, Zhang H, Wu FY, Garzanti E (2019) The Langjiexue Group is an in situ sedimentary sequences rather than an exotic block: constraints from coeval Upper Triassic strata of the Tethys Himalaya (Qulonggongba Formation). Sci China Earth Sci 62:83–79

Meng ZY, Wang JG, Garzanti E, Han Z, Chen G (2021) Late Triassic rifting and volcanism on the northeastern Indian margin: a new phase of Neo-Tethyan seafloor spreading and its paleogeographic implications. Palaeogeogr Palaeoclimatol Palaeoecol 570:110367

Metcalf K, Kapp P (2019) History of subduction erosion and accretion recorded in the Yarlung Suture Zone, southern Tibet. Geol Soc, Lond, Spec Publ 483(1):517–554

Mo XX, Niu YL, Dong GC, Zhao ZD, Hou ZQ, Zhou S, Ke S (2008) Contribution of syncollisional felsic magmatism to continental crust growth: a case study of the Paleocene Linzizong Volcanic Succession in southern Tibet. Chem Geol 250:49–67

Murphy MA, Yin A, Harrison TM, Dürr SB, Chen Z, Ryerson FJ, Kidd WSF, Wang X, Zhou X (1997) Did the Indo–Asian collision alone create the Tibetan Plateau? Geology 25(8):719–722

Najman Y, Appel E, Boudagher-Fadel M, Bown P, Carter A, Garzanti E, Godin L, Han J, Liebke U, Oliver G, Parrish R, Vezzoli G (2010) Timing of India–Asia collision: geological, biostratigraphic, and palaeomagnetic constraints. J Geophys Res, Solid Earth 115(B12):B12416

Najman Y, Jenks D, Godin L, Boudagher-Fadel M, Millar I, Garzanti E, Horstwood M, Bracciali L (2017) The Tethyan Himalayan detrital record shows that India–Asia terminal collision occurred by 54 Ma in the Western Himalaya. Earth Planet Sci Lett 459:301–310

Nicolas A, Girardeau J, Marcoux J, Dupre B, Wang XB, Cao YG, Zheng HX, Xiao XC (1981) The Xigaze ophiolite (Tibet): a peculiar oceanic lithosphere. Nature 294:414–417

Niu XL, Zhao ZD, Mo XX, Depaolo DJ, Dong G, Zhang SQ, Zhu DC, Guo TY (2006) Elemental and Sr-Nd-Pb isotopic geochemistry for basic rocks from Decun–Angren ophiolites in Xigaze area, Tibet: implications for the characteristics of the Tethyan upper mantle domain. Acta Petrol Sin (Yanshi Xuebao) 22(12):2875–2888

Orchard M, Nassichuk W, Rui L (1994) Conodonts from the lower Griesbachian Otoceras Latilobatum Bed of Selong, Tibet and the position of the Permian—Triassic Boundary

Orme DA, Carrapa B, Kapp P (2014) Sedimentology, provenance and geochronology of the upper Cretaceous–lower Eocene western Xigaze forearc basin, southern Tibet. Basin Res 387–411

Orme DA, Laskowski AK (2016) Basin analysis of the Albian-Santonian Xigaze Forearc, Lazi Region, South-Central Tibet. J Sediment Res 86(8):894–913

Ratschbacher L, Frisch W, Liu G, Chen C (1994) Distributed deformation in southern and western Tibet during and after the India–Asia collision. J Geophys Res Atmos 99:19917–19945

Reagan MK, Pearce JA, Petronotis K, Almeev RR, Avery AJ, Carvallo C, Chapman T, Christeson GL, Ferré EC, Godard M, Heaton DE, Kirchenbaur M, Kurz W, Kutterolf S, Li H, Li Y, Michibayashi K, Morgan S, Nelson WR, Prytulak J, Python M, Robertson AHF, Ryan JG, Sager WW, Sakuyama T, Shervais JW, Shimizu K, Whattam SA (2017) Subduction initiation and ophiolite crust: new insights from IODP drilling. Int Geol Rev 59(11):1439–1450

Reagan MK, Ishizuka O, Stern RJ, Kelley KA, Ohara Y, Blichert-Toft J, Bloomer SH, Cash J, Fryer P, Hanan BB, Hickey-Vargas R, Ishii T, Kimura J-I, Peate DW, Rowe MC, Woods M (2010) Fore-arc basalts and subduction initiation in the Izu-Bonin-Mariana system. Geochem Geophys Geosystems 11(3):Q03X12

Sciunnach D, Garzanti E (2012) Subsidence history of the Tethys Himalaya. Earth-Sci Rev 111:179–198

Shen SZ, Archbold NW, Shi GR, Zhong-Qiang C (2000) Permian brachiopods from the SelongXishan section, Xizang (Tibet), China Part 1: stratigraphy, strophomenida, productida and rhynchonellida. Geobios-Lyon 33:725–752

Shen S, Dongli S, Shi GR (2003a) A biogeographically mixed late Guadalupian (late Middle Permian) brachiopod fauna from an exotic limestone block at Xiukang in Lhaze county, Tibet. Journal of Asian Earth Sciences 21(10):1125–1137

Shen S, Shi GR, Archbold NW (2003b) A Wuchiapingian (Late Permian) brachiopod fauna from an exotic block in the Indus–Tsangpo suture zone, southern Tibet, and its palaeobiogeographical and tectonic implications. Palaeontology 46(2):225–256

Shen SZ, Cao CQ, Henderson CM, Wang XD, Shi GR, Wang Y, Wang W (2006) End-Permian mass extinction pattern in the northern peri-Gondwanan region. Palaeoworld 15:3–30

Sinclair H (1997) Tectonostratigraphic model for underfilled peripheral foreland basins: an Alpine perspective. Geol Soc Am Bull 109(3):324–346
Sinclair HD, Jaffey N (2001) Sedimentology of the Indus Group, Ladakh, northern India: implications for the timing of initiation of the palaeo-Indus River. J Geol Soc Lond 158:151–162
Stanley SM, Yang X (1994) A double mass extinction at the end of the Paleozoic era. Science 266:1340–1344
Sun GY, Hu XM, Wang JG (2011) Petrologic and provenance analysis of the Zongzhuo mélange in Baisha area, Gyangze, Southern Tibet. Acta Geol Sin 85(8):1343–1351
Sun S, McDonough W (1989) Chemical and isotopic systematics of oceanic basalts: implications for mantle composition and processes. In Saunders AD, Norry MJ (eds) Magmatism in the Ocean Basins. Geological Society [London] Special Publication 42:313–345
Tao J (1988) Plant fossils from the Liuqu Formation in Lhaze County, Xizang and their paleoclimatological significances. Memoirs of the Institute of Geology, Chinese Academy of Science (in Chinesewith English abstract). Science Press, Beijing, pp 223–238
Tapponnier P, Mercier JL, Proust F, Andrieux J, Armijo R, Bassoullet JP, Brunel M, Burg JP, Colchen M, Dupre B, Girardeau J, Marcoux J, Mascle G, Matte P, Nicolas A, Li T, Xiao X, Chang C, Lin B, Li G, Wang N, Chen G, Han T, Wang X, Den W, Zhen H, Sheng H, Cao Y, Zhou J, Qiu H (1981) The Tibetan side of the India–Eurasia collision. Nature 294(5840):405–410
Tapponnier P, Zhiqin X, Roger F, Meyer B, Arnaud N, Wittlinger G, Jingsui Y (2001) Oblique stepwise rise and growth of the Tibet Plateau. Science 294:1671–1677
Volkmer JE, Kapp P, Guynn JH, Lai Q (2007) Cretaceous-Tertiary structural evolution of the north central Lhasa terrane, Tibet. Tectonics 26:TC6007
Wan X, Wang L, Wang C, Jansa L (1998) Discovery and significance of Cretaceous fossils from the Xigaze forearc basin, Tibet. J Asian Earth Sci 16(2):217–224
Wan XQ, Ding L, Li JG, Cai HW (2001) Latest Cretaceous to Early Eocenemarine strata in the Zhongba region, Tibet. J Stratigr 25(4):267–272
Wan XQ, Lamolda MA, Si JL, Li GB (2005) Foraminiferal stratigraphy of Late Cretaceous red beds in southern Tibet. Cretac Res 26:43–48
Wang C, Liu Z (1999) Xigaze forearc basin and Yarlung Zangbo suture zone. Geological Publishing House, Tibet
Wang YJ, Mu XN (1980) Some new observation on the Permian biostratigraphy of the Himalayan province in southern Tibet. J Stratigr 4(2):145–151
Wang XD, Sugiyama T (2000) Diversity and extinction patterns of Permian coral faunas of China. Lethaia 33:285–294
Wang XB, Bao PS, Xiao XC (1987) Ophiolites of the Yarlung Zangbo River, Xizang (Tibet). Publishing House of Surveying and Mapping, Beijing, p 117
Wang C, Xia D, Zhou X, Chen J, Liu Z (1996) Field Trip Guide: T121/T387 geology between the Indus–Yarlung Zangbo Suture Zone and the Himalaya Mountains (Xizang), China. Geological Publishing House, Beijing, pp 49–156
Wang CS, Li XH, Hu XM, Jansa LF (2002) Latest marine horizon north of Qomolangma (Mt Everest): implications for closure of Tethys seaway and collision tectonics. Terra Nova 14:114–120
Wang CS, Hu XM, Sartid M, Scotte RW, Li XH (2005a) Upper Cretaceous oceanic red beds in southern Tibet: a major change from anoxic to oxic, deep-sea environments. Cretac Res 26:21–32
Wang R, Xia B, Zhou G, Zhang Y, Yang Z, Li W, Wei D, Zhong L, Xu L (2006) SHRIMP zircon U-Pb dating for gabbro from the Tiding ophiolite in Tibet. Chin Sci Bull 51(14):1776–1779
Wang JG, Hu XM, Wu FY, Jansa L (2010) Provenance of the Liuqu Conglomerate in southern Tibet: a Paleogene erosional record of the Himalayan–Tibetan orogen. Sed Geol 231(3–4):74–84
Wang JG, Hu XM, Jansa L, Huang ZC (2011) Provenance of the Upper Cretaceous-Eocene deep-water sandstones in Sangdanlin, southern Tibet: constraints on the timing of initial India–Asia collision. J Geol 119(3):293–309

Wang C, Li X, Liu Z, Li Y, Jansa L, Dai J, Wei Y (2012) Revision of the Cretaceous-Paleogene stratigraphic framework, facies architecture and provenance of the Xigaze forearc basin along the Yarlung Zangbo suture zone. Gondwana Res 22:415–433

Wang JG, Hu XM, Garzanti E, Wu FY (2013) Upper Oligocene-Lower Miocene Gangrinboche Conglomerate in the Xigaze area, southern Tibet: implications for Himalayan uplift and paleo-Yarlung-Zangbo initiation. J Geol 121(4):425–444

Wang JG, Hu X, BouDagher-Fadel M, Wu FY, Sun GY (2015) Early Eocene sedimentary recycling in the Kailas area, southwestern Tibet: implications for the initial India–Asia collision. Sed Geol 315:1–13

Wang C, Ding L, Zhang LY, Kapp P, Pullen A, Yue YH (2016a) Petrogenesis of Middle-Late Triassic volcanic rocks from the Gangdese belt, southern Lhasa terrane: Implications for early subduction of Neo-Tethyan oceanic lithosphere. Lithos 262:320–333

Wang JG, Wu FY, Garzanti E, Hu X, Ji WQ, Liu ZC, Liu XC (2016b) Upper Triassic turbidites of the northern Tethyan Himalaya (Langjiexue Group): the terminal of a sediment-routing system sourced in the Gondwanide Orogen. Gondwana Res 34:84–98

Wang JG, Hu X, Garzanti E, An W, Liu XC (2017a) The birth of the Xigaze forearc basin in southern Tibet. Earth Planet Sci Lett 465:38–47

Wang L, Wignall PB, Sun Y, Yan C, Zhang Z, Lai X (2017b) New Permian-Triassic conodont data from Selong (Tibet) and the youngest occurrence of Vjalovognathus. J Asian Earth Sci 146:152–167

Wang XC, Liu WL, Zhong Y, Hu XC, Xia B, Huang W (2018) Geochemical and zircon U-Pb age constraints on the origin of the Mesozoic Xigaze ophiolite, Yarlung Zangbo suture zone, SW China. Int Geol Rev 60(10):1267–1289

Wang JG, Hu X, Garzanti E, BouDagher-Fadel MK, Liu ZC, Li J, Wu FY (2020) From extension to tectonic inversion: Mid-Cretaceous onset of Andean-type orogeny in the Lhasa block and early topographic growth of Tibet. Geol Soc Am Bull 132(11–12):2432–2454

Wang CS, Li XH, Hu XM, Wan XQ, Yin JR, Huang YJ, Huang SJ, Li GB (2005) Tethyan Himalayan sedimentary geology and continental paleoceanography. Geological Publishing House, Beijing, p 373 (in Chinese)

Wei L, Liu X, Yan F, Mai X, Zhou X, Li G, Liu X (2009) Discovery and preliminary study on palynofossils from the Paleogene Liuqu Conglomerates in southern Xizang (Tibet). Acta Microbiol Sin 26:249–260

Willems H, Zhou Z, Zhang B, Gräfe KU (1996) Stratigraphy of the Upper Cretaceous and Lower Tertiary strata in the Tethyan Himalayas of Tibet (Tingri area, China). Geol Rundsch 85:723–754

Wu FY, Ji WQ, Liu CZ, Chung SL (2010) Detrital zircon U-Pb and Hf isotopic data from the Xigaze fore-arc basin: constraints on Transhimalayan magmatic evolution in southern Tibet. Chem Geol 271(1–2):13–25

Wu F, Ji W, Wang J, Liu C, Chung S, Clift PD (2014a) Zircon U-Pb and Hf isotopic constraints on the onset time of India–Asia collision. Am J Sci 314(2):548–579

Wu FY, Liu CZ, Zhang LL, Zhang C, Wang JG, Ji WQ, Liu XC (2014b) Yarlung Zangbo ophiolite: a critical updated view. Acta Petrol Sin (yanshi Xuebao) 30(2):293–325

Xiong Q, Griffin WL, Zheng JP, O'Reilly SY, Pearson NJ, Xu B, Belousova EA (2016) Southward trench migration at ~130–120 Ma caused accretion of the Neo-Tethyan forearc lithosphere in Tibetan ophiolites. Earth Planet Sci Lett 438:57–65

Xiong F, Yang J, Robinson PT, Gao J, Chen Y, Lai S (2017) Petrology and geochemistry of peridotites and podiform chromitite in the Xigaze ophiolite, Tibet: implications for a suprasubduction zone origin. J Asian Earth Sci 146(supplement C), 56–75

Yin A (2006) Cenozoic tectonic evolution of the Himalayan orogen as constrained by along-strike variation of structural geometry, exhumation history, and foreland sedimentation. Earth Sci Rev 76:1–131

Yin A, Harrison TM (2000) Geologic evolution of the Himalayan–Tibetan orogen. Annu Rev Earth Planet Sci 28:211–280

Yin A, Harrison TM, Ryerson FJ, Chen WJ, Kidd WSF, Copeland P (1994) Tertiary structural evolution of the Gangdese thrust system in southeastern Tibet. J Geophys Res 99:18175–18201

Yin J, Enay R, Wan X (1999) The first report of the late Triassic-Early Jurassic passage beds in the eastern tethyan himalaya. Comptes Rendus De Lacademie Des Sciences Serie II A Sciences De La Terre Et Des Planetes, 329, 0–133

Yin JR (2010) Jurassic ammonites of Tibet. Geological Publishing House, Beijing, pp 227–235 (in Chinese with English abstract)

Yu ZX, Zhen AZ (1979) Geologic map of the Lhasa region at a scale of 1:1000000. Geologic Publishing House

Yuan DX, Zhang YC, Shen SZ (2018) Conodont succession and reassessment of major events around the Permian–Triassic boundary at the Selong Xishan section, southern Tibet, China. Global Planet Change 161:194–210

Zhang QH, Willems H, Ding L, Gräfe KU, Appel E (2012) Initial India–Asia continental collision and foreland basin evolution in the Tethyan Himalaya of Tibet: evidence from stratigraphy and paleontology. J Geol 120:175–189

Zhang C, Liu CZ, Wu FY, Zhang LL, Ji WQ (2016a) Geochemistry and geochronology of mafic rocks from the Luobusa ophiolite, south Tibet. Lithos 245:93–108

Zhang LL, Liu CZ, Wu FY, Zhang C, Ji WQ, Wang JG (2016b) Sr-Nd-Hf isotopes of the intrusive rocks in the Cretaceous Xigaze ophiolite, southern Tibet: constraints on its formation setting. Lithos 258–259:133–148

Zhang XR, Chung SL, Lai YM, Ghani AA, Murtadha S, Lee HY, Hsu CC (2019a) A 6000-km-long Neo-Tethyan arc system with coherent magmatic flare-ups and lulls in South Asia. Geology 47:573–576

Zhang C, Liu CZ, Xu Y, Ji WB, Wang JM, Wu FY, Liu T, Zhang ZY, Zhang WQ (2019b) Subduction re-initiation at dying ridge of Neo-Tethys: insights from mafic and metamafic rocks in Lhaze ophiolitic mélange, Yarlung–Tsangbo suture zone. Earth Planet Sci Lett 523:115707

Zhang C, Liu CZ, Wu FY, Ji WB, Liu T, Xu Y (2017) Ultra-refractory mantle domains in the Luqu ophiolite (Tibet): petrology and tectonic setting. Lithos, 286–287(supplement C), 252–263

Zhang Y, Liu X, Watkins DK, Bruno MDR, Yao HW, Han KB, Guo HF, Chen X, The Cretaceous (early Albian to early 1 Campanian) biostratigraphy and paleotemperature reconstruction of the eastern Tethys: calcareous nannofossil evidences from southern Tibet, China. In review

Zhao ZD, Mo XX, Dilek Y, Niu YL, DePaolo DJ, Robinson P, Zhu DC, Sun CG, Dong GC, Zhou S, Luo ZH, Hou ZQ (2009) Geochemical and Sr-Nd-Pb-O isotopic compositions of the post-collisional ultrapotassic magmatism in SW Tibet: petrogenesis and implications for India intra-continental subduction beneath southern Tibet. Lithos 113:190–212

Zhu B, Kidd WSF, Rowley DB, Currie BS, Shafique N (2005) Age of initiation of the India-Asia collision in the east-central Himalaya. J Geol 113(3):265–285

Zhu J, Du Y, Liu Z, Feng Q, Tian W, Li J, Wang C (2006) Mesozoic radiolarian chert from the middle sector of the Yarlung Zangbo suture zone, Tibet and its tectonic implications. Sci China Ser D 49(4):348–357

Zhu DC, Pan GT, Chung SL, Liao ZL, Wang LQ, Li GM (2008) SHRIMP zircon age and geochemical constraints on the origin of Lower Jurassic volcanic rocks from the Yeba Formation, southern Gangdese, South Tibet. Int Geol Rev 50:442–471

Zhu DC, Zhao ZD, Niu YL, Mo XX, Chung SL, Hou ZQ, Wang LQ, Wu FY (2011) The Lhasa Terrane: record of a microcontinent and its histories of drift and growth. Earth Planet Sci Lett 301(1–2):241–255

Zhu DC, Wang Q, Zhao ZD, Chuang SL, Cawood PA, Niu YL, Liu S-A, Wu FY, Mo XX (2015) Magmatic record of India–Asia collision. Sci Rep 5:14289

Ziabrev S, Aitchison J, Abrajevitch A, Davis A, Luo H (2003) Precise radiolarian age constraints on the timing of ophiolite generation and sedimentation in the Dazhuqu terrane, Yarlung–Tsangpo suture zone, Tibet. J Geol Soc, London 160(4):591–599